Deciphering the functions of protein VII during adenovirus infection.

Edward Arthur Arnold IV

A dissertation

submitted in partial fulfillment of the

requirements for the degree of

Doctor of Philosophy

University of Washington

2024

Reading Committee:

Daphne C. Avgousti, Chair

Jason G. Smith

Adam P. Geballe

Program Authorized to Offer Degree:

Microbiology

University of Washington

Abstract

Deciphering the functions of protein VII during adenovirus infection.

Edward Arthur Arnold IV

Chair of the Supervisory Committee:

Daphne C. Avgousti

Microbiology (Medicine)

Adenoviruses are double-stranded DNA viruses that cause various common illnesses. Although usually considered self-limiting infections, adenoviruses pose significant risks for immunocompromised individuals. Thus, a comprehensive understanding of adenovirus pathogenesis is crucial for advancing strategies aimed at mitigating adenovirus-related diseases. As adenoviruses are nuclear replicating viruses, they necessarily interact with host chromatin. One way in which adenovirus controls host chromatin function is through the histone-like protein, protein VII. Protein VII is an essential viral protein that packages with and condenses the viral genome within the core of the virion. Much like histone proteins, protein VII contains several post-translational modifications (PTMs) that impact its localization within the nucleus. However, the specific impacts of these PTMs on protein VII function during infection remain unexplored. During late infection when protein VII is abundantly expressed, it localizes to and distorts host chromatin and interacts with several host chromatin-associated proteins, including high mobility group box one (HMGB1). In the nucleus HMGB1 binds to and bends DNA to reorganize chromatin. During times of stress or infection, HMGB1 is released from the cell as an alarmin, where it stimulates an inflammatory response. Protein VII retains HMGB1 on chromatin, yet the mechanism of this interaction and its implications during infection are poorly

understood. In human adenoviruses, protein VII (hVII) exhibits high conservation, whereas in different vertebrate adenoviruses, such as murine adenovirus-1 (MAdV-1), protein VII (mVII) shows significant divergence with only 39% similarity to hVII. Despite mVII's known role in viral genome packaging within virions, its specific functions remain largely unexplored. MAdVs serve as a valuable *in vivo* model for investigating adenovirus pathogenesis, thus understanding how mVII contributes to MAdV infection can elucidate how adenoviruses cause disease.

In this thesis, I addressed these gaps in our understanding of protein VII function. I investigated how protein VII interacts with HMGB1 and found that protein VII interacts with HMGB1's A-box and anchors it to chromatin using bacterial two-hybrid and human cell culture assays. Furthermore, I showed protein VII suppresses interferon β induction and exploits HMGB1 for this purpose. To determine how PTMs on protein VII impact adenovirus infection, I created mutant viruses that abrogated or mimicked PTMs on protein VII. I determined that acetylation on protein VII may impact expression of early viral genes, but the PTMs did not appear to impact later stages of infection or localization of protein VII. However, I also discovered that protein VII is likely modified at alternative residues, which may compensate for the mutations we introduced. Finally, I used a chimeric HAdV-5 with a protein VII from MAdV-1, to show that mVII does not directly interact with HMGB1, but HMGB1 is still retained on chromatin during infection. I also discovered that in this chimeric virus, mVII was expressed at lower levels than hVII during infection, resulting in a reduction in viral titers. Additionally, mVII frequently localized to the nucleolus, suggesting a potential divergence in function from hVII. These investigations significantly contributed to our knowledge of the interplay between protein VII and the host nuclear environment and its evolutionary adaptations across diverse adenoviral species.

Table of Contents

List of Figures

Acknowledgements

I would like to acknowledge several people with their technical assistance in multiple projects. I would like to thank Katie Leung and Monica Guo with their assistance in performing multiple bacterial two-hybrid assays in chapter two, figure 3.5 in chapter three, and figure 4.2 in chapter 4. I would like to thank Mia Brinkley and Daniel Nguyen for assistance with running western blots in chapters two and three. I would like to thank Laurel Kelnhofer-Millevolte for her assistance with analyzing immunofluorescence microscopy images for figures 2.1 and figures 3.1 and for assistance with ddPCR for figure 2.7. I would like to thank Julian Smith for assistance with RT-qPCR in figure 3.2. I would like to thank Kelsey Lynch, Jason Smith, and members of the Smith lab for assistance with bacterial recombineering to create the mutant viruses used in chapter three and the chimeric virus used in chapter four. I would like to thank Roland Strong for his advice in protein structure prediction used in figures 1.3, 3.4, and 4.1.

I would like to acknowledge several core facilities with their assistance in several projects and experiments. I would like to thank the Fred Hutch Cancer Center Flow Cytometry core for training and assistance in flow cytometry experiments, used in figure 4.6, and several other experiments not presented in this thesis. I would also like to thank the Fred Hutch Cancer Center Proteomics Core for assistance with mass spec experiments used in figures 3.4 and 4.7.

This work was supported financially by R35 GM133441 to Daphne Avgousti, R00 GM134153 to Monica Guo, R01 AI104920 to Jason Smith, and T32 AI083203 to Edward Arnold from the from the National Institute of Allergy and Infectious Disease. Additional support was provided by startup funds to Daphne Avgousti from Fred Hutch Cancer Center, startup funds to Monica Guo from the University of Washington, the University of Washington Magnuson Scholarship to L.E. Kelnhofer-Millevolte, and the Helen Riaboff Whiteley Fellowship from the University of Washington Microbiology Department to Edward Arnold.

I would like to thank my committee members, Daphne Avgousti, Jason Smith, Adam Geballe, Jennifer Hyde, and Brian Beliveau for their guidance and assistance on my projects throughout graduate school. A special thank you to Daphne, Jason, and Adam for serving as my reading committee members.

I would also like to acknowledge some of my previous mentors. To Duncan Krause, you were the first professor to let me join his lab and delve into the world of research. Thank you for letting me explore the wonderful world of microbiology. To Vincent Starai, your passion for microbiology while teaching my undergraduate courses was infectious and is one of the main reasons why I pursued a career in microbiology. Thank you for your support, and for helping me get into graduate school. To Caitlin Reeves Williams, you were the first graduate student I ever worked under and were so kind and patient with me when I barely knew how to hold a pipette. Thank you for teaching me the basics and helping me begin my career in research. To Patti Fields, thank you for supporting me in my position at the CDC and writing so many recommendation letters that got me into graduate school and a training grant. To Ana Posada, you were the first person to push me to attend graduate school and were a fantastic mentor for me at the CDC. Thank you for all the wonderful advice you gave me.

For more personal acknowledgements, I would like to thank current and previous members of the Avgousti lab for all of their assistance in lab and general feedback on experiments and presentations throughout my graduate school career. To Kelsey Lynch, I would like to thank you for your mentorship at the beginning of my graduate school career and keeping spirits up within the lab with your planned spirit days and happy hours in the park during the worst stages of the pandemic. To Hannah Lewis, I would like to thank you for your guidance and feedback on all my training grants and qualifying exams. To Melanie Dillon, thank you for always being there to help with technical issues in the lab, and for you and your family keeping the lab fed at the annual ‘beast feast’. To Monji Bat-Erdene, thank you for always being around

to chat when work and life were overwhelming. To Robin Kaai, we started in the Avgousti lab at the same time, and you were always a fantastic lab mate to have. I could always count on you to help out with anything, and you were always a great reminder to stay grounded, not worry about the things I couldn't control, and to just enjoy the ride. To Laurel Kelnhofer-Millevolte, we've struggled through the last stages of graduate school together, and I think we've both grown a bunch along the way with each other's help. To Daniel Nguyen and Lea Wison, thank you both for always being willing to help with any project and bringing youthful energy and excitement to the lab. To Julian Smith, we've only overlapped for half a year, but you have been supportive in my projects and extra helpful with my post-doc applications. To Allison, thank you for always handling any administrative problems with ease and bringing positive energy to the lab. Lastly, to Daphne, I want to extend an unquantifiable amount of gratitude. When I started graduate school, I felt very unprepared and out of place, but your mentorship has helped me grow not only as a scientist but as a person. I am very thankful for all the guidance you have given me, and I am excited to see where your lab goes after I have left.

I would like to give a special thanks to all of my cohort members: Jacob Frick, Ryan Yucha, Robin Cagle, Nikki Schwardt, and Joselyn Landazuri Vinueza. We all moved to Seattle to start graduate school in 2019, and within six months a global pandemic shut most of the world down. I believe we made it through not just the pandemic, but also through classes, teaching, qualifying exams, and the rest of the issues that graduate school and life can bring because we were all there for each other and willing to help each other no matter what. I don't think I could have made it without all of you, and I can't wait to see all of you graduate as well. I want to give an extra special thanks to Jacob for being my roommate for the first four years of graduate school, giving me advice on work, helping me navigate the field of academia, and most importantly, being a great friend.

I want to acknowledge all the current and former Microbiology graduate students. You all welcomed me with open arms and helped me navigate the first few years of graduate school when I often felt lost. I hope I've been able to repay this in kind to the younger graduate students as well. I truly feel as if the graduate students are a family, and I always look forward to our many parties, happy hours, camping trips, and student retreats. We work hard together, and we play hard together as well. Thank you all for your endless support.

To my family, I want to thank you for all the support and encouragement you have given me throughout my upbringing and my studies. I know it was difficult that I moved to the other side of the country to attend graduate school, and I wish I could have seen you more over the past several years but thank you for still supporting me and believing in me along the way. Thank you for attempting to understand what I worked on and being proud of my accomplishments. To my parents, thank you for allowing me to pursue whatever I wanted growing up. You didn't force me into a specific career path and allowed me to explore multiple academic topics and hobbies and were happy as long as I was happy and successful. I am who I am thanks to you. Also, thank you for always doing my needlessly complicated graduate school tax returns so that I didn't have to.

Finally, to Ale Valdez Cabrera, thank you so much for all the support you have given me these past few years. We suffered through graduate school together, been through many trials and tribulations together, and we will both be defending together. I am super excited to see where life takes us after graduate school, and I'm happy to have you and Shippo by my side on this journey.

Chapter 1: Introduction

Adenovirus

Pathogenesis: *Adenoviridae* is a family of double-stranded DNA viruses found throughout the animal kingdom, with most vertebrate animals having their own adenoviruses[1]. Adenovirus was first isolated from the adenoids of a pediatric patient in 1953, and it is from the adenoids that adenovirus gets its name[2]. There are over 50 serotypes, or types, of human adenovirus, which are classified into seven different species (A-G)[1,3]. Human adenovirus 5, a species C adenovirus (HAdV-C5), is one of the more commonly used serotypes in research, and most of the work presented throughout this thesis was performed with HAdV-C5. HAdVs primarily cause common-cold like diseases, with the most common manifestations presenting as respiratory infections, gastroenteritis, and conjunctivitis[4,5]. Respiratory infections are commonly associated with species B, C, and E; gastrointestinal infections with species A, F, and G; and ocular infections with species C and D[6,7]. While generally viewed as a self-limiting infection, adenovirus can be particularly harmful for immunocompromised individuals and is especially prevalent in patients who have undergone organ transplants or stem cell therapy[8–11]. For this reason, adenovirus should not be viewed as solely a common-cold causing virus, but as a potential threat for many at-risk individuals within the general public.

Adenovirus is primarily a lytic virus, and replicates to high titers within cells before killing the cell and releasing thousands of progeny. Adenovirus can also cause persistent infections. Persistent infection is conceptually similar to latency, such that the two terms are sometimes used interchangeably, but whether or not adenovirus can establish latency is still yet to be determined. For viruses that establish latency, the viral genome will remain dormant within the host cell, express minimal amounts of viral genes, and will not produce viral progeny until reactivated. Herpes simplex virus-1 is a common example of a virus that can establish latent

infections, usually remains dormant within neuronal cells, and spontaneously reactivates throughout the lifetime of the host[12]. Persistent adenovirus is thought to replicate at low to undetectable levels and is largely suppressed but not eliminated by the immune system[9]. This likely occurs in intestinal lymphocytes, which are not conducive to replication of adenovirus, and then a small amount of progeny can spillover into intestinal epithelial cells where it replicates to high titers[9,13]. Thus, adenovirus's ability to cause persistent disease in vulnerable individuals requires more study so that this phenomenon can be better understood.

Adenovirus is primarily spread through aerosols or the fecal-oral route and is highly stable on most surfaces[14]. There is no approved treatment for adenovirus infection and most individuals do not require medical intervention. In severe cases of adenovirus infection or in immunocompromised individuals, cidofovir/brincidofovir, an inhibitor of the viral DNA polymerase, can be administered to help treat patients[14–18]. However, cidofovir/brincidofovir are not specific to adenovirus, and cidofovir is potentially nephrotoxic, thus its use in treatment for severe adenovirus infection is limited. An adenovirus vaccine that targets HAdV-4 and -7 is only available to individuals within the US military, where these two serotypes are especially common in recruits likely due to the crowded conditions and high stress of military barracks[19,20]. These two serotypes are typically associated with cases of acute respiratory distress in infected individuals, and thus the vaccine was recommended for individuals in the military. Furthermore, the current vaccine is an attenuated, live, actively replicating virus that causes asymptomatic infection, and is deemed not suitable for the general public[21]. Therefore, study of adenovirus pathogenesis is important so that we can discover better therapies for adenovirus infection.

Adenovirus has also been integral as a tool in research laboratories, as well as in public health in the form of vaccines. Since adenovirus does not typically cause major disease, is genetically tractable, has a broad tropism, and is easy to mass produce, it is commonly used as a vector in vaccines, gene therapy, and in scientific research. Several of the vaccines used for

SARS-CoV-2 during and after the SARS-CoV-2 pandemic utilized an adenovirus vector, most notably by Johnson & Johnson and AstraZeneca[22]. It is also used as a gene vector to express transgenes in various target cell types or tissues, to help treat a specific disease, such as cancer[23–26]. Adenoviruses role as a gene vector is not restricted to public health and medicine and it is frequently used within research labs to deliver trans-genes to a target cell to study the gene's biological effects[26,27]. Unfortunately, adenoviruses illicit strong innate and adaptive immune responses, which can complicate their usage in gene therapy or as a vaccine vector where a reduced immune response may be desired[28–30]. This further highlights the need to understand how adenovirus subverts the immune response, to improve treatment for adenovirus infection and its use within medicine and public health.

Virion and genome structure: Adenovirus has a non-enveloped, icosahedral capsid that consists of 13 viral proteins and contains the viral genome (Figure 1.1A-B). The major capsid proteins are hexon, penton base, and fiber, which form the facets, vertices, and spike-like protrusions of the capsid, respectively[31]. The minor capsid proteins (also called cement proteins) IIIa, VI, VIII, and IX help stabilize the capsid and aid in cellular entry[32]. Six core proteins are located in the interior: TP, V, VII, μ, AVP, and IVa2. Proteins VII and μ bind and condense the viral genome [33–36], protein V links the genome to the interior of the capsid [37,38] and the terminal protein (TP) binds the 5' ends of the viral genome[39]. AVP is a viral protease, that cleaves several of the capsid proteins, which is essential for capsid maturation and escape from the endosome[40,41]. IVa2 exists at a low copy number within the virion and helps package the genome within the virion[42]. In total, the adenovirus virion consists of many structural and core proteins that are essential for gaining entry to a target host cell, protecting the viral genome, and transferring it to the nucleus to initiate viral gene expression and replication.

The HAdV genome varies in length depending on the species but is approximately 36 kb (Fig 1.1C). The ends of the genome contain inverted terminal repeats, important for genome replication, and the 5' end of the leading strand contains a packaging sequence important for packaging the genome into progeny virions. The more conserved viral genes tend to be found in the middle of the genome, while more species-specific genes are found near the ends. The viral genome can be broken into three transcription units: the early genes (E1A, E1B, E2, E3, E4),

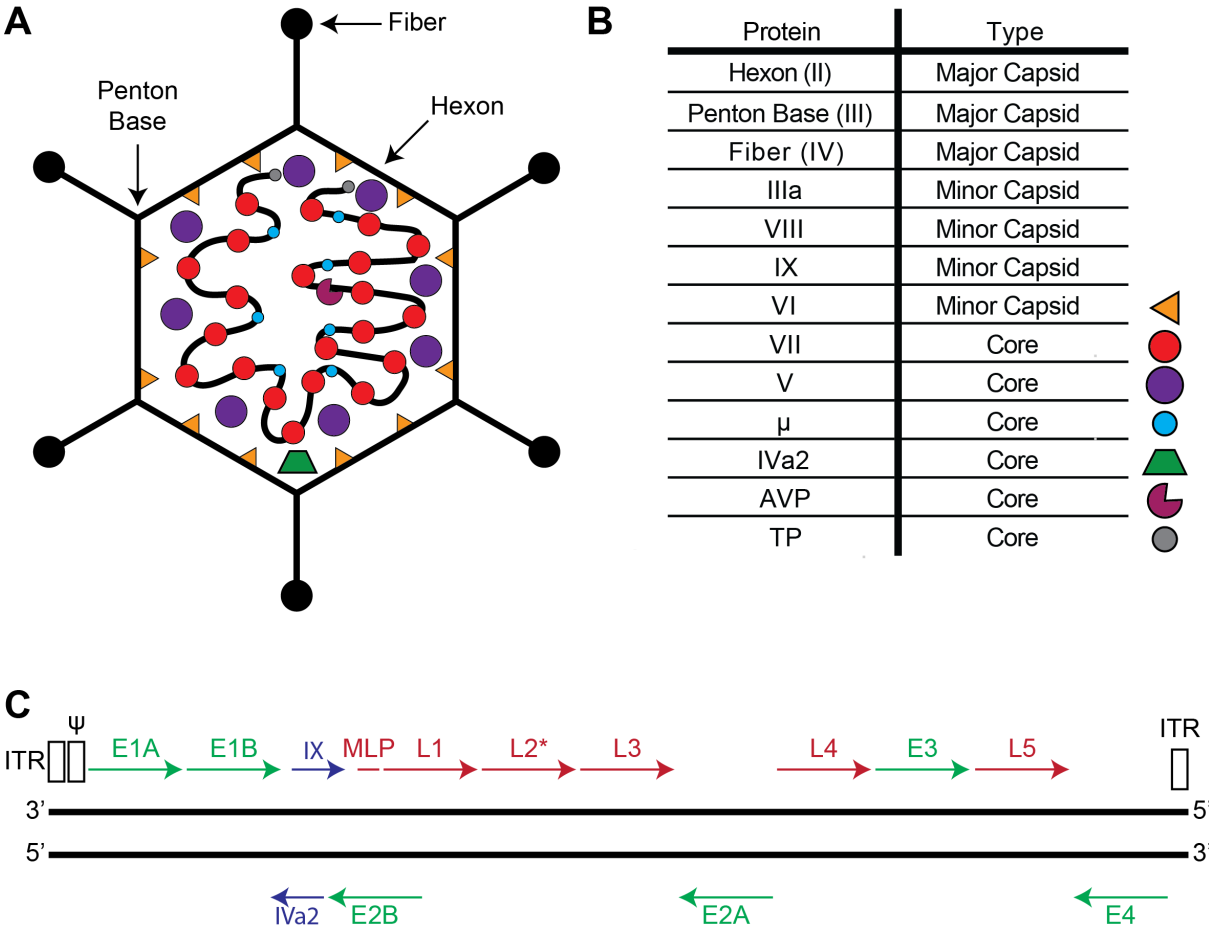

Protein	Type
Hexon (II)	Major Capsid
Penton Base (III)	Major Capsid
Fiber (IV)	Major Capsid
IIIa	Minor Capsid
VIII	Minor Capsid
IX	Minor Capsid
VI	Minor Capsid
VII	Core
V	Core
μ	Core
IVa2	Core
AVP	Core
TP	Core

Figure 1.1 Adenovirus virion and genome structure. A) Schematic of adenovirus virion with major capsid and core proteins identified. B) Table of major capsid, minor capsid, and core proteins that make up adenovirus virion. Key for core proteins and protein VI in cartoon schematic to the right of table. **C)** Schematic of HAdV-5 genome with approximate location and orientation of adenovirus genes. Green arrows are early genes, purple arrows are intermediate genes, and red arrows are late genes. Major Late Promoter (MLP) is a red line. Internal terminal repeats (ITR), and psi packaging sequence are black rectangles. L2* denotes the location of the protein VII gene. Genes not drawn to scale.

the intermediate genes (IVa2, IX, E2 late, and L4 intermediate), and the late genes (L1-L5) (Fig 1.1C). The early genes largely code for proteins that reprogram the cell, replicate the viral genome, or promote host immune evasion, while the intermediate gene IVa2 and late genes are mostly structural proteins and proteins involved in virion production and packaging.

Infection Cycle: Adenovirus infection begins with attachment and entry at the host cell membrane. This is facilitated by binding of fiber to the primary receptor (CAR in HAdV-C5) and binding of the RGD motif within penton base to integrins that contain the RGD motif, such as αvβ3 or αvβ5 [43] (Fig 1.2, [Stage 1]). Upon entry, the membrane lytic protein, protein VI, contains an amphipathic helix that when exposed lyses the endosome. The virion escapes the lysed endosome and traffics along microtubules toward the host cell nucleus[44,45] (Figure 1.2, [Stage 2]). The virion docks at nuclear pore complexes through interactions with the hexon and nuclear pore complex proteins[46,47]. From here, the viral genome enters the nucleus (Figure 1.2 [Stage 3]), where it is still bound by the core proteins, TP and VII. Once in the nucleus, the early phase of adenovirus infection begins with the expression of the early adenovirus genes (Fig 1.2 [Stage

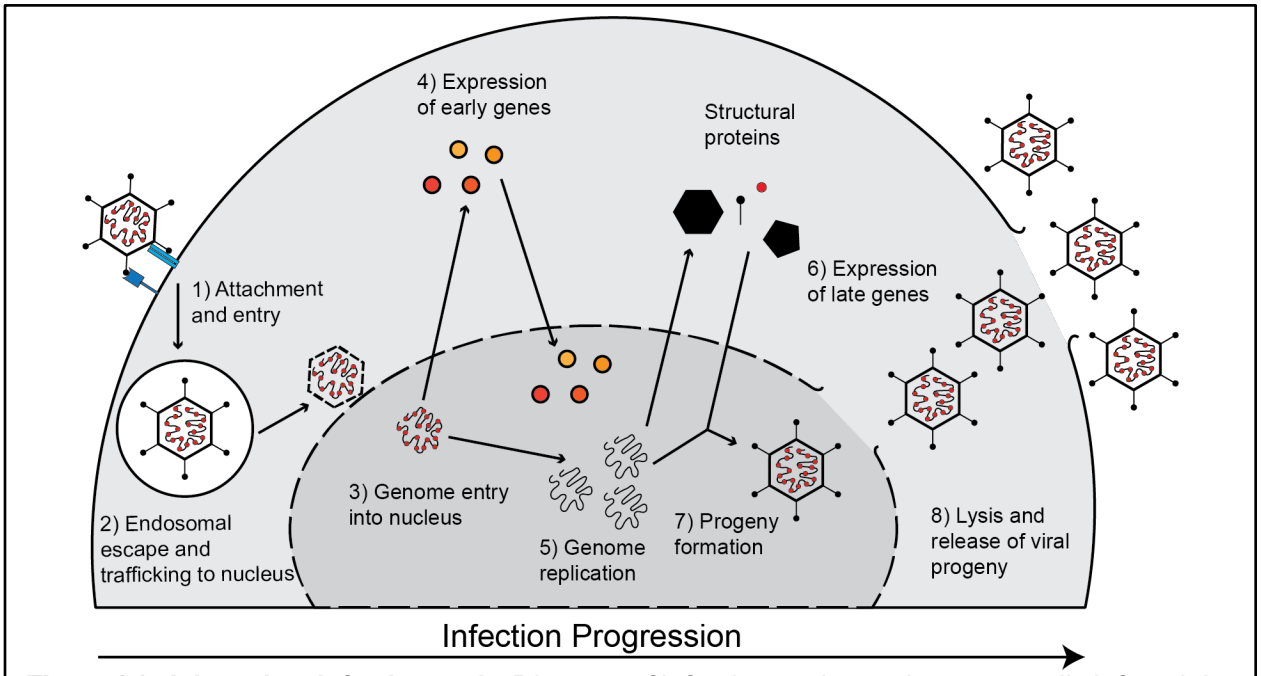

Figure 1.2: Adenovirus infection cycle. Diagram of infection cycle moving temporally left to right. Stages of infection are enumerated 1-8 and referenced as such within the text.

4]). The early genes have a wide range of functions but are ultimately responsible for pushing the host cell into a viral-like S-phase, evading the immune response, preventing cell death, and replicating the viral genome. Genome replication usually occurs around 6-8 h post-infection (p.i.) in most epithelial cell lines and is the switch that initiates the late stage of infection (Fig 1.2, [Stage 5]).

Adenovirus produces an excess of viral genomes during infection, exceeding the amount that can be packaged within viral progeny and effectively doubling the DNA content of the host cell[48]. The genome replicates within the nucleus at sites termed viral replication centers (VRCs). VRCs can be visualized in confocal microscopy by staining the early viral ssDNA binding protein, protein E2A, more commonly known as DNA binding protein (DBP)[49]. Multiple VRCs form throughout the nucleus during infection, start as small foci that slowly expand to larger ring-shaped structures, and eventually begin to merge to form large intranuclear structures termed the virus-induced post-replication (ViPR) bodies[49–52]. The early VRCs likely serve to produce new templates for transcription of viral genes. Later VRCs, which form ring-like shapes are likely producing an excess of viral genomes which are stored within the interior of the VRC. These VRCs eventually merge to form the ViPR body where the viral genomes can be packaged within progeny virions[53].

Viral late genes are expressed after the onset of genome replication (Fig 1.2 [Stage 6]). There are five viral late transcription units (L1-L5) controlled by the major late promoter (MLP) (Fig 1.1C). Each unit consists of more than one unique open reading frame for an individual protein. The late genes are transcribed as one long transcript, which is alternatively spliced into the individual genes, and then translated[54,55]. The late genes express structural proteins and proteins that aid in the formation of progeny virions in the nucleus within the ViPR bodies (Fig 1.2 [Stage 7]). Each infected cell can produce thousands of viral progeny, which are released

upon cell death and lysis; however, some adenoviruses release progeny through non-lytic mechanisms (Fig 1.2 [Stage 8]).

Protein VII

The adenovirus core contains multiple DNA binding proteins that are involved in compacting the viral genome and balancing the negative charge of the DNA. One of those proteins is protein VII, which functions within the virion and the host nucleus during early and late stages of viral infection. Protein VII is a small protein, about 20 kDa in size. It is a very basic protein that contains several lysine and arginine residues, giving it a net positive charge of 39 at

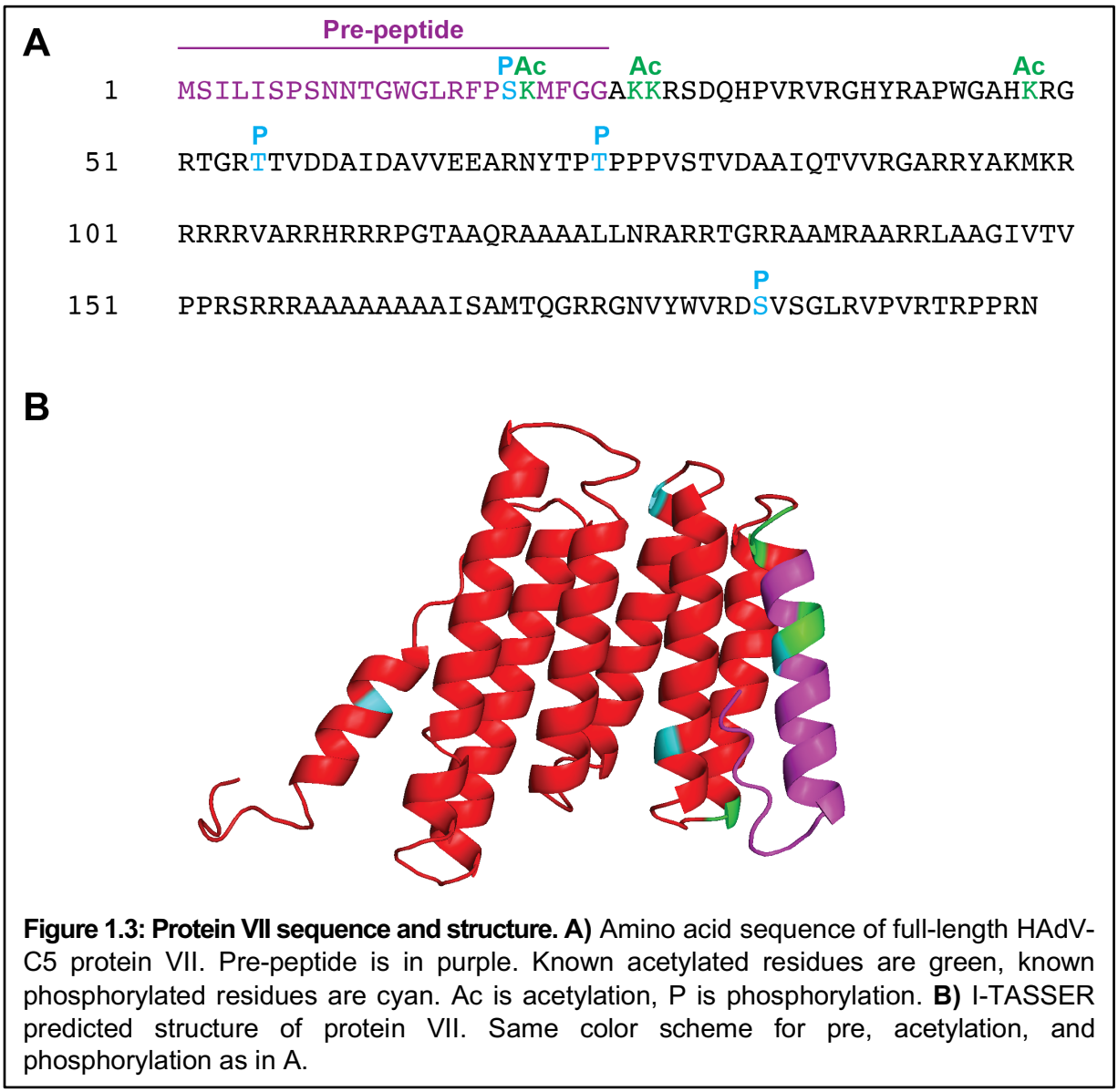

Figure 1.3: Protein VII sequence and structure. A) Amino acid sequence of full-length HAdV-C5 protein VII. Pre-peptide is in purple. Known acetylated residues are green, known phosphorylated residues are cyan. Ac is acetylation, P is phosphorylation. **B)** I-TASSER predicted structure of protein VII. Same color scheme for pre, acetylation, and phosphorylation as in A.

neutral pH. Protein VII is initially translated as preVII which is 198 amino acids long in HAdV-C5 (Fig 1.3A). The first 24 N-terminal amino acids make up the pre-portion of the peptide and are cleaved off by the viral protease, resulting in mature protein VII[40,56]. There is currently no structural data for the mature portion of protein VII, while a small segment of the pre-peptide has been resolved within virions[57]. The I-TASSER prediction software suggests that protein VII forms a bundle of approximately seven to eight α-helices, depending on the presence of the pre-peptide (Fig 1.3B)[58–60]. The lack of structural data for protein VII further highlights the need for it to be studied and fully characterized.

Protein VII was initially described as a histone-like protein in the 1970s and 80s. Digestion of adenovirus genomes extracted from virions showed that the viral genome was protected by the viral core proteins, forming 200 bp fragments[61]. Furthermore, electron microscopy of extracted adenovirus genomes showed that protein VII formed a beads-on-a-string-like structure on the viral genome, reminiscent of histones on DNA[36,62]. It was determined that 2-6 molecules of protein VII multimerize and 90-150 bp of DNA is wrapped around the protein VII multimer[36,63]. These results led researchers to conclude that protein VII compacts the viral genome within the virion and negates the negative charge of the viral DNA.

During infection, protein VII remains bound to the viral genome and functions throughout the early stages of infection[64–67]. Protein VII is one of two viral proteins that remains bound to the genome upon entry into the nucleus, the other being the terminal protein (TP). However, while the TP is covalently linked to the 5' ends of the viral genome, protein VII's interaction with DNA is likely more akin to that of the multiple hydrogen bonds formed between histone proteins and DNA[39]. When the viral capsid docks at nuclear pore complexes, protein VII interacts with several importin proteins (importin-α, -β, and -7), which facilitate its entry into the nucleus[68]. It is unknown if these importin proteins are necessary for facilitating nuclear entry of the AdV genome bound by VII during early infection, or if they are specifically for nuclear entry of protein

VII during late infection. Once inside the nucleus, AdV genomes can be visualized as foci by confocal microscopy through staining of protein VII, or through staining of the chromatin factor TAF-1β/SET, which quickly associates with protein VII after nuclear entry[66,69–71]. Protein VII foci will persist throughout early infection and begin to disappear around 10-12 hpi. The mechanism of protein VII's removal from the genome is unknown, with some studies reporting that transcription initiates its removal, while others reported that transcription is dispensable for protein VII's removal[65,67,72–74]. Thus, the exact mechanism of how protein VII is removed and what happens to it after removal remain to be explained. Protein VII's role in transcription is also a disputed topic. When protein VII is transfected into *Xenopus* eggs, protein VII condenses host chromosomes and prevents R-loop formation, suggesting it is a suppressor of transcription[75]. Furthermore, protein VII is believed to recruit E1A to the viral genome during early infection to initiate transcription[75]. However, when plasmids are coated in protein VII before transfection, protein VII enhances transcription of a reporter gene encoded by the plasmid[67,76]. Therefore, the exact roles that protein VII has during early infection remain unresolved. This topic will be explored further in chapter three of this thesis.

Protein VII is a late protein encoded on the L2 transcript and is expressed at high levels during the late stage of infection. Protein VII that is expressed during late infection is packaged with the viral genome as a core viral protein[36,64]. When visualized through IF microscopy, protein VII will localize at VRCs and within the ViPR body[51]. However, protein VII doesn't completely colocalize with DBP, suggesting that it isn't involved in active viral genome replication and is likely present to be packaged with newly replicated genomes[51,77]. The mechanism of how protein VII is packaged, and more broadly how adenovirus virions package their genome and core proteins, has yet to be completely elucidated. Current evidence favors a concerted model where the virion capsid forms around the viral genome and core proteins, but this model requires more evidence before being fully accepted[31,78]. Surprisingly, protein VII is dispensable

for virion formation as virions can be made with a HAdV-5 floxxed protein VII virus, which uses loxP sites and cre-recombinase to remove protein VII from the viral genome during infection[79]. However, the protein VII null viral progeny are no longer infectious[79]. Within the virion core, protein VII and protein VI compete for a binding pocket within the interior of the major capsid protein, hexon. This dynamic competition is hypothesized to force these proteins out of the pocket, where the viral protease can cleave either protein VII or VI into their mature forms[40,41,80]. This step is critical for protein VI, as it must be processed to gain its lytic function, which is essential for adenovirus to escape the endosome upon cellular entry[81]. Without protein VII this competition doesn't exist, and virions become trapped within endosomes[80], thus protein VII is essential for infection to be established in an indirect manner[79,80].

Protein VII expressed in late infection will also localize to and distort host chromatin[82]. This is observable through IF microscopy, where protein VII can form punctate foci that overlap with more intense DAPI staining, suggesting that the protein VII is distorting chromatin[82]. Expression of mature protein VII alone is enough to recapitulate this phenotype. During acid extraction of chromatin or high salt chromatin fractionation from cells infected with HAdV or ectopically expressing protein VII, protein VII has a strong association with host histones, confirming that protein VII is indeed interacting with host nucleosomes[82]. Exactly where protein VII interacts with host nucleosomes and the mechanism of how chromatin is distorted and for what purpose remains to be elucidated. Protein VII likely interacts with different regions of the nucleosome, binding the core histone proteins as well as the linker DNA. Furthermore, it is speculated that protein VII's distortion of host chromatin likely leads to broad changes in host gene expression, chromatin accessibility, and creates space for the replication and production of progeny virions.

Protein VII contains several post-translational modifications, and numerous studies have reported the presence of phosphorylation and acetylation sites on protein VII through mass

spectrometry[82–84]. On mature protein VII, lysine 2/3 and 24 are acetylated and threonine 31 and 50 and serine 159 are phosphorylated[82]. Since the PTMs are detected during ectopic expression of protein VII, a host enzyme must be responsible for depositing the PTMs. Functionally, the PTMs appear to be important for the localization of protein VII. During ectopic expression, when all five sites are modified to an alanine (ΔPTM), protein VII localizes to the nucleolus. When only lysine two and three are mutated to alanine (K2AK3A), again protein VII localizes to the nucleolus. When lysine three is mutated to glutamine (K3Q), which acts as an acetyl mimic, protein VII localizes to chromatin[82]. Interestingly, during adenovirus infection, the nucleolus becomes disrupted, and many nucleolar proteins localize to viral replication centers and have been reported to be involved in viral progeny production[85]. The changes in localization of protein VII support a model where modification of protein VII dictates whether it localizes to host chromatin (modified) or to viral genomes (unmodified). Mass spectrometry performed on purified adenovirus detected no acetylation on protein VII and only one phosphorylation at S79[82–84]. The lack of PTMs on protein VII within virions supports the model that modification determines the localization of protein VII to either chromatin or to be packaged in viral progeny[82]. However, these mutation studies have only been studied in the context of ectopic expression, and part of this dissertation (chapter 3) will address the function of PTMs within the context of infection.

Protein VII's distortion of host chromatin leads to large changes in the composition of chromatin. Mass spectrometry of chromatin isolated during adenovirus infection or ectopic expression of protein VII identified several host factors that are enriched on chromatin compared to cells that were uninfected or not expressing protein VII. Many of these proteins are affiliated with the immune response and DNA damage, and some of the most abundant proteins enriched on chromatin were SET (also called TAF-1β) and HMGB proteins, with the most abundant being high mobility group box one (HMGB1)[82]. Briefly, HMGB1 is an alarmin protein

that is released from the nucleus and the cell during times of stress or infection to help stimulate an inflammatory response[86]. Protein VII interacts with and retains HMGB1 on chromatin during adenovirus infection, preventing this alarmin response[82]. SET is a histone chaperone whose interaction with protein VII has been extensively studied[70,87,88]. SET interacts directly with protein VII, forming a tertiary complex with protein VII and DNA, and facilitates the deposition of histones on the adenovirus genome driving transcription of early genes and the potential removal of protein VII[70,87,88]. This interaction is observable by confocal microscopy during early infection. Adenovirus genomes can be visualized with protein VII staining as foci and SET staining will also colocalize with protein VII as foci during early infection[69,70].

Protein VII also inhibits the DNA damage response (DDR). The MRE11-RAD50-NBS (MRN) sensor complex is a set of proteins that bind to damaged DNA and recruit proteins involved in DNA repair[89]. The MRN complex can detect the ends of the adenovirus genome as double-stranded breaks and initiate a DDR response[90]. Protein VII coated on the early viral genome prevents the MRN sensor complex from recognizing the viral genome and activating the downstream DDR response[65]. Protein VII will also prevent the accumulation and spread of γH2AX on the host genome[91]. γH2AX is the activated form of H2AX, a histone variant that recruits other DDR mediators to the site of DNA damage to amplify a repair response that could block the cell cycle or induce apoptosis[92,93]. Loss of the host protein SET causes an increase in γH2AX accumulation, even in the presence of protein VII, suggesting that SET either aids protein VII in inhibiting γH2AX accumulation or loss of SET signals for γH2AX accumulation[91]. Lastly, protein VII can block cell cycle progression, and it recruits SET and HMGB1 to achieve this. Since humans have multiple HMGB proteins with overlapping functions, the block was first characterized in yeast, which only express one homolog of SET (Nap1) and HMGB1 (Hmo1). Expression of protein VII in budding yeast led to a growth defect and dysregulation of cell cycle progression; however, knockout of the Nap1 and/or Hmo1 rescued this growth defect,

suggesting that these host proteins are important for blocking cell cycle progression[94]. Protein VII is hypothesized to compete with the linker histone, H1, for access to the nucleosome. Protein VII can utilize HMGB1, an H1 antagonist, and SET, a histone chaperone, to evict H1 from the nucleosome[91,94]. Yeast, also only have one homolog of histone H1, Hho1. Knockout of Hho1 in VII expressing yeast led to growth defects worse than those seen in the presence of Hho1, suggesting that the presence of the linker histone alleviates the inhibitory effects of protein VII on yeast growth. This result was further characterized in eukaryotic cells, where nuclear markers of G2 phase and mitosis were depleted during wild-type HAdV-5 infection in comparison to infection with the HAdV-5 floxxed protein VII virus, suggesting that protein VII is acting during late infection to hijack host chromatin and dysregulate the cell cycle[79,94]. By blocking cell cycle progression, protein VII prevents mitosis of the host cell before viral progeny have begun forming[94]. This would prevent cellular resources from being redirected to mitosis and keep them focused on viral replication and progeny production. In total, these findings show that protein VII engages in multiple virus-host interactions and is an essential protein for adenovirus infection. Thus, it is important that we continue to detangle the interactions of protein VII with host factors and how they impact adenovirus infection.

HMGB1

Protein VII interacts with many host chromatin factors during infection. One of the key binding partners of protein VII is HMGB1. HMGB1 is a multifunctional protein that acts as a chromatin factor within the nucleus and as an alarmin when secreted from the cell. HMGB1 is enriched on chromatin when protein VII is expressed, meaning that it is a potentially important interaction during adenovirus infection, of which the functional output needs to be further characterized and understood. HMGB1 is a small, largely nuclear protein of 215 amino acids. It contains three domains: the A box, B box, and C terminal tail (Fig 1.4A). The box domains each form an L-shape and are connected by a flexible linker, and the C-terminal tail is an intrinsically disordered region of the protein (Fig 1.4B**)**. The two box domains are responsible for binding to and bending DNA, while the C-terminal tail helps facilitate HMGB1's interaction with other proteins and DNA[95–97]. Both box domains contain bulky hydrophobic residues (F38, F103, I122) that are inserted into the minor groove of DNA (Fig 1.4B). The hydrophobic residues are flanked by basic residues that help enhance the interaction with DNA. Once inserted, HMGB1 undergoes a conformational change, and the DNA is bent to extreme angles[98,99]. This interaction is transient and has been described as a 'hit-and-run' interaction with DNA. When the bulky residues are mutated to alanine, HMGB1 no longer localizes to chromatin and its interaction and ability to bend DNA is greatly reduced[100,101]. The C-terminal tail is a long stretch of ~30 glutamic and aspartic acids (Fig 1.4A-B). The large negative charge of the tail allows it to fold back and sit in between the box domains to inhibit binding to DNA by the box domains. In fact, removal of the tail greatly enhances HMGB1's ability to bind and bend DNA[101]. The C-terminal tail will also regulate binding to other proteins and interacts with histone proteins H1 and H3[102]. HMGB1 can be heavily modified and contains several sites of acetylation, phosphorylation, and methylation, mostly located within the A-box[103–106]. Modification affects HMGB1 function and localization. Normally, HMGB1 within the nucleus is unmodified, however,

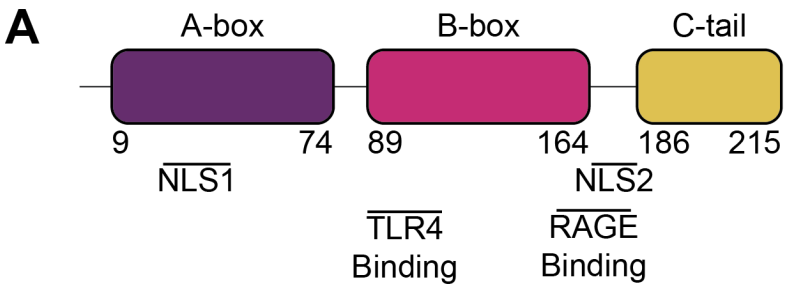

Figure 1.4: High mobility group box one. A) Diagram of HMGB1, its three domains (A-box, B-box, and C-tail). Residues corresponding to each domain indicated. Regions of the two NLS, TLR4 binding, and RAGE binding indicated. **B)** AlphaFold3 predicted structure of HMGB1. A-box is in purple, B-box is in pink, C-terminal tail is in yellow, linker regions are in green. Three hydrophobic residues (F38, F103, and I121) are in cyan. Three cysteine residues (C23, C45, and C106) are in blue.

the addition of PTMs facilitate its translocation from the nucleus to the cytoplasm. This likely occurs through an increased association with the nuclear export protein CRM1[107]. HMGB1 also has redox sensing potential and has three cysteine residues (C23, C45, and C106), with C23 and C45 capable of forming a disulfide bridge (Fig 1.4B). The oxidation state of the three residues can impact HMGB1's function and localization. Within the nucleus, usually HMGB1 exists in a reduced state, however, mutation of C106 to an alanine results in translocation to the cytoplasm[108]. Extracellularly, all-thiol HMGB1 (reduced) can exert chemo-attractive effects by binding CXCL12 or induce autophagy by binding RAGE[109]. Oxidation and disulfide bridge formation between C23 and C45 reduces HMGB1's ability to bind DNA and results in

translocation to the cytoplasm[110]. The disulfide bridge form of HMGB1 also induces an inflammatory response when it binds TLR4[111]. The completely oxidized form of HMGB1 appears to be inert in function[112]. In total, HMGB1 localization and function are highly regulated, and variable based on its modification and oxidation state.

Evolution: HMGB1 likely emerged within multicellular animals over 500 million years ago[113]. It is a highly conserved protein amongst animals and HMGB1 in humans is 99% identical to HMGB1 in mice at the amino acid level. HMGB1 is also found in eukaryotes outside of animals. Yeast have an HMGB1 homolog, Hmo1, that lacks the C-terminal tail, suggesting that this portion evolved later[114]. Deletion of HMGB1 in mice is embryonic lethal, which means that HMGB1likely plays a crucial role in development in animals[115]. There are two other proteins within the HMGB family found within metazoans: HMGB2 and HMGB3.There is also HMGB4, which is only found in mammals[116]. HMGB1-3 are similar at the structural and amino acid level, sharing over 80% amino acid identity and largely differing in length[117,118]. All four HMGBs contain an A and B box domain, while HMGB4 lacks an acidic C-terminal tail and is more divergent at the nucleotide level[119,120]. HMGBs have varying levels of overlapping functions, especially within the nucleus[117,121]. While all are expressed to some degree within most cells, some are more abundantly expressed in specific cell types. HMGB1 is highly expressed in most tissues[122], whereas HMGB2 is more specific to the thymus and testis[123], HMGB3 in hematopoietic stem cells[124], and HMGB4 in neural cells and the testis[125]. HMGB1 is the most abundant of the four HMGBs and is one of the most abundant non-histone nuclear proteins.

Functions: HMGB1 is a multifunctional protein that operates largely within the nucleus but also has roles within the cytoplasm and extracellularly. Within the nucleus, HMGB1 is a DNA-binding protein where it bends DNA to extreme angles[95,96]. This bind and bend interaction is believed to help facilitate transcription factor binding, replication, DNA repair, and chromatin remodeling. DNA binding by HMGB1 is not sequence specific but rather it recognizes non-

canonical DNA structures, such as four-way junctions, DNA bulges, and hemi-catenated DNA[126,127]. The interaction with DNA is very transient, which makes a ChIP of HMGB1 difficult. The first ChIP of HMGB1 was performed recently (2021) and required harsh conditions to achieve this. The ChIP needed fixation and crosslinking times of up to 40 minutes to succeed, and ultimately showed that HMGB1 likely plays a role in senescence and cell proliferation[128].

HMGB1 is also known as an alarmin or danger-associated molecular pattern (DAMP). During times of cellular stress, damage, or infection, HMGB1 is passively secreted by most cell types to trigger inflammation[86]. Immune cells, such as macrophages and monocytes, and non-immune cells, such as hepatocytes and neurons, will actively secrete HMGB1 into the extracellular environment[129–132]. In the extracellular space, HMGB1 binds other DAMPS (nucleosomes, extracellular DNA) or pathogen-associated molecular patterns (LPS). It will then bind known receptors TLR4 or RAGE (Fig 1.4A) with the bound DAMPs/PAMPs, which leads to a signaling cascade and activation of an interferon response or the release of pro-inflammatory cytokines[131,133]. HMGB1 has also been reported to bind to other known receptors to produce an immune response, such as TLR2 and TLR9, but TLR4 and RAGE are currently the only accepted receptors of HMGB1.

HMGB1 localizes to the nucleus under normal physiological conditions, HMGB1 is occasionally found within the cytosol, where it has been shown to modulate autophagy[134]. HMGB1 will interact with free nucleic acids within the cytosol. HMGB1 will bind to immune stimulatory U-turn DNA, leading to an activation of the cGAS-STING response and nucleic acid-based immune responses[135,136].

Since HMGB1 is a potential mediator of inflammatory and immune responses to infection, it is not surprising that viruses have evolved strategies to interact with and hijack HMGB1. The influenza virus nucleoprotein (NP) interacts with HMGB1 during infection, which enhances viral transcription and replication[137]. The borna disease virus phosphoprotein also

interacts with the A-box of HMGB1 to repress HMGB1's interaction with and stimulation of p53 mediated transcription[138]. HMGB1 was a strong hit in a CRISPR screen of cells infected with SARS-Cov-2, and was shown to regulate expression of ACE2, the primary receptor for SARS-CoV-1 and 2 binding and entry[139].

Adenovirus protein VII interacts with HMGB1 and retains it on chromatin during infection, preventing it from being released to act as an alarmin[82]. Furthermore, this retention of HMGB1 aids in protein VII's ability to block cell cycle progression[94]. The mechanism of how protein VII interacts with HMGB1 and what effect this has on transcription will be addressed in Chapter 2 of this thesis.

Chapter 2: Adenovirus Protein VII binds A-box of HMGB1 to repress interferon responses*

Abstract

HMGB1 is an abundant host nuclear protein that can also be released from infected cells as an alarmin to amplify inflammatory responses. Protein VII binds and sequesters HMGB1 in chromatin and prevents its release, thus inhibiting downstream inflammatory signaling. However, the consequences of this chromatin sequestration on host transcription are unknown. In this chapter, I demonstrate the mechanism of how protein VII directly binds HMGB1, what domain it binds to, the role that HMGB1's interaction with DNA has on this interaction, and the role that PTMs on protein VII have on this interaction. Lastly, I demonstrate that protein VII inhibits expression of interferon β, in an HMGB1-dependent manner, but does not affect transcription of downstream interferon-stimulated genes. Together, our results demonstrate that protein VII specifically harnesses HMGB1 through its A-box domain to depress the innate immune response and promote infection.

Introduction

Nuclear-replicating viruses interact with and hijack host chromatin to promote viral replication, evade the immune system, and create viral progeny. Adenovirus is a double-stranded DNA virus that manipulates the nuclear environment and host chromatin to promote a productive infection [6,140]. Adenoviruses encode an essential core viral protein, known as protein VII, that packages with the viral genome inside virions [35,36,141]. Protein VII is initially translated as a precursor protein, pre or pVII, which is cleaved by a viral protease to remove the N-terminal 24 amino acids and produce the packaged mature protein VII [40,56,142], herein referred to as

*Work in this chapter is adapted from, Arnold EA, Kaai RJ, Leung K, Brinkley MR, Kelnhofer-Millevolte LE, Guo MS, et al. (2023) Adenovirus protein VII binds the A-box of HMGB1 to repress interferon responses. PLoS Pathog 19(9): e1011633.

protein VII. Protein VII is delivered with the viral genome into the nucleus and is released upon initiation of viral transcription[66,67,70]. Late during infection, high levels of protein VII are produced, the majority of which localize to and distort host chromatin[82]. Protein VII is also post-translationally modified at five sites (K2-acetyl, K24-acetyl, T32-phospho, T50-phospho, S159-phospho) that are responsible for localization of protein VII to host chromatin[82,91]. When all five are mutated to alanine, abrogating modification, protein VII localizes to the nucleolus instead of chromatin[82]. Virus lacking protein VII can be generated, but these virions cannot establish infection and are markedly less stable, indicating that protein VII is dispensable for virion formation but not infection[33,79,143].

During infection, protein VII interacts with and sequesters in chromatin the host alarmin high mobility group box 1 (HMGB1)[82,94]. HMGB1 is a multifunctional protein that acts both extracellularly as an alarmin and within the cell as a transcription co-factor[144]. In the nucleus, HMGB1 is one of the most abundant proteins that transiently binds to DNA in a non-sequence specific manner, subsequently inducing DNA bending[95,96]. HMGB1 consists of three domains, an A-box and B-box that function to bind DNA[97], and a highly charged acidic C-terminal tail. The A-box and B-box domains have bulky hydrophobic residues that insert into the minor groove of DNA, as well as basic residues that bind the phosphodiester backbone, allowing HMGB1 to bend DNA to extreme angles[145]. The C-terminal tail, a 30 amino acid stretch of glutamic and aspartic acid residues, interacts with the A- and B-box domains to regulate their binding to DNA or other proteins[101,102,146,147].

Upon cellular stress, HMGB1 is shuttled from the nucleus to the cytoplasm and is rapidly released from the cell[86]. HMGB1 is therefore considered a typical damage-associated molecular pattern, or DAMP, that induces migration of immune cells and pro-inflammatory cytokines [148]. Extracellular HMGB1 has two characterized cellular receptors, the receptor for advanced glycation endproducts (RAGE) and toll like receptor 4 (TLR4) and is predicted to bind several

other host cell receptors as well [112,131,149,150]. Interestingly, HMGB1 has also been characterized as a nucleic acid sensor in the cytoplasm where it facilitates innate immune proteins like cyclic GMP–AMP synthase (cGAS) to recognize pathogen-associated molecular patterns (PAMPs), including exogenous RNAs and DNAs[135,136]. The downstream outcome of these pathways is expression of type-I interferons (IFNs), which are released in turn and lead to the expression of numerous interferon-stimulated genes (ISGs) that have multiple antiviral functions[151–154]. While HMGB1 functions to stimulate and amplify inflammatory responses, it is unknown whether HMGB1's activity as a transcriptional co-factor may also directly impact the transcription of interferon or ISGs. Thus, protein VII preventing HMGB1 release may have multipronged effects on immune responses.

In this study, we demonstrate the mechanism of the protein VII-HMGB1 interaction and the consequence to transcription of immune response genes on the host genome. We show that adenovirus protein VII directly interacts with the A-box of HMGB1, causing HMGB1 to become insoluble and unable to be released from the cell. We further show that the protein VII-HMGB1 interaction is not dependent on HMGB1's association with DNA, nor is it dependent on post translational modifications (PTMs) on protein VII, although protein VII PTMs are required to render HMGB1 insoluble. Finally, we demonstrate that protein VII represses the immune response to infection by dampening transcription of interferon beta (IFNβ) in an HMGB1-dependent manner. This study is the first to demonstrate the mechanism of protein VII hijacking of HMGB1, thereby uncovering a key aspect of immune evasion by adenoviruses.

Results

Protein VII directly interacts with HMGB1 by bacterial two-hybrid analysis.

To identify which domains of HMGB1 mediate physical interaction with protein VII, we performed a bacterial two-hybrid analysis (B2H) based on the reconstitution of the split *Bordetella pertussis* adenylate cyclase (*Of note: B2H assays were performed by K. Leung in Monica Guo's lab, and not by the author of this thesis*)[155]. Briefly, "bait" and "prey" proteins were fused to either the T18 or T25 fragment of adenylate cyclase and co-expressed in *Escherichia coli* (Fig 2.1A). Protein-protein interaction between bait and prey reconstitutes adenylate cyclase, drives synthesis of cyclic-AMP, and leads to a red colony coloring on MacConkey agar

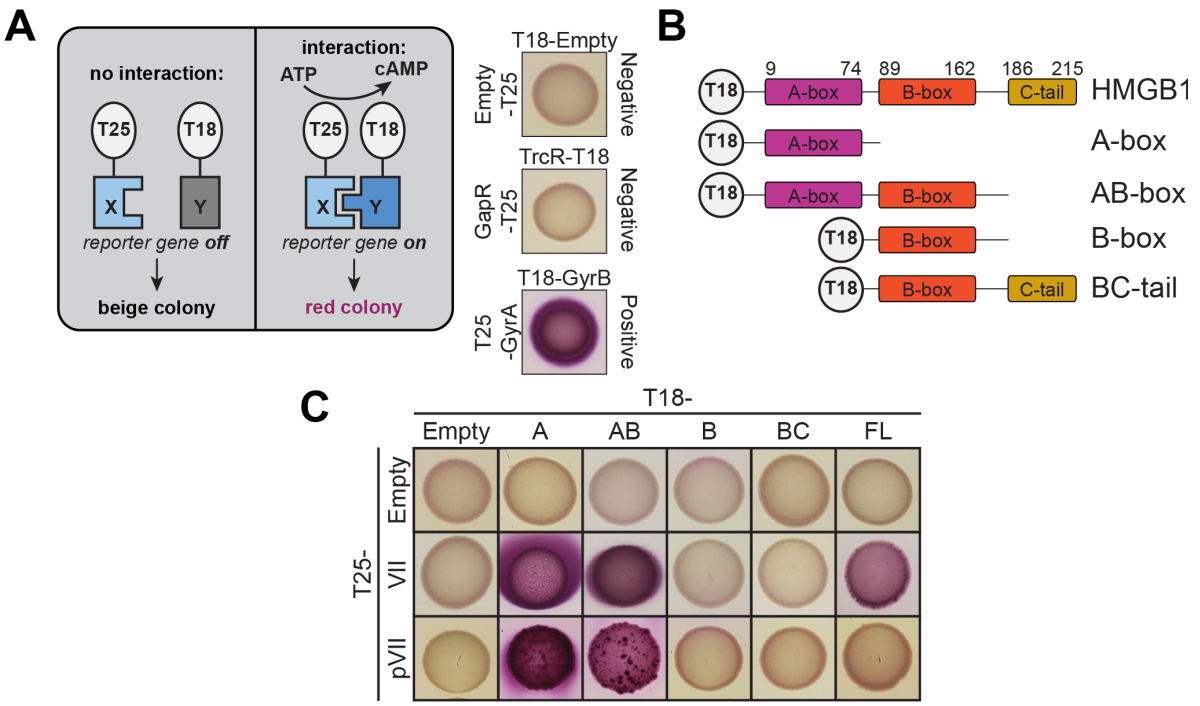

Figure 2.1: Protein VII directly binds HMGB1. A) *Left:* Schematic of the bacterial two-hybrid (B2H) assay. *Right:* Empty vectors or no interaction between the bait and prey proteins results in beige colony (top and middle) while a direct interaction results in pink colony (bottom). **B)** Diagram of different HMGB1 constructs used for B2H assay. **C)** B2H results of interactions between HMGB1 constructs as indicated above with N-terminal T18. Protein VII constructs are indicated with N-terminal T25. Protein VII strongly binds A-box containing constructs of HMGB1 while pVII only binds A-box and AB-box constructs. **Performed by K. Leung.*

plates (Fig 2.1A). This B2H system has previously been employed to quantitatively interrogate protein-protein interaction of various bacterial, fungal, and mammalian proteins[155–158]. We first sought to replicate our previous finding that protein VII interacts with HMGB1[82] using C-terminal fusions of protein VII and HMGB1 to T25 and T18, respectively (T25-protein VII and T18-HMGB1, Fig 1B). We found that T25-protein VII and T18-HMGB1 directly interact (Fig 2.1C), validating our B2H assay system.

There are three domains of HMGB1: the DNA binding A-box (amino acids 9-79) and B-box (amino acids 89-162), and the acidic C-terminal tail (amino acids 186-215) (Fig 2.1B). To determine the domain(s) responsible for binding protein VII, we generated several constructs of HMGB1 as follows: only the A-box, the A- and B-boxes together, only the B-box, and the B-box together with the C-terminal tail alone (abbreviated as shown in Fig 2.1B). We found that loss of the A-box completely abrogated HMGB1 interaction with protein VII, while loss of the C-terminal tail increased interaction (Fig 2.1C). Next, we asked if either the A-box or B-box was sufficient for protein VII binding and found that protein VII interacted with the A-box and did not interact with the B-box (Figs 2.1C, 2.2A). As a control, we repeated the B2H assay with all other possible orientations of protein VII with HMGB1, truncation mutants of the A-box, and A-box alone (Fig 2.2, see S2.1 Table). Although interaction between full-length HMGB1 and protein VII was not observed in any of these alternative orientations, we captured a strong interaction between protein VII and the HMGB1 A-box in all but one orientation tested (2.2B Fig, see Table 2.12). Together these data indicate that protein VII directly binds to the HMGB1 A-box.

Protein VII is synthesized as a precursor form (pVII) with the precursor portion subsequently cleaved during the late stages of infection during virion maturation[40,56,142]. We assayed binding of pVII to HMGB1 and discovered that pVII did not interact with full-length HMGB1 due to inhibition from the C-terminal tail, as pVII was able to interact with the A-box and with the AB-box lacking this inhibitory tail (Fig 2.1C, bottom row).

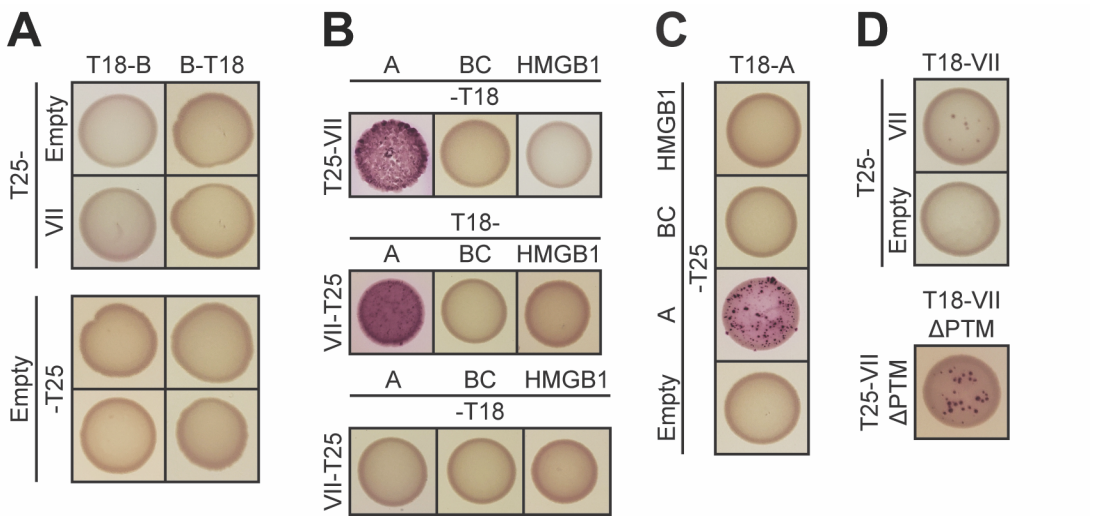

Figure 2.2: A-box of HMGB1 and protein VIIΔPTM weakly self-interact. A) B2H assay of HMGB1 B-box in different orientations with protein VII. **B)** B2H assay between protein VII and indicated HMGB1 variants in three additional orientations. **C)** B2H assay of HMGB1 A-box with indicated HMGB1 variants showing self-interaction in one instance. **D)** B2H assay of protein VII N-terminal T25- and N-terminal T18-fusions (top) and an assay of protein VII mutants with alanine substitutions to PTM sites (VIIΔPTM) N-terminal T25- and N-terminal T18-fusions (bottom). Both assays show modest self-association. For results of interactions and controls in additional orientations, see Table 2.12 at end of results section.

Lastly, we tested the ability of HMGB1 and protein VII to self-dimerize. Human HMGB1 dimerizes in the presence of reactive oxygen species[159,160], and other HMGB1 homologs, such as human mitochondrial transcription factor A (mtTFA) and HMGa from maize, also form dimers[161,162]. Similarly, protein VII is found as a multimer when packaged with viral genomes, though the stoichiometry of these multimers is unknown[36,63]. We found that full-length HMGB1 did not self-interact, but the A-box did dimerize if C-terminally tagged A-box was paired with N-terminally tagged A-box (T18-Abox with Abox-T25, Fig 2.2C, see Table 2.12, end of results section). These results suggest that HMGB1 dimerization may only occur when A-boxes are properly oriented and that steric effects or other interactions from the B-box and C-terminal tail may inhibit dimerization. We additionally found that protein VII self-association is extremely weak but is enhanced when the sites of post-translational modification are altered (VIIΔPTM,

see Fig 2.5) (Fig 2.2D, see Table 2.12), suggesting that the PTM residues may be integral to protein VII self-interaction.

HMGB1 is co-localized with protein VII during adenovirus infection.

Given the direct interaction between protein VII and HMGB1, we next hypothesized that protein VII binds specifically to the A-box of HMGB1 within the nucleus during infection. To test our hypothesis, we generated cell lines expressing different constructs of HMGB1 with a GFP tag and visualized localization in the presence or absence of adenovirus infection (Figs 2.3A and Fig 2.4). Given that HMGB1 and its homologs can self-associate[159–162] and our findings above show that HMGB1 can self-dimerize through the A-box, we used A549 cells devoid of endogenous HMGB1 through CRISPR-Cas9 knock-out[91] and introduced our constructs into this null background. Thus, we were able to interrogate protein VII's interaction with our HMGB1 constructs without the complication of dimerization with endogenous HMGB1. We first validated that all cell lines expressed HMGB1 constructs to comparable levels both with each other and endogenous HMGB1 by western blot (Fig 2.3B). We then visualized the localization pattern of the HMGB1 constructs by immunofluorescence microscopy and found that the A-box, B-box, and BC-tail were diffusely nuclear while the AB-box was somewhat nucleolar (Fig 2.3C, mock). Of note, the A-box, while mostly nuclear, had an observable cytoplasmic signal. This is likely due to lack of the second reported NLS site on HMGB1 in this construct (residues 179-185)[104]. Upon infection with human adenovirus type 5 (Ad5), we observed that the HMGB1 constructs had three different localization patterns: a diffusely nuclear pattern similar to that of mock infection (Fig 2.3C, triangle), a ring-like pattern, referred to as pattern I (Fig 2.3C, circle), or a punctate pattern, referred to as pattern II (Fig 2.3C, star). We quantified the different patterns seen during infection for each cell line and plotted the frequency of the pattern as a percentage (Fig 2.3D). We observed that all constructs containing an A-box had noticeable shift away from

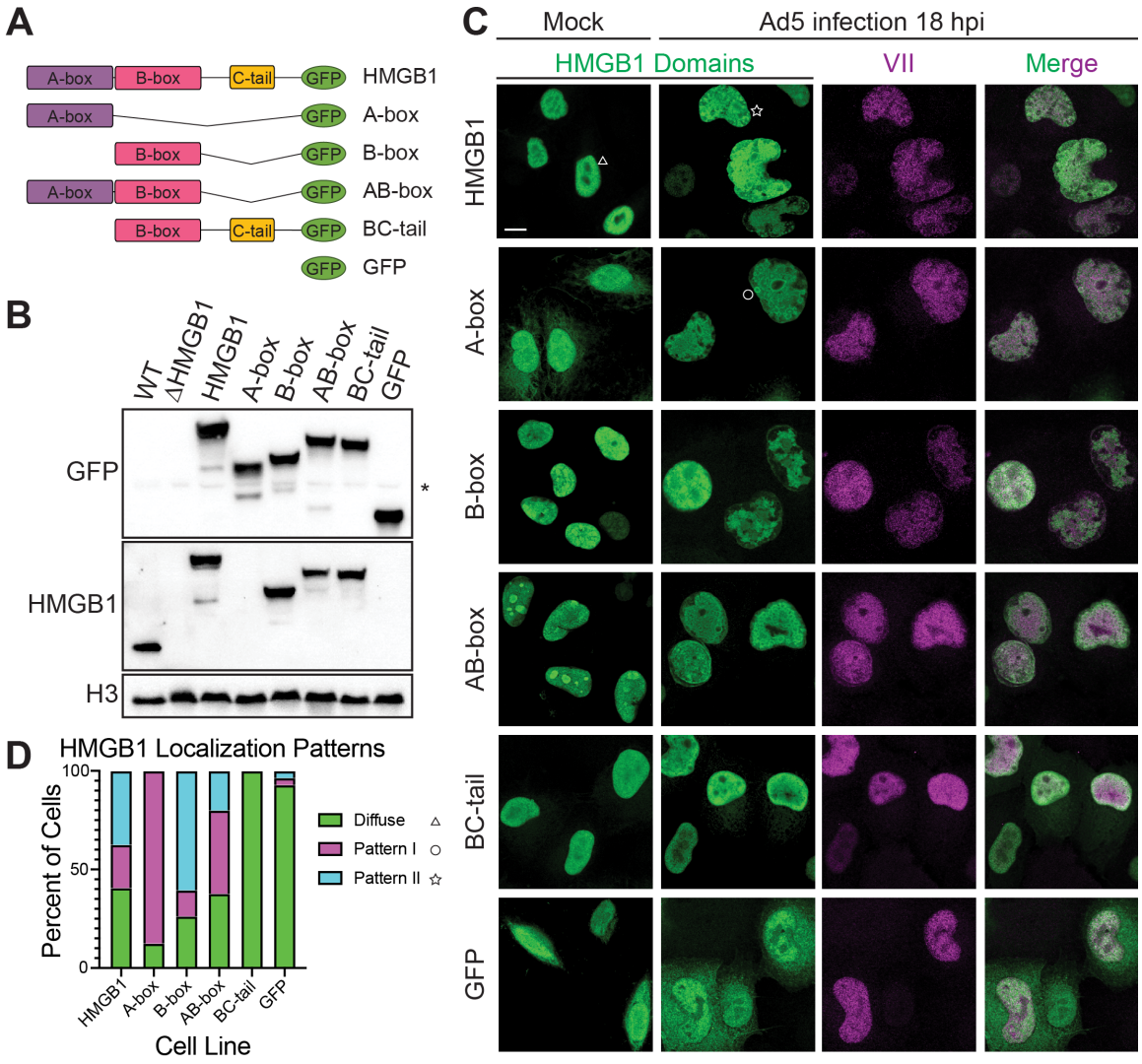

Figure 2.3: Protein VII mislocalizes A-box containing constructs of HMGB1 during infection. **A)** Schematic of HMGB1 constructs expressed in HMGB1-deleted A549 cells. **B)** Representative western blot showing expression from cell lines generated as in (A) indicating similar expression levels to endogenous HMGB1. *Top:* GFP, *middle:* HMGB1, *bottom:* H3 loading control. *Note:* HMGB1 antibody binds the B-box, thus no signal is detected for A-box cell line, * denotes non-specific band. **C)**Immunofluorescence images of cell lines as in (A) showing HMGB1 domains in green and protein VII in magenta. Left column is mock-infected cells showing HMGB1 construct distribution and right three columns are Ad5 infected, MOI of 10, at 18 hours post infection (hpi). Scale bar is 10 μm. **D)** Table summarizing localization changes of HMGB1 constructs during infection as presented in (C). Frequency of HMGB1 localization patterns observed for each cell line depicted as percentage of total cells. N>20 cells for each cell line.

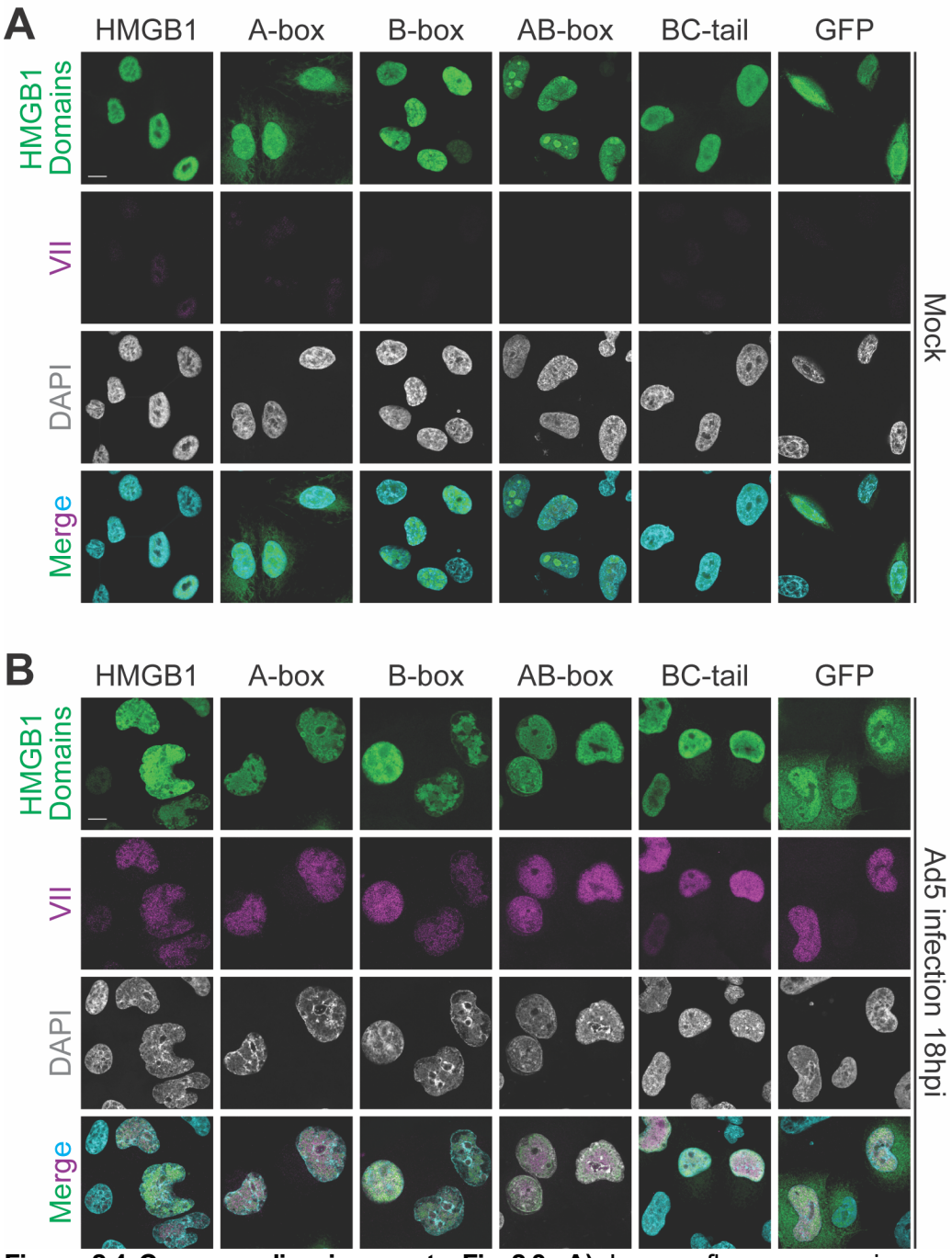

Figure 2.4 Corresponding images to Fig 2.3. A) Immunofluorescence images showing all channels of mock infected cells from Fig 2.3C with HMGB1 in green, protein VII in magenta, and DAPI in gray (cyan in merge). Scale bar is 10 μm. **B)** Immunofluorescence images of Ad5 infected cells showing all channels from Fig 2.3C with HMGB1 in green, protein VII in magenta, and DAPI in gray (cyan in merge). Scale bar is 10 μm.

diffuse to patterns I and II. Full length HMGB1 had an even distribution of all three patterns whereas the A-box and AB-box constructs both favored pattern I. Interestingly, the B-box construct also had a observable shift from diffuse to pattern II. Both the BC-tail and GFP cells remained diffusely nuclear, suggesting that these constructs are not being mislocalized during infection.

To investigate whether the changes in pattern are due to differences in binding chromatin, we extracted soluble proteins prior to fixation (termed pre-extraction) and then visualized the patterns by immunofluorescence microscopy as above. Furthermore, we used a virus with HA-tagged protein VII (Ad5 VII-HA) to allow for better resolution of protein VII with a commercial antibody and focused on constructs with or without the A-box. When we infected our HMGB1, AB-box, and BC-tail cells with Ad5 VII-HA and fixed the cells under the previously used conditions, as expected we observed similar patterns to our Ad5 WT virus (compare Fig 2.C with Fig 2.5A). When we pre-extracted mock infected cells, soluble HMGB1 leaked out of the nuclei in all conditions such that HMGB1 is no longer visible upon imaging (Fig 2.5B). Imaging Ad5 VII-HA infected cells after pre-extraction revealed full-length HMGB1 and the AB-box construct remained nuclear, and the signal fully overlapped with that of protein VII (Fig 2.5B). In contrast, the BC-tail construct was extracted along with other soluble proteins, resulting in little to no signal upon imaging (Fig 2.5B). We quantified these localization patterns (Fig 2.5C and 2.5D) and conclude that the A-box is required for protein VII to render HMGB1 bound to the chromatin during infection.

Protein VII is sufficient to render HMGB1 insoluble.

The release of HMGB1 from cells is a key step in inflammatory signaling. Therefore, we hypothesized that protein VII may prevent HMGB1 release by immobilization in chromatin through direct interaction. Because HMGB1 release is critical for extracellular signaling, we

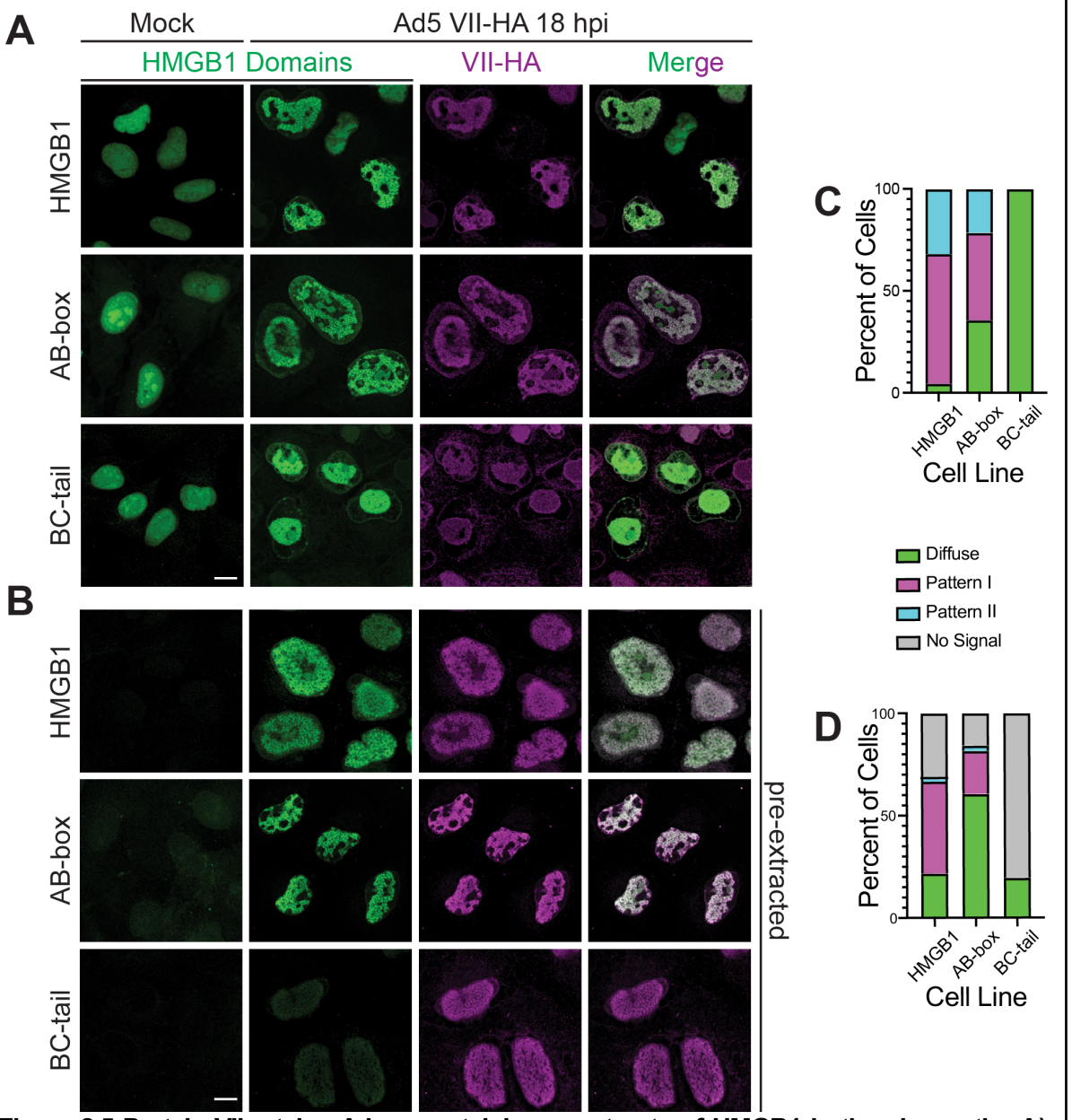

Figure 2.5 Protein VII retains A-box containing constructs of HMGB1 in the chromatin. A) Immunofluorescence images of HMGB1, AB-box and BC-tail cell lines, showing HMGB1 domains in green and protein VII in magenta. Left column is mock-infected cells showing HMGB1 construct distribution and right three columns are Ad5 VII-HA infected, MOI of 10, at 18 hours post infection (hpi). Scale bar is 10 μm. **B)** Same as in (A), but cells were pre-extracted before fixation, staining, and imaging. **C)** Frequency of HMGB1 localization patterns observed for each cell line depicted as percentage of total cells during Ad5 VII-HA infection. Total N>30. **D)** Same as in C, but cells were under pre-extraction conditions. N>30 for each cell line.

chose to use cellular fractionation to measure HMGB1 solubility as a proxy for HMGB1 release. We used simple fractionation by mild detergent to separate cells (termed whole cell lysate or WCL) into either soluble or insoluble fractions (Fig 2.6A). Soluble nuclear and cytoplasmic

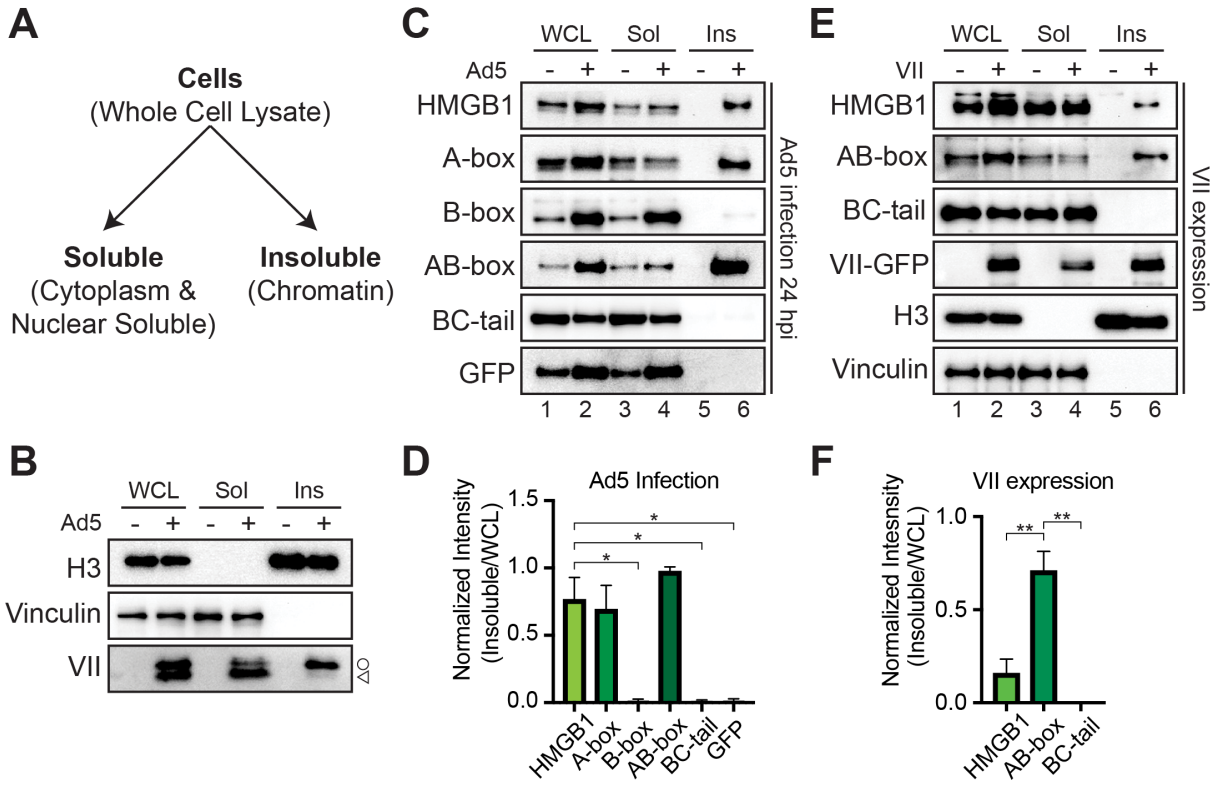

Figure 2.6: Protein VII causes A-box containing constructs of HMGB1 to be insoluble. A) Schematic of fractionation assay. **B)** Western blot of fractionated cells showing representative blots of three biological replicates. Whole cell lysate (WCL) in left two lanes, soluble (Sol) fraction in middle two lanes, and insoluble (Ins) fraction in right two lanes with or without Ad5 infections as indicated by +. H3 indicates insoluble chromatin while vinculin is cytoplasmic and soluble. ○ denotes pVII and ◁ is mature protein VII. **C)** Representative western blots of fractionated Ad5 infected cells at 24 hpi of cell lines as indicated showing predominantly A-box containing constructs of HMGB1 are rendered insoluble during infection. Lanes are numbered 1-6. 1: WCL mock, 2: WCL infected, 3: soluble mock, 4: soluble infected, 5: insoluble mock, 6: insoluble infected. **D)** Densitometry of western blots in (C) of HMGB1 in the insoluble fraction of infected cells normalized to HMGB1 in the WCL fraction. Error bar represents SD of three biological replicates, * is $p<0.05$ by Welch's t-test. **E)** Representative western blots upon ectopic protein VII expression of cell lines as indicated showing that protein VII is sufficient to render A-box containing constructs insoluble. Lanes numbered 1-6, same as (C) with expression of protein VII instead of infection. **F)** Same as (D) for western blots from (E). Error bar represents SD of three biological replicates, ** is $p<0.01$ by Welch's t-test.

proteins are found in the soluble fraction (termed Sol), while insoluble proteins, made up of chromatin-bound proteins and histones, are found in the insoluble fraction (termed Ins) (Fig 2.6B). We used this method to assay the solubility of several proteins during infection and found vinculin, a large cytoskeletal protein, to be soluble, histone H3 to be insoluble, and protein VII in both soluble and insoluble fractions (Figs 2.6 and 2.7), consistent with previous findings[82,163]. Interestingly, we were able to resolve the two bands of protein VII and pVII and found that pVII is predominantly insoluble while the mature form is more soluble, suggesting a separation of properties that may be indicative of function. We next investigated the solubility of GFP-tagged

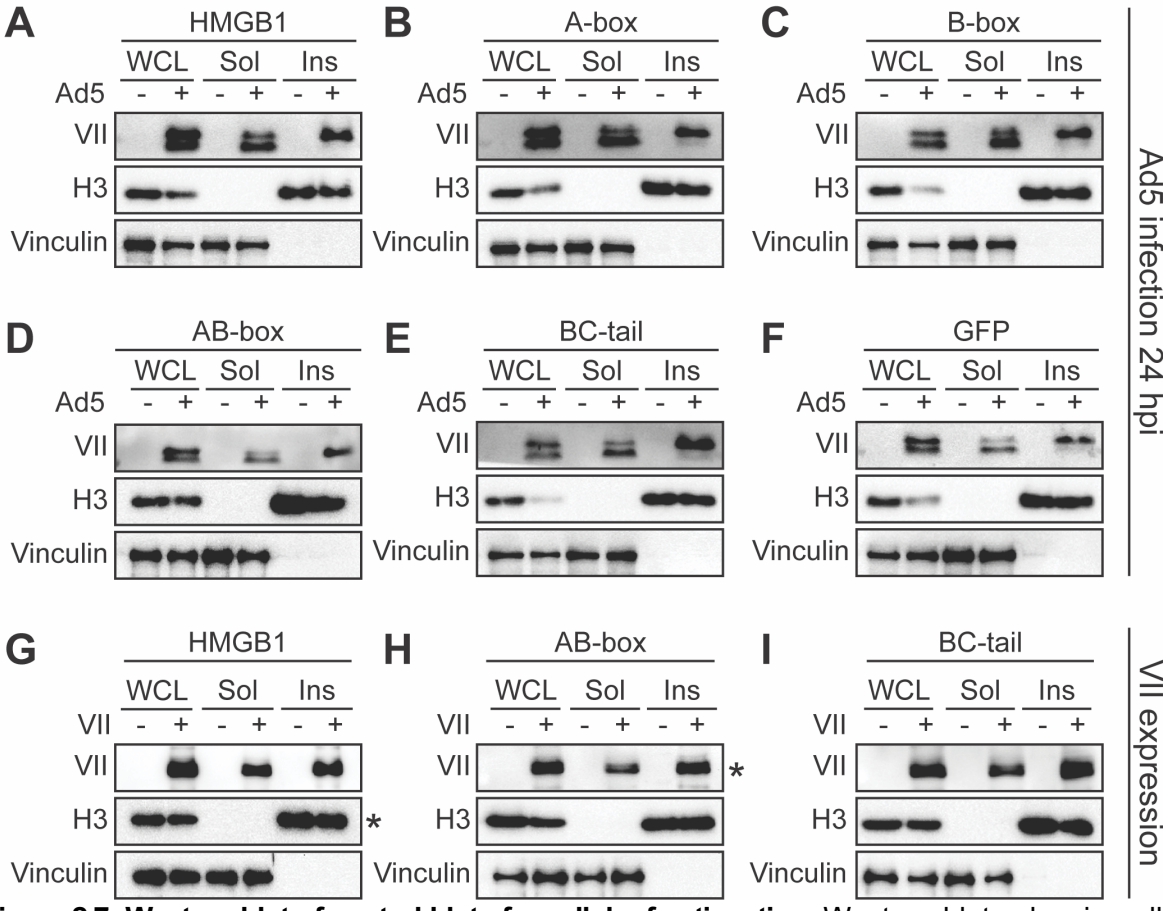

Figure 2.7: Western blot of control blots for cellular fractionation. Western blots showing all controls that correspond with Fig 2.6C for protein VII, H3, GFP, and vinculin: HMGB1 **(A)**, A-box **(B)**, B-box **(C)**, AB-box **(D)**, BC-tail **(E)**, and GFP **(F)**. Western blots showing all controls that correspond with Fig 2.6E for protein VII, H3, GFP, and vinculin; HMGB1 **(G)**, AB-box **(H)**, and BC-tail **(I)**.

HMGB1 constructs from the cell lines described above using this fractionation assay. We found that in the absence of infection, all HMGB1 constructs are soluble (Fig 2.6C, compare lanes 3 and 5). In contrast, during infection we find that full length HMGB1, A-box only, and AB-box, that is constructs containing the A-box, are insoluble whereas the B-box alone and BC-tail constructs are soluble (Fig 2.6C, lane 6). There is a slight band present for the B-box alone in the insoluble fraction during infection, suggesting that there may be weak retention of the B-box in chromatin. When the C-terminal tail is added to the B-box, there is no observable signal in the insoluble fraction. Because all HMGB1 constructs have the same GFP tag, we were able to directly compare the levels in the insoluble fraction by densitometry of the western blots normalized to the infected WCL. We found that there is significantly more HMGB1 retained in the insoluble fraction of the full length, A-box, and AB-box cells compared to the negative GFP control (Fig 2.6D). Importantly, we examined viral protein levels in our cell lines and observed that they were unaffected by the various HMGB1 constructs (Fig 2.8), suggesting that the impact of the protein VII-HMGB1 interaction is likely beyond a single infected cell. This notion is consistent with insolubility as a proxy for HMGB1 release affecting systemic inflammatory responses to infection.

To determine whether protein VII was sufficient for the change in solubility of the HMGB1 constructs, we expressed protein VII alone and investigated HMGB1 solubility. To do this, we transduced cells with an E1-deleted replication incompetent recombinant adenovirus (rAd) that expresses only protein VII-GFP and assayed for solubility. We found that indeed protein VII is sufficient to render HMGB1 insoluble, consistent with previous reports [82]. Further, we found that only A-box containing constructs were rendered insoluble by protein VII (Fig 2.6E), consistent with our findings above that protein VII directly interacts with the A-box. Interestingly, the retention of full length HMGB1 in the insoluble fraction is much weaker than that of the AB-box, further supporting the idea that the C-terminal tail may inhibit the interaction

between protein VII and the A-box. Consistent with this interpretation, our densitometry analysis confirmed that there was significantly more insoluble AB-box than HMGB1 or BC-tail (Fig 2.6F). Taken together, these results indicate that during infection protein VII binds the A-box of HMGB1, rendering it insoluble and sequestered in chromatin.

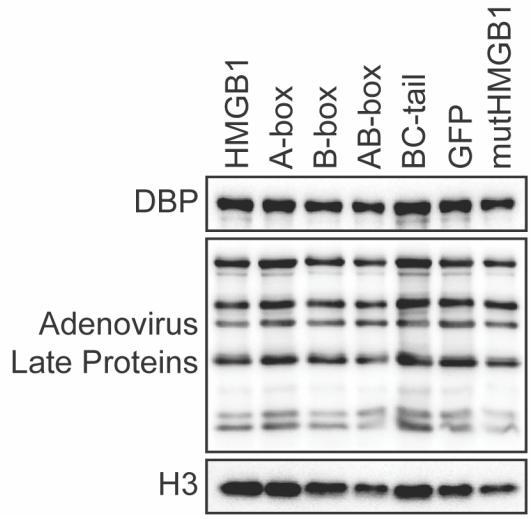

Figure 2.8: HAdV-5 infection produces similar amounts of viral protein in different HMGB1 cell lines. Western blot of DBP (early viral protein), adenoviral late proteins, and H3 loading control of infected WCL samples of cell lines from Fig 2.6C showing similar amounts of viral protein accumulation during infection of each cell line.

Protein VII interacts with, mislocalizes, and sequesters HMGB1 in chromatin independent of HMGB1's interaction with DNA.

Since HMGB1 can directly bind DNA[99], we next asked whether the interaction between protein VII and HMGB1 is dependent on this DNA binding. To test this, we changed the three hydrophobic residues in HMGB1 that are responsible for the DNA interaction to alanine: F38A, F103A and I122A (mutHMGB1, Fig 2.9A), and investigated the protein VII interaction by B2H assay. F38 is found in the A-box while F103 and I122 are in the B-box (Fig 2.9A). We tested protein VII interaction with mutated HMGB1 in the A-box only, the AB-box and full-length HMGB1 (FL) and found that these mutations did not eliminate interaction with protein VII (Fig

2.9B). We note that although the protein VII with AB-box and FL B2H colonies are red, indicating a positive interaction, the colonies exhibit a speckled pattern (compare to A-box or to Fig 2.1C), indicating that there may be a decrease in interaction efficiency. To further exclude the possibility that our B2H assays captured an indirect, DNA-mediated interaction between HMGB1 and protein VII, we validated that two non-specific DNA-binding proteins do not interact in the B2H assay (Fig 2.1A). Therefore, we conclude that these mutations to HMGB1 do not abrogate binding to protein VII. We next investigated the interaction of mutHMGB1 with protein VII in human cells. We expressed mutHMGB1 in A549ΔHMGB1 cells and infected these cells with Ad5. We observed by immunofluorescence microscopy that mutHMGB1 localization closely resembled that of wild-type (WT) HMGB1: mutHMGB1 was disperse throughout the nucleus in the absence of infection and a mixture of patterns I and II upon Ad5 infection (Fig 2.9C, compare to Fig 2.3C). We also performed pre-extraction on Ad5 VII-HA infected mutHMGB1 cells, as in Fig 2.5 Much like WT HMGB1, during mock infection mutHMGB1 is not visible within the nucleus of pre-extracted cells but remains bound to the chromatin in infected cells (Fig 2.9C). These results closely recapitulate those of wild-type HMGB1 suggesting that these mutations do not impact protein VII's ability to bring HMGB1 into insoluble chromatin (Fig 2.9D-E). Thus, we conclude that protein VII mislocalizes HMGB1 independent of HMGB1 binding DNA.

Next, we examined the solubility of mutHMGB1 during Ad5 infection. We found that mutHMGB1 is strongly retained in the insoluble fraction upon Ad5 infection (Fig 2.9D, lane 6). When compared to FL HMGB1 by densitometry analysis, mutHMGB1 had slightly increased retention, although the difference was not statistically significant (Fig 2.9E). Taken together, these results indicate that protein VII interacts with, mislocalizes, and sequesters HMGB1 in chromatin independently of HMGB1 DNA binding.

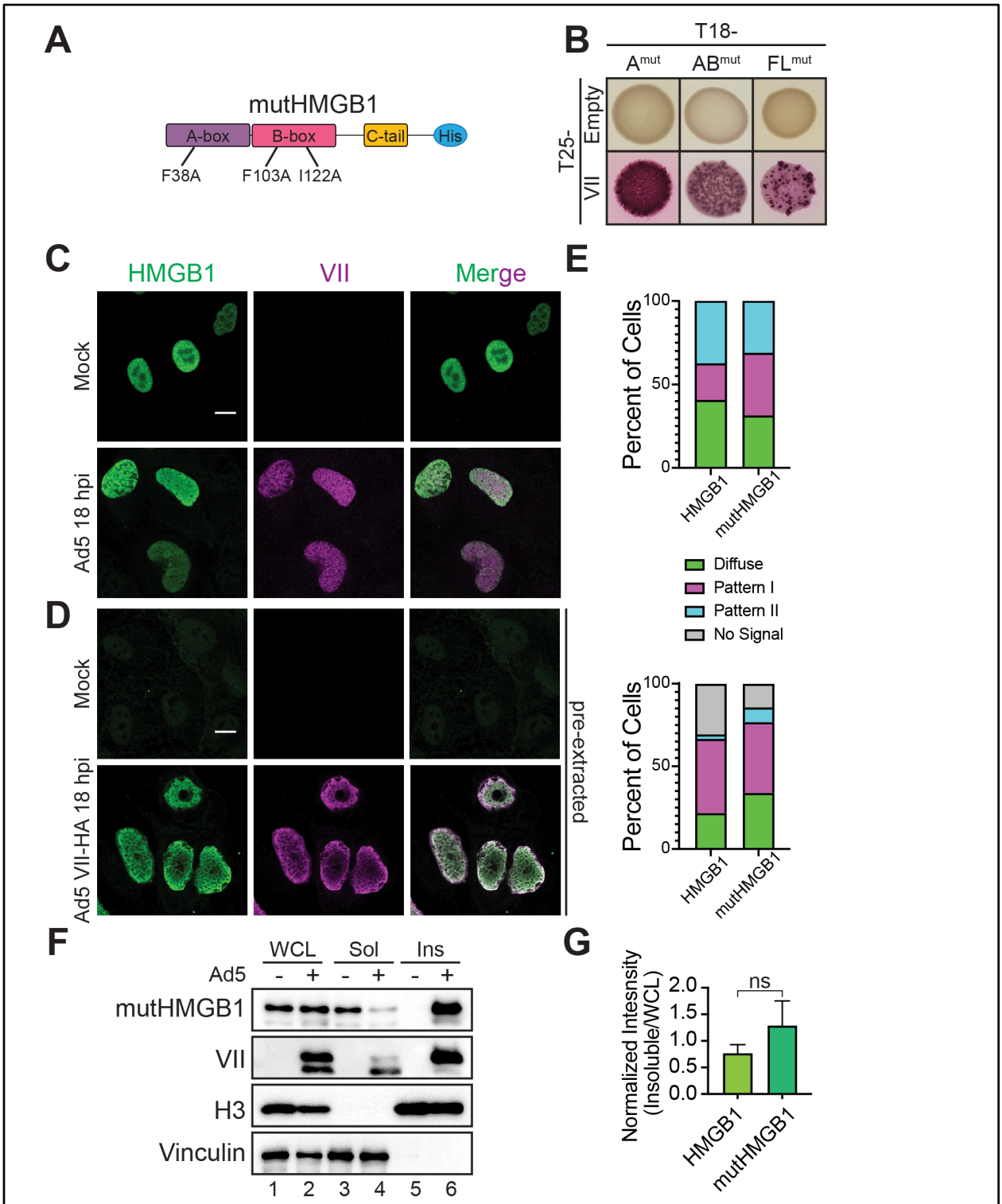

Figure 2.9: Protein VII's interaction with HMGB1 is not dependent on HMGB1's interaction with DNA. A) Schematic of mutHMGB1 expressed in A549ΔHMGB1 cells with point mutations as indicated. **B)** B2H results of interaction between protein VII and mutHMGB1 constructs as indicated. **Performed by K. Leung. C-G on next page.*

C) Immunofluorescence images of full length mutHMGB1 cells as in (A) showing HMGB1 in green and protein VII in magenta. Top row is mock infected showing mutHMGB1 distribution and bottom row is Ad5 infected, MOI of 10, at 18hpi. Scale bar is 10 μm. **D)** Same as in (C), but under pre-extraction conditions, and infection is with Ad5 VII-HA. Scale bar is 10 μm. **E)** Frequency of HMGB1 localization patterns observed for each cell line depicted as percentage of total cells during Ad5 infection for top graph. N>30 for each cell line. Bottom graph is same as top, but for Ad5 VII-HA infection and under pre-extraction conditions. N>30 for each cell line. **F)** Representative western blots of fractionated Ad5 infected mutHMGB1 cells at 24 hpi showing mutHMGB1 constructs are rendered insoluble in the presence of infection. Lanes as in Fig 3C. **G)** Densitometry of western blots as in (D) of mutHMGB1 in the insoluble fraction of infected cells normalized to HMGB1 in the WCL fraction. Wild type HMGB1 results from Fig 3E. Error bar represents SD of three biological replicates, * is $p<0.05$ by Welch's t-test.

Post-translational modifications on protein VII do not affect binding to HMGB1 but are important for sequestering HMGB1 in chromatin.

Protein VII contains five post-translational modifications (PTMs) that affect protein VII's localization in the nucleus[82]. When the PTMs on protein VII are present, protein VII localizes to the host chromatin. In contrast, when these sites are mutated to alanine, referred to as VIIΔPTM (Fig 2.10A), protein VII localizes to the nucleolus[82]. This change in localization is thought to facilitate protein VII distinguishing between the host and viral genomes during infection as the nucleolus is disrupted during late stages of infection, causing many nucleolar proteins to localize with viral replication centers[82,85]. Because these PTMs affect protein VII localization, we next asked how the PTMs on protein VII affect the interaction with HMGB1 and HMGB1 localization in the nucleus. We first examined the interaction by B2H and found that VIIΔPTM still interacted with the A-box alone and the AB-box construct, indicating that the interaction between protein VII and the A-box is not dependent on these sites. However, we found that VIIΔPTM no longer interacted with FL HMGB1 (Fig 2.10B), suggesting that the C-terminal tail fully inhibited the interaction in a bacterial context. Furthermore, B2H interactions between VIIΔPTM and A-box alone and the AB-construct led to weakly pink and speckled colonies, again indicating a

potential decrease in interaction compared to wild-type protein VII. This speckling pattern was also observed when we examined self-association of VIIΔPTM (Fig 2.2D). Although, protein VII self-association was extremely weak, VIIΔPTM exhibited a stronger interaction suggesting that these sites may be important for multimerization of protein VII. It is important to note that in bacteria, WT protein VII is unlikely to be modified as the enzymes responsible for modification would only be present in human cells, therefore, we conclude that these residues are likely important for protein VII multimerization.

We next examined the localization of HMGB1 in the presence of VIIΔPTM in human cells by visualizing endogenous HMGB1 in A549 cells that express HA-tagged VIIΔPTM from a doxycycline (dox) inducible promoter[82]. We observed that without dox, HMGB1 exhibited the characteristic disperse nuclear pattern (Fig 2.10C). In contrast, upon addition of dox and subsequent induction of protein VIIΔPTM expression, we found that HMGB1 adopted the same pattern as VIIΔPTM and was concentrated in the nucleolus. When pre-extracting the cells prior to fixation, we observed that although the pattern of VIIΔPTM is altered by pre-extraction itself, HMGB1 is strongly localized to the nucleolus when VIIΔPTM is present (Fig 2.10D). We quantified these patterns as disperse, nucleolar, or no signal (Fig 2.10E). When we plotted the frequency of these patterns, we found that approximately 50% of the cells have nucleolar HMGB1 when VIIΔPTM is present in either fixation condition. Taken together, these results indicate that VIIΔPTM binds endogenous HMGB1 and causes it to re-localize to the nucleolus. To investigate how the interaction with VIIΔPTM potentially impacts HMGB1 release, we assayed for solubility by fractionation. Without doxycycline treatment, thus in the absence of protein VII, we found that endogenous HMGB1 was completely soluble, recapitulating HMGB1 solubility in uninfected cells (Fig 2.10E, lane 3). Interestingly, expression of VIIΔPTM did not cause HMGB1 to become insoluble (Fig 2.10E, lane 6), unlike WT protein VII. The B2H and

microscopy results support a model in which VIIΔPTM binds HMGB1 and the two co-localize to the nucleolus, however, the VIIΔPTM-HMGB1 complex is soluble. This suggests that HMGB1

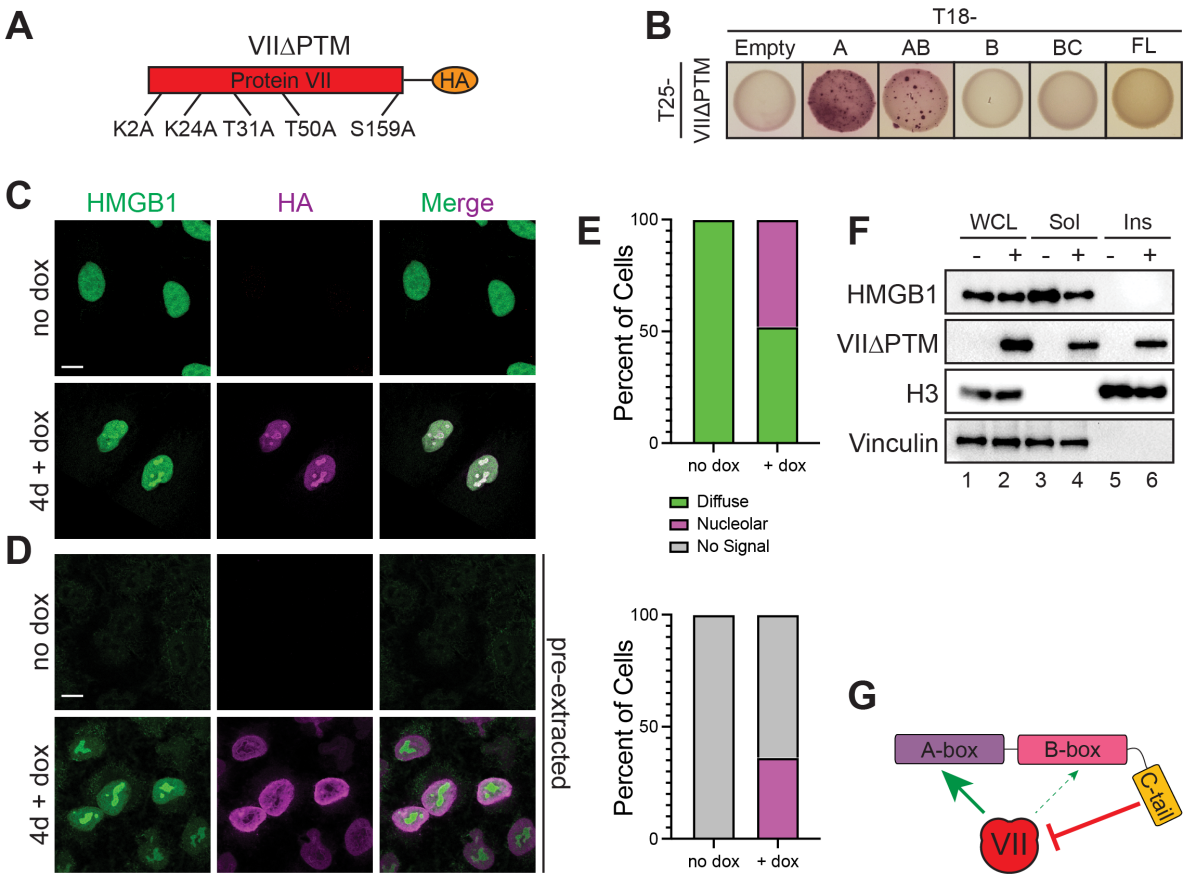

Figure 2.10: Post-translational modifications on protein VII are not required for HMGB1 binding but are important to render HMGB1 insoluble. A) Schematic of point mutations in VIIΔPTM expressed in A549 cells with doxycycline (dox) inducible promoter. **B)** B2H results of interaction between protein VIIΔPTM and HMGB1 constructs as depicted. *Performed by K. Leung.* **C)** Immunofluorescence images of A549 cells expressing dox inducible VIIΔPTM, as in (A), with endogenous HMGB1 in green and VIIΔPTM in magenta, showing predominant nucleolar localization of HMGB1 when VIIΔPTM is expressed. Top row is without dox and bottom row is with 4 days of dox treatment. Scale bar is 10 μm. **D)** Same as in (C) under pre-extraction conditions. Scale bar is 10 μm. **E)** Frequency of HMGB1 localization patterns observed for each no dox and + dox conditions, depicted as percentage of total cells for top graph. N>30 for each condition. Bottom graph is for pre-extraction conditions. N>30 for each condition. **F)** Representative western blots of three biological replicates depicting fractionation of A549 VIIΔPTM cells with and without dox addition. **G)** Schematic summarizing the interaction of protein VII and HMGB1. Protein VII primarily interacts with the A-box of HMGB1 with some impact on the B-box while the C-terminal tail inhibits the interaction.

may not be analogously sequestered in the chromatin. Taken together, these results indicate that while VIIΔPTM can bind the A-box of HMGB1 and mislocalize endogenous HMGB1 to the nucleolus, it cannot cause HMGB1 to be insoluble, suggesting that the PTMs of protein VII may be required to sequester HMGB1 in chromatin.

Protein VII inhibits interferon signaling by decreasing IFNβ1 expression.

Since protein VII immobilizes HMGB1 in chromatin and HMGB1 is implicated as a transcriptional co-factor[164–166], we hypothesized that protein VII may be harnessing this role of HMGB1 to promote immune evasion. Protein VII was originally described as a transcriptional repressor[75], therefore, we hypothesized that protein VII may hijack HMGB1 to repress the innate immune response. To investigate this hypothesis, we used A549 cells that express dox-inducible protein VII[82], similar to the cells used for VIIΔPTM in Fig 2.10. We induced expression of protein VII, and then treated the cells with interferon to induce the expression of downstream ISGs. We used quantitative PCR to measure the levels of ISGs in the presence or absence of dox and interferon. In the absence of protein VII, we found a robust, statistically significant increase in MX2 and ISG15, but not upstream NF-kB over the no treatment control (Fig 2.11A). When we expressed protein VII, we saw that ISG induction was equally robust and was not significantly different than the cells that were not expressing protein VII, suggesting that protein VII is not affecting the downstream effects of the type-I interferon response (Fig 2.11A).

Because protein VII strongly binds to chromatin and sequesters HMGB1[82], we hypothesized that any effect on immune responses may be upstream of ISGs, such as the expression of interferon itself. To test this, we expressed protein VII-GFP or a GFP control (as in Fig 2.6E) in wildtype (WT) A549 cells and A549ΔHMGB1 cells. We then treated these cells with poly(dA:dT) to mimic exogenous dsDNA and measured IFNβ mRNA levels by droplet-digital PCR (ddPCR) (Fig 2.11B). In this assay, we normalized IFNβ expression to 18S expression.

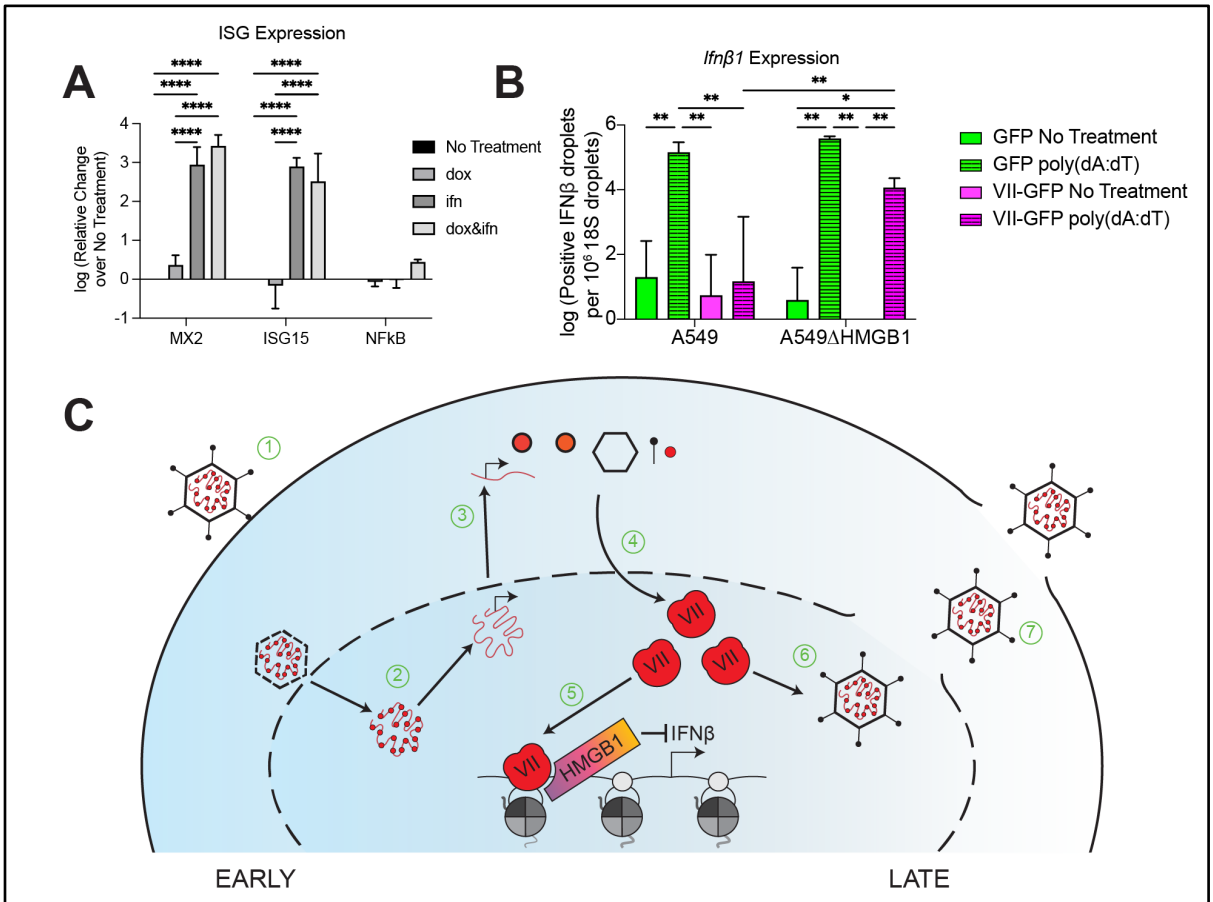

Figure 2.11: Protein VII inhibits expression of IFNβ1. A) Quantification MX2, ISG15 and NF-κB mRNA levels by RT-qPCR in A549 cells with dox inducible protein VII treated with or without human IFNβ as indicated. Error bar represents SD of three biological replicates. **** is $p<0.0001$ by 2-way ANOVA with Tukey multiple comparisons test. **B)** Quantification of IFNβ mRNA levels by ddPCR in A549 and A549ΔHMGB1 cells with or without protein VII as indicated, with or without poly(dA:dT) treatment as indicated. Error bar represents SD of three biological replicates. * is $p<0.05$, ** is $p<0.01$, by 2-way ANOVA with Tukey multiple comparisons test. **C)** Schematic detailing adenovirus infection with proposed mechanism of action by protein VII binding HMGB1 for inhibition of IFNβ. 1) Adenovirus enters into the cell and nucleus. 2) Protein VII is removed from the viral genome, histones take its place, and viral transcription begins. 3) Viral transcripts are translated in the cytoplasm. 4) Newly translated protein VII accumulates in the nucleus at later times during infection. 5) Protein VII binds HMGB1, sequesters it on host chromatin, where it inhibits transcription of Ifnβ, thus dampening the type-I interferon response. 6) Protein VII, without HMGB1, is packaged with progeny viral genomes. 7) Viral progeny are released through cell lysis.

Since 18S is highly expressed, we normalized IFNβ droplets to every 1 million 18S-positive droplets. In A549 WT cells without protein VII, we observed a robust increase in IFNβ expression upon stimulation with poly(dA:dT) compared to mock treated (Fig 2.11B). Upon expression of protein VII, we found a significant decrease in the levels of IFNβ compared to poly(dA:dT) treated cells without protein VII. The decrease of IFNβ induction resulting from protein VII expression was not significantly greater than untreated conditions. These findings strongly indicate that protein VII inhibits expression of IFNβ. In the absence of HMGB1 (A549ΔHMGB1 cells), we found a robust and significant increase in IFNβ expression upon stimulation with poly(dA:dT). When the A549ΔHMGB1 cells expressing VII-GFP were treated with poly(dA:dT), we still detected a decrease in IFNβ levels compared to the GFP control; however, it was less pronounced than in WT cells and was significantly higher than the untreated cells expressing VII-GFP. Furthermore, IFNβ expression was significantly higher in the poly(dA:dT) treated A549ΔHMGB1 cells expressing protein VII-GFP than in the poly(dA:dT) treated A549 WT cells expressing protein VII-GFP. Thus, we conclude that protein VII causes a significant reduction in IFNβ expression, and that this inhibition is promoted by the presence of HMGB1. Because the loss of HMGB1 did not fully rescue protein VII from dampening IFNβ induction to baseline levels, we predict that other factors such as HMGB2 may also support protein VII's repressive function. Taken together, these results indicate that protein VII binds the A-box of HMGB1 to inhibit interferon signaling by decreasing the expression of IFNβ.

GENOTYPE	PHENOTYPE
pUT18C pKT25	-
pUT18C-GyrB pKT25-GyrA	+++
pUT18-TrcR pKNT25-GapR	-
pUT18C-HMGB1(Abox) pKT25	-
pUT18C-HMGB1 (AB) pKT25	-
pUT18C-HMGB1 (Bbox) pKT25	-
pUT18C-HMGB1 (BC) pKT25	-
pUT18C-HMGB1 pKT25	-
pUT18C pKT25-protein VII	-
pUT18C-HMGB1(Abox) pKT25-protein VII	++++
pUT18C-HMGB1 (AB) pKT25-protein VII	+++/++++
pUT18C-HMGB1 (Bbox) pKT25-protein VII	-
pUT18C-HMGB1 (BC) pKT25-protein VII	-
pUT18C-HMGB1 pKT25-protein VII	++
pUT18C-HMGB1(Abox DNA bending mutant) pKT25	-
pUT18C-HMGB1(AB DNA bending mutant) pKT25	-
pUT18C-HMGB1(DNA bending mutant) pKT25	-
pUT18C-HMGB1(Abox DNA bending mutant) pKT25-protein VII	+++
pUT18C-HMGB1(AB DNA bending mutant) pKT25-protein VII	++
pUT18C-HMGB1 (DNA bending mutant) pKT25-protein VII	++
pUT18C pKT25-VIIΔPTM	-
pUT18C-HMGB1(Abox) pKT25-VIIΔPTM	++
pUT18C-HMGB1 (AB) pKT25-VIIΔPTM	+
pUT18C-HMGB1 (Bbox) pKT25-VIIΔPTM	-
pUT18C-HMGB1 (BC) pKT25-VIIΔPTM	-
pUT18C-HMGB1 pKT25-VIIΔPTM	-
pUT18C pKT25-pVII	-
pUT18C-HMGB1(Abox) pKT25-pVII	+++
pUT18C-HMGB1 (AB) pKT25-pVII	++/+++
pUT18C-HMGB1 (Bbox) pKT25-pVII	-
pUT18C-HMGB1 (BC) pKT25-pVII	-
pUT18C-HMGB1 pKT25-pVII	-
pUT18 pKT25	-
pUT18-HMGB1 (Abox) pKT25	-
pUT18-HMGB1 (BC) pKT25	-
pUT18-HMGB1 pKT25	-
pUT18 pKT25-protein VII	-
pUT18-HMGB1 (Abox) pKT25-protein VII	++
pUT18-HMGB1 (BC) pKT25-protein VII	-
pUT18-HMGB1 pKT25-protein VII	-
pUT18 pKNT25	-

pUT18-HMGB1 (Abox) pKNT25	-
pUT18-HMGB1 (BC) pKNT25	-
pUT18-HMGB1 pKNT25	-
pUT18 pKNT25-protein VII	-
pUT18-HMGB1 (Abox) pKNT25-protein VII	++
pUT18-HMGB1 (BC) pKNT25-protein VII	-
pUT18-HMGB1 pKNT25-protein VII	-
pUT18C pKNT25	-
pUT18C-HMGB1 (Abox) pKNT25	-
pUT18C-HMGB1 (BC) pKNT25	-
pUT18C-HMGB1 pKNT25	-
pUT18C pKNT25-protein VII	-
pUT18C-HMGB1 (Abox) pKNT25-protein VII	-
pUT18C-HMGB1 (BC) pKNT25-protein VII	-
pUT18C-HMGB1 pKNT25-protein VII	-
pUT18C-protein VII pKT25	-
pUT18C-protein VII pKT25-protein VII	-/+
pUT18C-protein VII pKNT25	-
pUT18C-protein VII pKNT25-protein VII	-
pUT18-protein VII pKT25	-
pUT18-protein VII pKT25-protein VII	-
pUT18-protein VII pKNT25	-
pUT18-protein VII pKNT25-protein VII	-
pUT18C-protein VII pKNT25-HMGB1 (Abox)	++
pUT18C-protein VII pKNT25-HMGB1 (BC)	-
pUT18C-protein VII pKNT25-HMGB1	-
pUT18C-protein VII pKT25-HMGB1 (Abox)	+++
pUT18C-protein VII pKT25-HMGB1 (BC)	-
pUT18C-protein VII pKT25-HMGB1	++
pUT18C-HMGB1 (Abox) pKNT25-HMGB1 (Abox)	++
pUT18C-HMGB1 (Abox) pKNT25-HMGB1 (BC)	-
pUT18C-HMGB1 (Abox) pKNT25-HMGB1	-
pUT18C-HMGB1 (Abox) pKT25-HMGB1 (Abox)	-
pUT18C-HMGB1 (Abox) pKT25-HMGB1 (BC)	-
pUT18C-HMGB1 (Abox) pKT25-HMGB1	-
pUT18-HMGB1 (Abox) pKNT25-HMGB1 (Abox)	-
pUT18-HMGB1 (BC) pKNT25-HMGB1 (BC)	-
pUT18-HMGB1 pKNT25-HMGB1	-
pUT18C-HMGB1 (BC) pKNT25-HMGB1 (BC)	-
pUT18C-HMGB1 pKNT25-HMGB1	-
pUT18C-HMGB1 (AB) pKT25-HMGB1 (AB)	-
pUT18C-HMGB1 (Abox) pKT25-HMGB1 (Bbox)	-

pUT18C-HMGB1 (AB) pKT25-HMGB1 (Bbox)	-
pUT18C-HMGB1 (Bbox) pKT25-HMGB1 (Bbox)	-
pUT18C-HMGB1 (Abox DNA bending mutant) pKT25-HMGB1 (Abox DNA bending mutant)	-
pUT18C-HMGB1 (AB DNA bending mutant) pKT25-HMGB1 (AB DNA bending mutant)	-
pUT18C-HMGB1 (DNA bending mutant) pKT25- HMGB1 (DNA bending mutant)	-
pUT18C-VIIΔPTM pKT25-VIIΔPTM	+
pUT18C-pVII pKT25-pVII	-

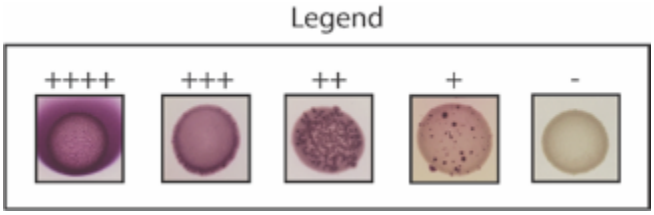

Table 2.12: List of tested protein VII and HMGB1 bacterial two-hybrid interactions. Each interaction was tested using four biological replicates. Legend with representative images for each phenotype is provided at the bottom. Positive interactions are indicated in green.

Discussion

Manipulation of the nuclear environment and the extracellular milieu is critical to the success of nuclear-replicating viruses such as adenovirus. Specifically, adenovirus protein VII prevents the release of HMGB1 and inhibits HMGB1-associated downstream inflammation[82,94]. We hypothesized that protein VII retains HMGB1 in the chromatin not only to prevent its activity as a DAMP, but also to affect transcription; in this case, by inhibiting interferon b expression. In this study, we leveraged bacterial and human culture systems to define the mechanism of protein VII binding to HMGB1 and the consequent effect on host responses.

In our B2H analysis, we demonstrated that both the protein VII precursor, pVII, and mature protein VII directly bind to the A-box or AB-box of HMGB1. In contrast, only mature protein VII binds full-length HMGB1 (Fig 2.1). The preference of mature protein VII over pVII for HMGB1 is intriguing, as it points to a potential mechanism of the first 24 amino acids in pVII inhibiting the interaction with HMGB1. Interestingly, we also noted by western blot that it was mostly pVII that was found in the insoluble fraction during infection when HMGB1 was also insoluble (Fig 2.6B), suggesting that in human cells, HMGB1 likely does interact with pVII. One possibility is that pVII is also post-translationally modified in the first 24 amino acids and that these modifications increase affinity for HMGB1. Indeed, we previously reported two modifications in the precursor fragment, S18 phosphorylation and K19 acetylation. These marks identified by mass spectrometry of pVII purified from infected cells may be important for mediating the HMGB1 interaction[82]. These observations indicate that the precursor fragment may be important for modulating the protein VII-HMGB1 interaction during infection.

At late times during infection, the nucleolus becomes disrupted, and nucleolar proteins co-localize with viral replication centers[85]. This is particularly significant in light of the observation that VIIΔPTM is localized to the nucleolus upon ectopic expression because the PTMs may promote distinguishing between viral or host genomes. Interestingly, these PTMs

were not identified in purified virus particles[82,83], suggesting that their presence may promote host chromatin binding, while their absence causes localization to the viral genomes and eventual packaging[82,94]. We observed that mutation of the PTM sites also promotes self-dimerization in the B2H assay. While these PTMs are not likely to occur in bacteria, it is possible that the amino acids changed provide a structural function for protein VII that has yet to be determined. Future structural studies will shed light on their relevance to binding DNA and other factors. Furthermore, virus particles without protein VII are less stable than wild type virions [33]. Thus, because protein VII forms a multimer when compacted with the viral genome inside of virus particles[63], it is possible that these sites promote protein VII multimerization and stabilizes the packaged viral genome.

We further demonstrated that point mutations affecting the DNA binding of HMGB1 did not abrogate the interaction of these two proteins (Fig 2.9). This does not rule out the potential importance of DNA in the interaction between protein VII and HMGB1, only that it is not required by HMGB1. Protein VII also has high affinity for DNA, but this is likewise not required for the protein VII-HMGB1 interaction as the two proteins bind strongly *in vitro* in the absence of any other factors [82]. In contrast, the C-terminal tail diminished HMGB1 affinity for protein VII in all contexts tested. This includes mature protein VII, pVII, and VIIΔPTM. We were unable to examine any interaction with the C-terminal tail alone as it is highly charged and unstable. Nevertheless, previous studies reported that the C-terminal tail negatively regulates the DNA binding capacity of the A- and B-boxes[101,167,168], consistent with our findings. The HMGB1 C-terminal tail also disrupts the interaction with protein VII, suggesting that the high charge and disordered nature of the C-terminal tail is disruptive to protein-protein or protein-DNA interactions. Interestingly, although HMGB1 is a highly conserved protein from yeast to humans, the yeast homolog, HMO1, does not contain an acidic C-terminus[114], suggesting that this feature evolved later as a means of modulating HMGB1 function.

We found a slight effect of protein VII on solubility and localization of the B-box alone during infection. We observed that there is some B-box in the insoluble fraction upon infection but becomes completely soluble upon addition of the C-terminal tail, similar to full-length HMGB1 in the absence of protein VII. Furthermore, the localization pattern of the B-box was altered during infection though it did not copy the pattern of the A-box containing proteins. Instead, the pattern more resembled that of endogenous HMGB1 upon infection with a protein VII-null virus [94]. This pattern was again completely lost upon addition of the C-terminal tail in the BC-tail construct. This suggests that (1) other viral proteins may affect HMGB1 during infection independently of protein VII and that (2) the presence of the C-terminal tail still diminishes this effect.

In our B2H system, several interactions between mutated protein VII or HMGB1 resulted in a speckled pattern compared to a more uniform pink with WT proteins (Figs 2.1, 2.2, 2.9, 2.10), suggesting a weaker interaction, although our B2H assay does not inform on kinetics. Finally, direct interaction was specific to certain orientations of HMGB1 and/or protein VII with the T18 and T25 subunits of adenylate cyclase, suggesting that the physical interaction is stereotyped in specific orientations. Future structural and kinetic studies will be needed to define the spatial dynamics of the protein VII-HMGB1 interaction. Together, these observations indicate that the interaction between protein VII and HMGB1 is robust but can be modulated by the C-terminal tail and post-translational modifications. Our data support a model in which VII interacts with the A-box, and very slightly with the B-box, while the C-terminal tail inhibits this interaction (Fig 2.10E). The process of HMGB1 release from the cell is heavily reliant on modification of HMGB1 and the oxidation state of its three cysteine residues[108]. HMGB1 within the nucleus is thought to be unmodified and in a reduced state. Upon stimulation for release, the NLS sites of HMGB1 become heavily acetylated, phosphorylated, or glycosylated, which promotes its translocation to the cytoplasm[86,169–171]. The release of HMGB1 from the cytoplasm

into the extracellular milieu occurs through secretory lysosomes or autophagosomes and is cell-type specific[104,148]. It will be interesting for future work to determine how the oxidation state of HMGB1 impacts the interaction with protein VII.

To investigate the relevance of the protein VII-HMGB1 interaction on chromatin, we focused on the type-I immune response through interferon. Our results show that in the presence of protein VII, expression of IFNβ is reduced to baseline levels. When HMGB1 is lost, this repression is partially rescued such that IFNβ levels were still induced by poly (dA:dT) treatment, though not to the same degree as in the control (Fig 2.11). We suspect that the presence of HMGB2 or HMGB3 in these cells may compensate for the lack of HMGB1, allowing protein VII to still repress IFNβ to a significant degree. This appears to be specific for IFNβ because transcription of downstream interferon stimulated genes was unchanged. These results indicate that protein VII's ability to repress IFNβ is not due to a general repression in host transcription, but a specific effect on IFNβ expression. HMGB1 and the remaining HMGB family of proteins are highly conserved across eukaryotes[172], while the interferon response is only found amongst vertebrate animals[173]. Because protein VII is well conserved in human serotypes[3,174], this suggests a potential mechanism by which protein VII from human adenoviruses has evolved to evade the innate immune system. Thus, hijacking HMGB1 by protein VII has a two-fold payoff: (1) it prevents HMGB1 release to dampen systemic inflammatory defenses and (2) it restricts IFNβ expression and in turn the downstream effects of interferon, both of which promote viral infection.

There has been extensive work characterizing how many of the early adenovirus proteins inhibit the innate immune response to adenovirus infection. For example, E1A, E1B-55K, E4orf3, and E4orf6 all use strategies ranging from inhibiting transcription, and degrading host proteins, to sequestering host proteins to prevent the innate immune response[154,175–177]. Here, we propose a model in which protein VII hijacks HMGB1 to suppress IFNβ expression

(Fig 2.11C). This is a unique strategy from the perspective of the virus since protein VII is a late viral protein and will likely not impact the death of the infected cell, but rather prevents large amounts of interferon from being released upon cell death and lysis, thus dampening the systemic immune response. Furthermore, this appears to be separate from protein VII preventing the extracellular HMGB1-associated inflammation response.

In the past decade, several studies have reported that different viruses interact with and utilize HMGB1 for viral benefit. For example, the influenza virus nucleoprotein binds HMGB1 to promote replication[137] and SARS-CoV-2 infection also relies on HMGB1 to promote ACE2 expression[139]. In light of these studies, it will be fascinating to uncover the mechanisms by which HMGB1 functions not just in extracellular signaling as a response to infection but also as a target for hijacking within the nucleus to subvert host defenses.

Materials and Methods

Bacterial growth conditions and chemical treatments.

Escherichia coli strains were grown in LB (5 g / L NaCl, 10 g / L tryptone, 5 g / L yeast extract) at 37 °C with shaking at 200 rpm. Antibiotics were supplemented as needed (carbenicillin: 50 µg / mL liquid / 100 µg / mL plate, and kanamycin: 30 µg / mL / 50 µg / mL). Optical density was measured at 600 nm using an Eppendorf BioPhotometer. For bacterial two-hybrid assays, *E. coli* BTH101 was grown in M63 minimal media (0.4 g / L ammonium sulfate, 2.72 g / L monopotassium phosphate, 0.1 mg / L ferrous sulfate heptahydrate [pH 7.0], 1 mM magnesium sulfate, 0.2 % maltose, 0.4 % glucose, and 0.0001% vitamin B1) supplemented with carbenicillin, kanamycin, and 1 mM IPTG for 48 hours at 30°C with shaking before spotting on MacConkey agar (BD Difco) plates.

Plasmid construction.

HMGB1 plasmids for cell line construction were generated in a 2nd generation pLVX-M-puro transfer plasmid (Addgene plasmid# 125839). The HMGB1 sequence was obtained from the pcDNA3.1 Flag hHMGB1 plasmid (Addgene plasmid #31609). Different HMGB1 constructs (A-box, B-box, AB-box, BC-tail, GFP) were PCR amplified from the HMGB1 sequence, restriction enzyme digested and cloned into the pLVX transfer plasmid using traditional cloning methods. The mutHMGB1 with 6xHis tag was custom generated by GeneWiz, and then cloned into pLVX transfer plasmid using traditional cloning methods.

Constructs of HMGB1 and protein VII for B2H assays were PCR amplified from the HMGMB1.pLVX and protein VII plasmids using KOD DNA polymerase. PCR products were verified on a 1% TAE agarose gel and extracted using the Zymo Research DNA Clean and Concentrator Kit. PCR products were then digested using KpnI-HF and XbaI (New England Biolabs) and ligated into pUT18, pUT18C, pKT25, or pKNT25 digested with the same enzymes

pre-treated with quick CIP (New England Biolabs). Ligated plasmids were then transformed into DH5α *E. coli* and validated by sanger sequencing.

Bacterial two-hybrid analysis

Plasmids (pUT18, pUT18C, pKT25, and pKNT25) containing fusion constructs of HMGB1, protein VII, and variants were co-transformed into the B2H assay strain BTH101. Four replicates from each transformation were picked, grown in M63 minimal media for 48 hours, and spotted on MacConkey agar plates supplemented with carbenicillin, kanamycin, 1% maltose, and 1mM IPTG. Plates were incubated at 30 °C and imaged after 72 hrs. Interaction between protein VII and HMGB1, A-box, B-box, BC, and itself (VII dimerization experiments) was probed in four orientations (e.g., T25-VII with T18-HMGB1, T25-VII with HMGB1-T18, VII-T25 with T18 HMGB1, and VII-T25 with HMGB1-T18). Protein VII with AB and HMGB1 DNA-bending mutants was examined using C-terminal fusions (e.g., T25-VII with T18-AB). Similarly, pre-VII and VIIΔPTM with HMGB1 variants or self-interaction experiments were examined with C-terminal fusions. A-box, BC, and HMGB1 self-interactions, and A-box dimerization with BC or HMGB1 were assayed with N-terminal fusions and cross-oriented tags (e.g., BC-T25 with T18-BC and BC-T25 with BC-T18) to assess if dimerization occurred in the same orientation as the observed interaction between HMGB1 and protein VII. AB, B-box, DNA-bending mutant self-interactions, and B-box dimerization with A-box or AB was assayed using C-terminal fusions (e.g., T25-A^{mut} with T18-A^{mut}).

Cell culture, cell line generation and viral infections

A549 cells were purchased from ATCC and cultured using standard methods in Kaighn's modification of Ham's F-12 medium (F-12K) containing 100 U/ml of penicillin and 100 mg/ml of streptomycin and supplemented with 10% fetal bovine serum (FBS). Tetracycline negative FBS was used for cell lines containing dox-inducible protein VII constructs. HEK293T cells were purchased from ATCC and cultured using standard methods in Dubelco's Modified Eagle

Medium (DMEM) containing 100 U/mL of penicillin and 100 mg/ml of streptomycin and supplemented with 10% fetal bovine serum (FBS) and used for generating lentivirus. Lentiviruses were generated using 2nd generation pLVX transfer plasmid containing different constructs of HMGB1 (HMGB1.eGFP, Abox.eGFP, Bbox.eGFP, ABbox.eGFP, BCtail.eGFP, eGFP, and mutHMGB1.His). The pLVX, psPAX.2, and pMDG.2 plasmids were transfected into a confluent 10cm^2 dish HEK293T cells at a ratio of 1: 3.75: 2.5, respectively. Supernatant was collected at 24-, 48-, and 72-hours post transduction and stored at -80˚C. A549ΔHMGB1 cells were seeded in a 6-well plate and then transduced with the different HMGB1 construct lentivirus. At 24 hours post transduction, puromycin was added with fresh media at 2 µg/mL to select for transduced cells. Successfully transduced cells were kept under puromycin selection while they were expanded to be frozen or used for experiments.

All infections were performed using standard protocols with a multiplicity of infection of 10 (Ad5), 100 (rAd VII-GFP), or 50 (rAd GFP). Wild-type Ad5 was obtained from ATCC and recombinant adenovirus vectors rAd VII-GFP and rAd GFP were a gift from D. Curiel [178]. Ad5 VII-HA was generated using bacterial recombineering with an E3-deleted Ad5 bacterial artificial chromosome (BAC) vector [179,180]. Briefly, an HA tag was added to the protein VII gene through PCR amplification, and then protein VII was introduced into the Ad5 genome through recombineering. Successful recombineering was verified through restriction digest and Sanger sequencing. The Ad5 VII-HA genome was linearized by PacI endonuclease digestion, transfected into 293 cells, and amplified over several passages. Following amplification, the virus was extracted from cell pellets by freeze thawing. All viruses were purified using two rounds of ultracentrifugation on a cesium chloride gradient and stored in 20% glycerol at -80˚C. Viral titers were determined by plaque assay.

Immunofluorescence microscopy

Immunofluorescence microscopy was performed using standard methods as previously described [94]. Briefly, cells were seeded on poly-L-lysine coated coverslips in a 24-well plate. Cells were infected with Ad5, and coverslips were collected at 18 hours post infection and fixed with 4% paraformaldehyde. After fixation, cells were permeabilized with 0.5% Triton-X, and blocked with 3% BSA. Cells were incubated with primary antibodies for 1 hour, washed three times in PBS, incubated with secondary antibody and DAPI for 1 hour in the dark, and then washed three times in PBS. Coverslips were then mounted on slides with ProLong Gold Antifade Mountant (Thermo Fisher Scientific), and then allowed to dry overnight. High resolution confocal microscopy was performed with a Leica Stellaris Confocal Microscope using a 63x oil objective.

Nuclear pre-extraction.

Cells were prepared for immunofluorescence microscopy as stated above. Before fixation, cells were treated with nuclear pre-extraction buffer (20mM Hepes, 20mM NaCl, 5mM $MgCl_2$, 1mM DTT, 0.5% NP-40, 1X phosphatase inhibitor and 1X protease inhibitor) for 20 minutes on ice. After this treatment, cells were washed with PBS and then fixation with paraformaldehyde and the staining process proceeded as stated above.

Fractionation and western blotting.

The cellular fractionation protocol was adapted from Suzuki *et al.* [181]. Briefly, cell pellets were thawed on ice for 5 minutes and then resuspended in 900µL of ice-cold 0.5% NP-40. 300 µL was added to 100µL of 4X sample buffer as whole cell lysate. The remaining 600µL was incubated at room temperature for 5 minutes and then centrifuged at 13,000 RPM for 30 seconds. 300µL of the supernatant was added to 100µL of 4X sample buffer as the soluble fraction. The remaining 300µL was discarded and the pellet was resuspended in 900µL of ice-cold 0.5% NP-40 and incubated at room temperature for 5 minutes. The mixture was

centrifuged at 13,000 RPM for 30 seconds, the supernatant was discarded, and the remaining pellet was resuspended in 200µL of 1X sample buffer as the insoluble fraction. All three fractions were boiled at 95˚C for 20 minutes. Samples were run on 12% poly-acrylimide gels and then transferred to nitrocellulose. The membranes were blocked in 5% milk in TBST, and then probed with primary antibodies at 4˚C overnight. Blots were then probed with secondary antibodies for one hour, developed with Clarity Western ECL Substrate, and then imaged with a Biorad ChemiDoc MP Imaging System.

Antibodies.

Commercially available antibodies were purchased through Abcam (GFP [ab290], HMGB1 [18256], H3 [ab1791]), Sigma-Aldrich (Vinculin [V9131]) and Clontech (His [631212]). Protein VII antibodies were a generous gift from the Gerace and Wodrich labs [69,182]. DBP antibodies were a generous gift from the Levine lab [183]. Secondary antibodies used for immunoblotting were obtained from Jackson ImmunoResearch (115-035-003 and 111-035-045). Secondary antibodies for immunofluorescence microscopy were obtained from Thermo Fisher Scientific (A11008, A-11011, A-21245, A-11001, A32727, A-21236).

Interferon and poly(dA:dT) treatment.

For the interferon treatment, A549 VII-HA cells were treated with or without doxycycline for four days at 0.2 µg/mL, with fresh doxycycline added each day. On day three, cells were treated with or without recombinant human IFNβ at 1000 U/mL. Cell pellets were collected on day four for RNA extraction using the NEB Monarch Total RNA Miniprep Kit. One µg of RNA was converted into cDNA using iScript Reverse Transcription Supermix (Bio-Rad), and then cDNA was used for qPCR with iTaq Universal SYBR Green Supermix. Final data for RT-qPCR for ISG expression was log transformed before plotting on graph. For poly(dA:dT) treatment, cells were transduced with recombinant adenovirus vector rAd VII-GFP at an MOI of 100 or recombinant adenovirus vector rAd GFP at an MOI of 50 to achieve equal levels of GFP positive cells

(greater than 90%). This is because the recombinant adenovirus vector rAd VII-GFP is less stable, thus a higher apparent MOI was required to achive the same levels of GFP positive cells. At 24 hours post transduction cells were treated with poly(dA:dT) at 1 μg/mL for 8 hours, and then cell pellets were collected for droplet digital PCR. RNA was extracted from the cell pellets and 1 ug of RNA was converted to cDNA as above, for droplet digital PCR (ddPCR). The cDNA was serial diluted and then mixed with a primer-probe mix for IFNβ and commercially available Eukaryotic 18S rRNA Endogenous Control (VIC/MGB probe, primer (4319413E). The ddPCR mixture consisted of 12.5 μL of of a 2X ddPCR Supermix for Probes no dUTP (Bio-Rad: 1863024), 1.25 μL of each primer-probe mix, and 10 μL of the diluted template cDNA. 20 μL of each reaction mixture was loaded onto a disposable Dg8 cartridge (Bio-Rad 1864008) with 70 μL of droplet generation oil (Bio-Rad 1863005) and oil droplets were generated (QX200 Droplet Generator). Generated droplets were transferred to a 96-well PCR plate (Bio-Rad 12001925), and PCR amplification was performed with a Bio-Rad C100 Touch Thermal Cycler under the following conditions: 95˚C for 10 minutes, 40 cycles of 94˚C for 30 seconds and 60˚C for 1 minute with a ramp rate of 2˚C/sec, followed by 98˚C for 10 minutes, and then held at 12˚C. Following amplification, the plates were loaded on a droplet reader (Bio-Rad QX200) and droplets were analyzed with droplet reader oil (Bio-Rad 1863004). Data was analyzed using the Quantasoft analysis software, and after accounting for fold-dilution of cDNA, the number of IFNβ positive droplets was normalized to every 1 million positive 18S rRNA positive droplets and then log transformed.

Statistical analysis.

All statistical analyses were performed using GraphPad Prism v9 or v10. Statistical tests and n values are described in the figure legends. Statistical significance was defined as $p<0.05\%$ in all experiments. Specifically, we used a Welch's t-test and 2-way ANOVA with Tukey's multiple

comparisons test where described. Statistical tests for Fig 2.11A-B were performed on log transformed data. Only p-values less than cutoff are reported in figures.

Primers

Primer	Sequence 5' to 3'	Use
DA645_mEGFP (F) 5'-EcoRI	TAGAATTCATGGTGAGCAAGG	Cloning
DA646_HMGB1 A box (F) 5'-EcoRI	GAAGGAATTCATGGGCAAAGGAGATCCTAA	Cloning
DA647_HMGB1 B box (F) 5'-EcoRI	GTCGAATTCCATGGAGACAAAAAAGAAGTTCAAGG	Cloning
DA648_HMGB1 linker+C term (F) 5'-EcoRI	CAGGAATTCTATGCGAGCTAAAGGAAAGCC	Cloning
DA649_mEGFP (R) 5'-XbaI	CGTATCTAGATTACTTGTACAGCTCGT	Cloning
DA040MX2_Fwd	CACATCCATATTTCAGAGTTCTCC	RT-qPCR
DA041_MX2_Rev	GGTGGCTCTCCCTTATTTGTC	RT-qPCR
DA030_ISG15_Fwd	CAGATCACCCAGAAGATCGG	RT-qPCR
DA031_ISG15_Rev	GCCCTTGTTATTCCTCACCA	RT-qPCR
DA799_Interferon-Beta_Probe1_FAM	/5FAM/CAATTGAATGGGAGGCTTGAATAC/3BHQ1/	RT-ddPCR
DA_800IFNBeta_Fwd 4	GCCTTTGCTCTGGCACAAC	RT-ddPCR
DA_801IFNBeta_Rev 4	GCTGTAGTGGAGAAGGACAAC	RT-ddPCR

Plasmids

Plasmid	Use
pLVX_HMGB1_eGFP	Lentivirus and Cell Line Generation
pLVX_Abox_eGFP	Lentivirus and Cell Line Generation
pLVX_Bbox_eGFP	Lentivirus and Cell Line Generation
pLVX_ABbox_eGFP	Lentivirus and Cell Line Generation
pLVX_BCterm_eGFP	Lentivirus and Cell Line Generation
pLVX_eGFP	Lentivirus and Cell Line Generation
HMGB1_His_TripleDNAMutant	Lentivirus and Cell Line Generation
pMD2.G	Lentivirus and Cell Line Generation
psPAX2	Lentivirus and Cell Line Generation

Chapter 3: Post-translational modifications on protein VII are important during early stages of adenovirus infection

Abstract

Protein VII is peppered with several PTMs whose addition contributes its localization either to host chromatin or to the nucleolus, but the impact of these PTMs has not been characterized during adenovirus infection. In this chapter, I used mutant viruses that abrogate or mimic these PTMs on protein to demonstrate how PTMs impact protein VII function during adenovirus infection. I discovered that acetylation of the lysine in positions 2 or 3 (K2 or K3) is important during early infection as mutation to alanine led to greater intake of protein VII to the nucleus and enhanced early gene expression. Furthermore, I detected that protein VII is acetylated at alternative residues to compensate for mutated lysine sites. Lastly, I demonstrated that protein VII interacts with the early viral gene E1A through a chromatin-mediated interaction, and that PTMs on protein VII are dispensable for this interaction. Together, these results demonstrate that a single amino acid change in a key viral protein can influence the onset of infection.

Introduction

Chromatin is a complex of DNA and histone proteins that serves to compact the host genome and regulate gene expression[184]. Histones are heavily post-translationally modified (PTM) with marks such as phosphorylation, acetylation, and methylation, among others, that impact DNA accessibility through compaction. For example, acetylation of histone H3 at lysine 18 (H3K18ac) is associated with open chromatin and active gene expression[185,186]. In contrast, methylation at lysine 9 (H3K9me) is commonly associated with repressed chromatin[185,186].

Phosphorylation of histones is frequently involved in the activation of many signaling pathways independent of chromatin, such as phosphorylation of H3S10 (H3S10ph) during mitosis[185,187–189]. Similar to histones, protamines are small arginine rich basic proteins that, in mammals, serve to compact the paternal genome within sperm. The paternal genome is compacted within the restricted space of sperm cells supporting the notion that protamines are more efficient at compacting the genome than histone proteins[190,191]. Upon fertilization, protamines are extensively modified, which is hypothesized to reduce their high charge and promote their replacement with histones[190]. Thus, PTMs are an essential aspect of the relationship between DNA and histones or histone-like-proteins.

Adenovirus is a double-stranded DNA virus that encodes a core protein, called protein VII, which is bound to the viral genome within the virion and has been described as a histone or protamine-like protein[35,141,192]. Protein VII is a small, basic protein of 198 amino acids that is initially expressed as a precursor, preVII, before a viral protease cleaves the first 24 amino acids resulting in the packaged mature protein VII[40,56,142]. In a wild-type infection, protein VII is delivered with the genome to the nucleus[64,66,67,70] and is commonly used as a marker for incoming viral genomes. By immunostaining, these incoming genomes can be visualized as foci within the cell that persist up to 10-12 h post-infection (p.i.)[65,66,70,74,193]. Protein VII is essential in that although protein VII-null virions can be made, the incoming virions remain trapped in the endosome during viral entry and are unable to establish an infection[79]. Chromatin immunoprecipitation of protein VII during early infection showed that protein VII associates with the viral genome throughout early stages of infection up to 10-12 h p.i.[66,67,72,73,75,194] and is slowly removed over time, independent of transcription or DNA replication[67,72,73]. In contrast, other reports showed that protein VII foci decreased with the onset of transcription of early viral genes and that protein VII foci persisted when transcription was inhibited or in the absence of early viral gene E1A[65,74]. E1A binds to the host genome and facilitates transitioning the cell into and

viral ‘S phase’, and importantly activates transcription of other early viral genes[195], among other functions. Protein VII also protects the incoming viral genome from recognition by the host DNA damage response[65,91], although how the presence of VII impacts the onset of viral gene expression is unclear.

Because remodeling of the incoming viral genome to deposit histones and initiate transcription is closely tied to the removal of protein VII, protein VII was hypothesized to act as a transcriptional repressor[196–198]. A recent study used chromatin profiling techniques to map protein VII on the early viral genome and found that protein VII forms a repeating complex with DNA, termed adenosomes, that are reminiscent of host nucleosomes[199]. Schwartz *et al* found that lower amounts of protein VII on a viral gene, for example early genes, was correlated with transcription, supporting the idea of protein VII as a repressor[199]. In contrast, other studies proposed that protein VII activates transcription, likely through its interactions with the chromatin factor TAF-Iβ/SET that promote remodeling of the incoming viral genome for gene expression[67,70]. Further, it was hypothesized that protein VII directly binds and recruits E1A, to the viral genome to drive early gene transcription[74], adding a layer of complexity to the early stages of infection.

Interestingly, protein VII is also able to bind fully formed nucleosomes[82], which suggests that the interaction of protein VII with DNA or newly deposited nucleosomes on the viral genome may be more nuanced than previously thought. During late stages of infection, protein VII is expressed with other late genes to high levels. At this time, protein VII localizes both to viral replication compartments (VRCs) for assembly into nascent virions, and to host chromatin where it is thought to bind nucleosomes directly with the aid of host factors SET and HMGB1[82,94,200]. The mechanisms by which protein VII distinguishes between viral and host chromatin are unknown.

Much like histones and protamines, protein VII is also post-translationally modified. The mature protein contains two acetylation sites (K2 or K3 and K24) and three phosphorylation sites (T38, T48 or T50, and S159)[82]. Additional phosphorylation (S19) and acetylation (K20) sites were also identified on the N-terminal precursor fragment[82]. Wild-type mature protein VII localizes to host chromatin upon ectopic expression; however, if all five PTM sites are mutated to alanine to abrogate modification, protein VII no longer localizes to chromatin but to the nucleolus[82]. Further analysis suggested that acetylation of either K2 or K3, which appear to be redundant, is critical for host chromatin localization. As such, mutation of both lysine residues to alanine in ectopically expressed protein VII phenocopied the mutation all five PTM sites and resulted in nucleolar localization whereas mutation of either lysine residue to the acetyl mimic glutamine recapitulated the wild-type protein localization to chromatin[82]. These data support a model for the distribution of protein VII during infection wherein unmodified protein VII localizes to viral genomes in VRCs to be packaged while modified protein VII localizes to host chromatin. Consistent with this model, mass spectrometry on purified virions identified no acetylation on protein VII or phosphorylation at T72 or S79[82–84], suggesting that PTMs may contribute to protein VII's ability to distinguish between viral and host chromatin.

Here, to investigate the function of PTMs on protein VII during infection, we generated mutant viruses with point mutations in protein VII. We demonstrate that preventing acetylation of K2 and K3 by mutating both residues to alanine led to enhanced nuclear entry of the viral genome which causes earlier onset of expression of the early viral gene E1A. Interestingly, this acceleration of early gene expression caused by mutating protein VII had no impact at later stages of infection. We found that mutated protein VII is still acetylated during infection, likely at alternate residues. To elucidate the dynamics of early infection, we discovered that protein VII and E1A interact in a chromatin dependent manner, adding a new dimension to our understanding of the remodeling of the incoming viral genome and early transcription onset.

Together, our findings establish that modifications on protein VII are critical for early viral entry and gene expression.

Results

Post-translational modifications on protein VII contribute to nuclear entry.

Due to protein VII's role in establishing infection, we hypothesized that PTMs on protein VII may impact early stages of infection. To test this, using recombineering[179,200] we created replication-competent E3-deleted human adenovirus type 5 (HAdV-5) mutants with point mutations and a C-terminal HA tag on protein VII. We generated three mutant viruses in which (1) all five PTMs sites on protein VII were mutated to alanine (ΔPTM), (2) only the second and third lysine residue were mutated to alanine (K2AK3A), or (3) the third lysine residue was mutated to the acetyl mimic glutamine (K3Q) (Fig 3.1). We then infected A549 cells with these viruses and visualized incoming genomes at early time points of infection. To ensure comparable infection dynamics, we synchronized infection by cold incubation prior to initial infection (see Methods). We then immunostained cells for HA to observe the localization of protein VII, as an indicator of viral genomes, and the early viral protein E1A to monitor the onset

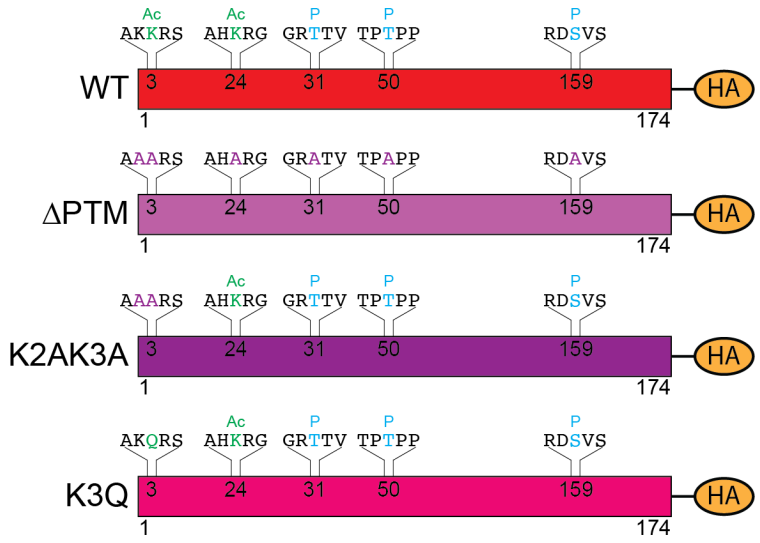

Figure 3.1 WT and protein VII mutant virus design. Schematic of protein VII from wild-type (WT) and mutant viruses. WT mature protein VII (top) is shown with the amino acid sequence of modified sites and corresponding residue positions indicated. Amino acid changes and their predicted effects on modifications are shown for mutant viruses below. Ac is acetylation and in green, P is phosphorylation and in cyan, and alanine substitutions are in purple.

of early viral gene expression (Fig 3.2A). Next, we quantified the integrated density of HA staining within the nucleus of infected cells (Fig 3.2B). At 2 h p.i., the majority of HA-positive foci localized to the cytoplasm in all samples, with very little positive staining in the nucleus (Fig 3.2A and 3.2B). This is somewhat unexpected since adenovirus genomes have been reported to reach the nucleus by approximately 45 minutes after infection[201,202]; however, since our system uses an HA-tagged protein VII in an E3-deleted virus with cold synchronization, these differences could account for a delay in kinetics. At 4 h p.i., we observed HA-positive foci both in the nucleus and the cytoplasm, and the nuclear localization of ΔPTM and K2AK3A viral genomes was significantly greater than WT (Fig 3.2A and 3.2B). At 6 h p.i., this difference became more pronounced, with even more foci in the nucleus upon infection with the K2AK3A and ΔPTM compared to the other viruses. By 8 h p.i., the pattern remained the same for all four viruses, with the K2AK3A virus infected cells containing the most nuclear foci; however, the HA signal became more diffuse at this time, suggesting that protein VII may no longer be associated with viral genomes. By quantification, we observed that the WT and K3Q viruses had similar patterns of nuclear entry, meaning that the distribution of foci at 4 h p.i. were very similar, suggesting that the K3Q virus is phenotypically similar to the WT. Interestingly, the K2AK3A and ΔPTM viruses also had comparable patterns at 4 h p.i. with a significantly higher proportion in the nucleus compared to the other two viruses. We also observed that the K2AK3A virus had a higher integrated density plateau in our quantification analysis. We hypothesized that this may be due to a higher particle to pfu ratio of our K2AK3A virus. To ensure comparable amounts of virus were used in each condition, we performed qPCR to determine the average number of genomes per cell and found that the K2AK3A had the highest at ~250 (Fig 3.2C) and that the WT and K2AK3A viruses were both significantly higher than the K3Q virus (Fig 3.2C), suggesting more viral genomes were present. Nevertheless, this slightly higher plateau does not

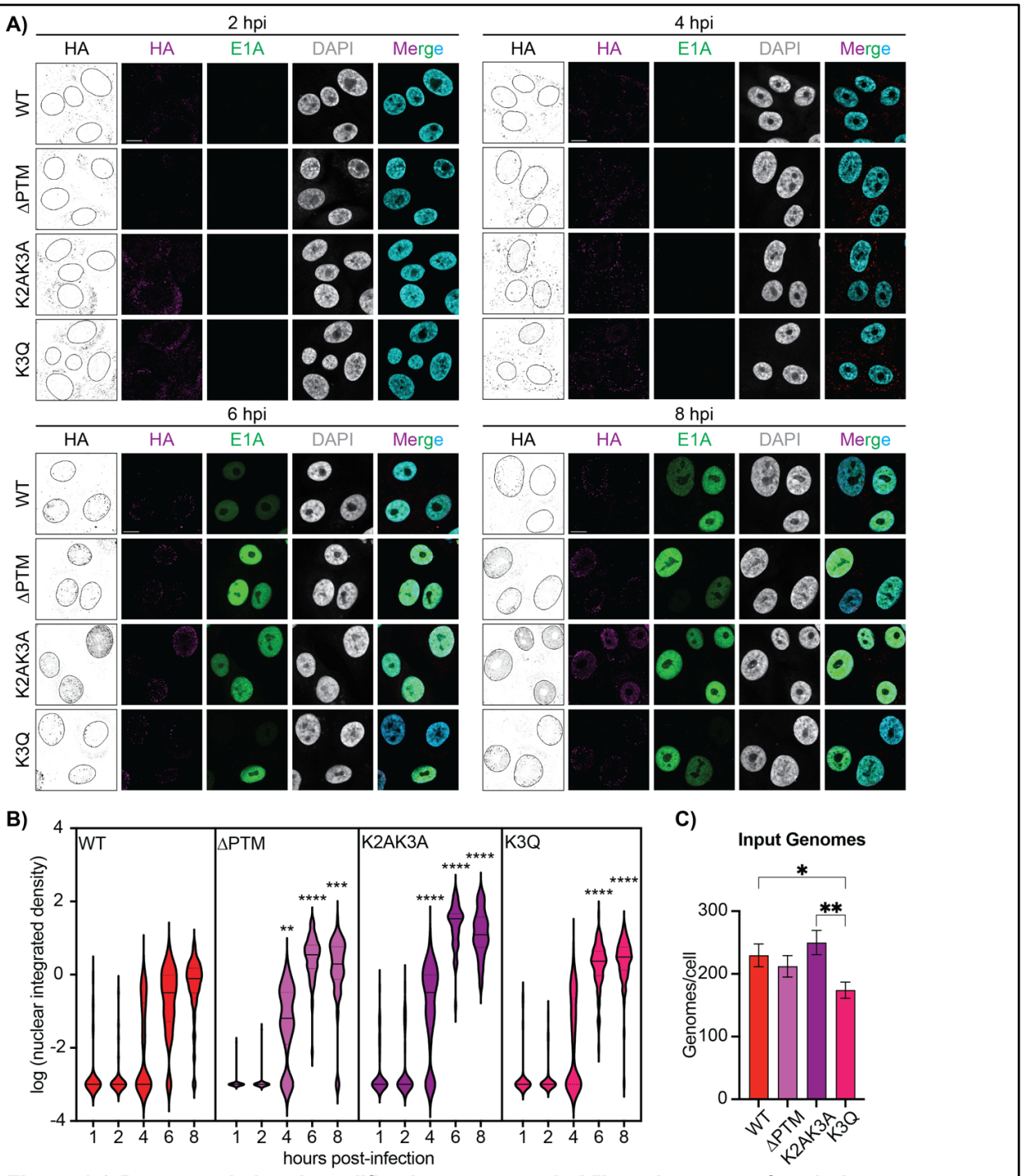

Figure 3.2 Post-translational modifications on protein VII are important for viral genome entry into the nucleus. A) Representative immunofluorescence images of A549 cells infected with WT and mutant viruses as described in Fig 3.1 at 2 (top left), 4 (top right), 6 (bottom left), and 8 (bottom right) h p.i., showing HA in magenta, E1A in green, and DAPI in grey (cyan in merge). Additional panels of HA staining in black and white and nuclei outlined are provided for better visualization. Scale bar is 10 μm. *Legend continues on next page.*

B) Quantification of the integrated density of HA staining within the nucleus for each time point. N>30 nuclei for each virus at each time point. ** is p<0.01, *** is p<0.001 **** is p<0.0001 by one-way ANOVA with Dunnett's multiple comparisons test. **C)** Quantification of input viral genomes per cell by qPCR of infected A549 cells with indicated viruses at MOI of 25 pfu per cell. Input genomes are presented as mean and error bars represent standard deviation. * is p<.05, ** is p<.01 by two-way ANOVA with Tukey's multiple comparisons test. n=3 biological replicates.

account for the significantly greater foci detected in the nuclei of cells infected with the K2AK3A and ΔPTM viruses. Taken together, these results suggest that mutation of the K2 or K3 residues enhances viral entry into the nucleus.

We observed that E1A became detectable at 6 h p.i. and increased in intensity by 8 h p.i. We found both a greater number of E1A positive cells as well as more intense E1A signal in the K2AK3A and ΔPTM infected cells compared to the WT and K3Q infected cells at 6h p.i. These results suggest that the increased nuclear entry observed by immunofluorescence also leads to increased expression of E1A. Together, these results suggest that acetylation at the K2/K3 lysine impacts accumulation of viral genomes within the nucleus.

K2AK3A mutations in protein VII enhance early gene expression.

Next, we hypothesized that transcription may also be starting earlier with mutation of K2 and K3 on protein VII. To investigate this, we performed infections over a time course with our mutant viruses and measured viral mRNA by RT-qPCR at 0.5, 1, 1.5, 2 and 4 h p.i. and protein expression by western blotting at 4, 6 and 8 h p.i. (Fig 3.3). We found an increase in relative abundance of E1A mRNA in the K2AK3A virus, and to a lesser extent in the ΔPTM virus, compared to the control housekeeping gene, RPLP0, at all early time points tested (Fig 3.3A). These differences were noticeable by 1 h p.i. and the E1A mRNA remained consistently higher for the K2AK3A and ΔPTM virus until 4 h p.i. when the difference reached statistical significance for both the K2AK3A and ΔPTM viruses compared to WT. The K3Q virus produced mRNA levels similar to those of the WT virus throughout the time course, consistent with the idea that

K3Q is a mimic of acetylation which is present on WT protein VII, while the K2AK3A and ΔPTM viruses exhibited earlier expression, consistent with earlier entry into the nucleus.

We next examined the expression of early viral proteins by western blot and found that E1A protein levels in the K2AK3A virus infection were greater compared to the other viruses at 4 and 6 h p.i. (Fig 3.3B). By 8 h p.i., E1A expression appeared to reach similar levels across all four viruses. We also probed for another early viral protein, E2A, more commonly referred to as DNA binding protein (DBP)[49,203,204], which mirrored the E1A results. At 4 h p.i., DBP was only visible in the K2AK3A virus, and was more intense at 6 and 8 h p.i. compared to the other viruses. Taken together, these findings suggest that mutation of these lysine residues on protein VII results in greater numbers of genomes entering the nucleus, leading to increased early gene expression.

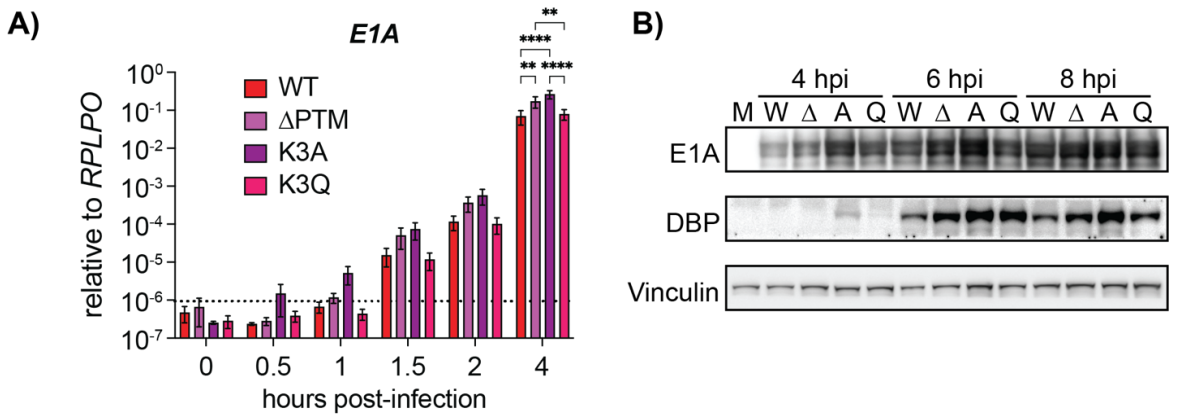

Figure 3.3 Mutation of lysine 2 and 3 on protein VII enhances early gene expression. A) E1A mRNA levels measured by RT-qPCR of A549 cells infected with corresponding viruses, cold synchronized for 1 h on ice, and then collected at the indicated time points. mRNA levels are presented as mean, error bars represent standard deviation. **, p<0.01, and ****, p<0.0001 by two-way ANOVA with Tukey's multiple comparisons test, n = 3 biological replicates. Dotted line represents the limit of detection. **B)** Representative western blots of A549 cells infected with the indicated viruses and harvested at 4, 6, and 8 h p.i. Blots were stained for viral early proteins E1A and DBP and vinculin as a loading control. M is mock, W is WT, Δ is ΔPTM, A is K2AK3A, and Q is K2Q. n = 3 biological replicates.

Post translational modifications on protein VII do not impact later stages of infection.

Due to the effects of protein VII mutations on early viral gene expression, we next investigated their impact at later stages of infection. To measure this, we examined genome replication, protein production, and infectious progeny production. We performed qPCR to measure relative genome amounts and observed no statistically significant difference in genome replication across the four viruses (Fig 3.4A). Similarly, there were no observable differences in protein expression between the four viruses (Fig 3.4B). Lastly, we measured the amount of viral progeny produced during infection by plaque assay. All four viruses had similar titers at the three time points tested, suggesting that these mutations did not impact progeny production (Fig 3.4C). Despite the enhanced early gene expression upon K2AK3A mutation, and to a lesser extent in the ΔPTM virus, our data show that all four viruses appear to function similarly by later stages of infection.

PTMs on protein VII impact localization of the ectopically expressed protein such that WT and K3Q protein VII localized to chromatin, while ΔPTM and K2AK3A protein VII localized to the nucleolus[82]. To assess the impact of these PTMs on localization during infection, we infected A549 cells with the WT and mutant viruses and examined cells at 14 h p.i. by confocal microscopy. We immunostained for HA to visualize protein VII localization, DBP to visualize infection progression together with DAPI[50,205,206]. We found that WT protein VII had a dispersed nuclear localization, forming large puncta throughout the nucleus consistent with previous reports (Fig 3.4D). Surprisingly, there was no clear difference in protein VII localization across the mutant viruses. In fact, contrary to ectopic expression[82], the ΔPTM and K2AK3A mutants did not localize to the nucleolus and were equivalent to WT and K3Q. Thus, we conclude that protein VII localization during infection is not impacted by mutation of protein VII at these specific residues.

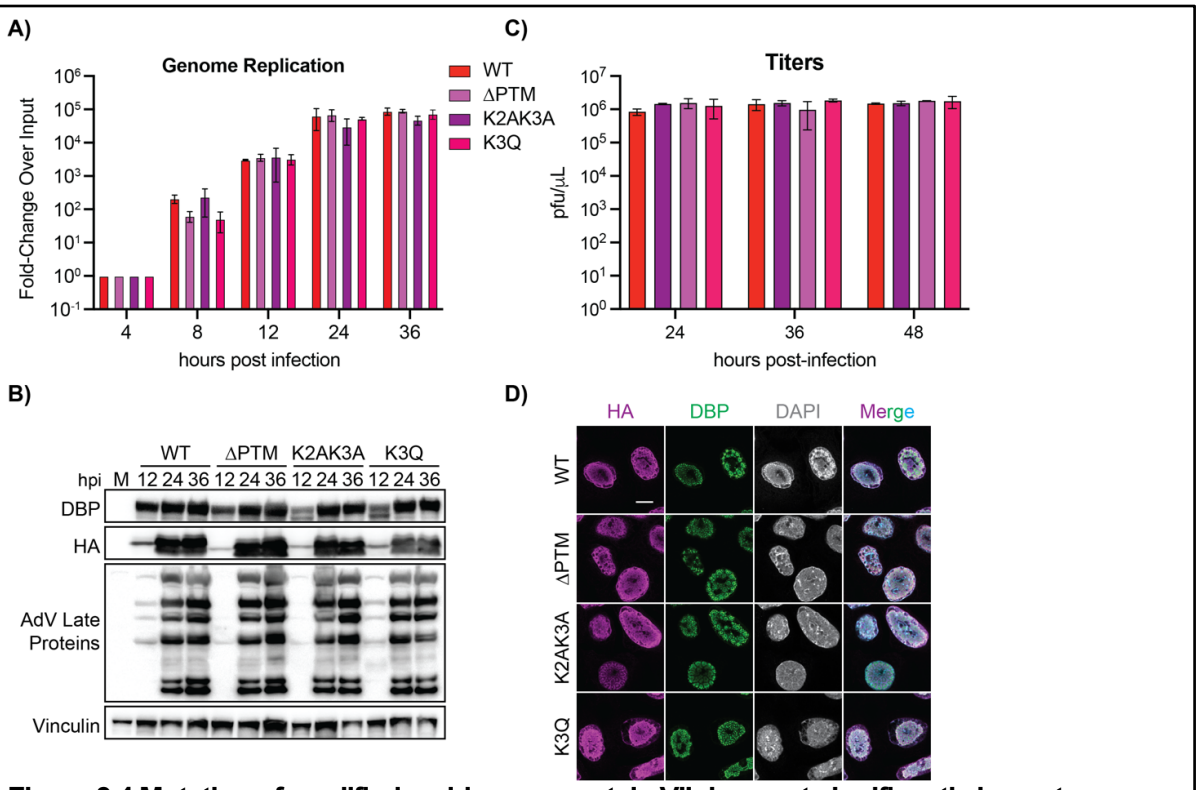

Figure 3.4 Mutation of modified residues on protein VII does not significantly impact genome replication, late protein production, and infectious progeny production. A) Genome quantification as measured by qPCR of A549 cells infected with indicated viruses at 4, 8 12, 24, and 36 h p.i., depicted as mean with error bars representing standard deviation. n = 3 biological replicates. No significance by two-way ANOVA with Tukey's multiple comparisons test. **B)** Representative western blot of A549 cells infected with indicated viruses at time points as indicated. Blots were stained for protein VII (HA), early viral protein DBP, late viral proteins, and vinculin as a loading control. n = 3 biological replicates. No significance by two-way ANOVA with multiple comparisons. **C)** Infectious progeny of the indicated viruses upon infection of A549 cells were quantified at 24, 36, and 48 h p.i. Titers are presented as mean with error bars representing standard deviation. n = 3 biological replicates. No significance by two-way ANOVA with Tukey's multiple comparisons test. **D)** Immunofluorescence images of A549 cells infected with WT and mutant viruses at 14 h p.i. HA is magenta, DBP is green, DAPI is gray (cyan in merge). Scale bar is 10μm. n>30 nuclei for each virus.

VIIΔPTM is acetylated at alternative residues in infected cells.

Upon ectopic expression of protein VII, mutation of K2 and K3 to alanine either as a pair (K2AK3A) or in combination with all other known PTM sites (ΔPTM) drastically changes the localization of protein VII compared to WT[82]. In contrast, our mutant viruses had no major

phenotypic changes in comparison to the WT virus at later stages of infection, and all four appeared to have similar localization patterns. If acetylation of protein VII alone is sufficient to alter its localization, we hypothesized that during infection, ΔPTM and K2AK3A may be modified at different nearby residues to compensate for the mutations. While the structure of protein VII has not been solved, we used the protein prediction software I-TASSER to model protein VII[58,59]. This analysis produced a structure of a bundle of seven α-helices (red, Fig 3.5A), with an eighth helix for the N-terminal precursor fragment (purple, Fig 3.5A). The remaining lysine residues are K20 in the precursor fragment and K73 and K75 of the mature protein (K97 and K99 of preVII) (dark gray, Fig 3.5A). In the predicted structure, K20 within the precursor fragment is in close physical proximity to the known acetylated lysine residues K2 and K3 (K24 and K25 of preVII, green Fig 3.5A). K73 and K75 (dark gray, Fig 3.5A) are also predicted to be on the end of a helix, making them available for acetylation, which may compensate for the loss of the K2 and K3 site. Due to the locations of lysine residues within the predicted structure of protein VII, we hypothesized that in the absence of the preferentially modified lysine residues (K2, K3, and K24), an acetyl transferase enzyme may modify other nearby lysine residues. To test this, we performed an immunoprecipitation (IP) of protein VII in WT and ΔPTM infected cells. We performed the IP at 24 h p.i. when protein VII is expressed to high quantities and probed with a pan lysine-acetyl antibody. We found that both the WT and ΔPTM viruses showed the double banding pattern typical of the pre- and mature protein VII (Fig 3.5B, compare to banding pattern in Fig 3.4B). Furthermore, the ΔPTM signal appeared to lower on the western blot than the WT, as we have noted previously (compare to bands in Fig 3.4B). Taken together, these data suggest that both WT and ΔPTM protein VII are acetylated during infection, suggesting that mutation of known sites to prevent modification may result in acetylation at other sites.

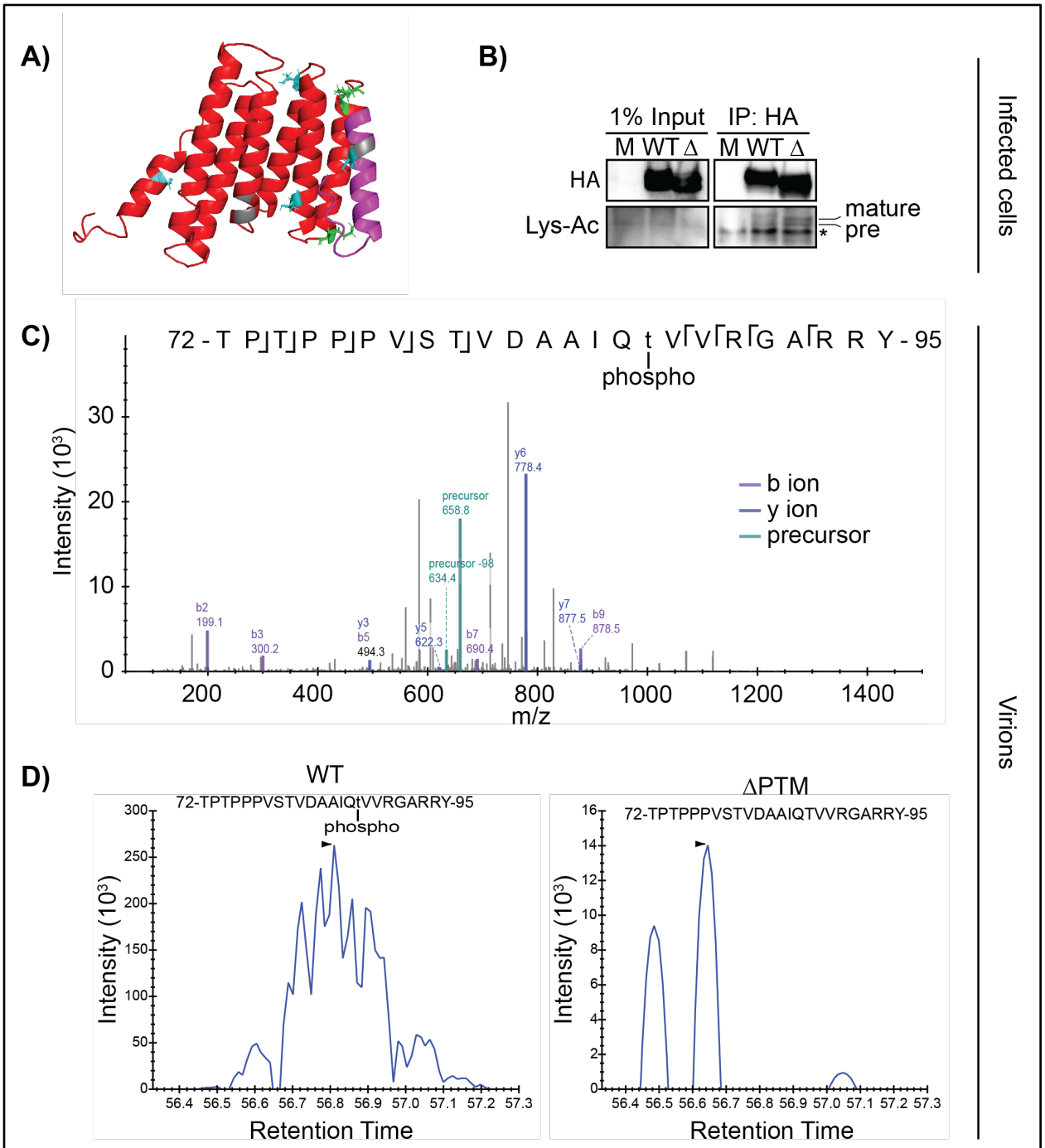

Figure 3.5 VIIΔPTM is acetylated at alternative residues in infected cells. A) I-TASSER structural prediction of protein VII. Protein VII is in red, pre-peptide is in magenta, acetylation sites are in green, and phosphorylation sites are in cyan. Potential lysine residues that could be acetylated in protein VII are in dark gray. **B)** Western blot of protein VII IP at 24 h p.i. for mock, WT, and ΔPTMviruses. Left side is 1% input and right is HA IP. Blots were stained for HA (protein VII) and acetylated lysine. *Legend continues on next page.*

Bands for pre-VII and mature VII are labeled, * denotes the light chain of the IgG1 antibody used for IP. **C)** Mass spectrometry spectra of a modified peptide from virions containing WT protein VII. B ions are in purple, y ions are in blue, and the precursor peptide with and without the phospho group is in teal. The sequence of the identified peptide is shown above the graph. The phosphorylated residue is indicated by lower case. Bars within the peptide sequence indicate the location of b and y ions, with b ions moving left to right (bars underneath residues) and y ions moving right to left (bars above residues). **D)** Chromatograms of the retention times of peptide from HPLC depicting peak that is present in VII and absence of peak in PTM.

Within the virion, either zero or one phosphorylation site was detected on protein VII at T72 or S29[82–84]. We sought to test whether the ΔPTM virus also contained any alternate modifications to compensate for the loss of modification at the mutated sites. We examined the WT and ΔPTM virions by mass spectrometry and did not detect modifications on protein VII from the ΔPTM virus particles. In the WT virus, we detected a 24 amino acid phosphopeptide ("precursor",Fig 3.4C) as well as the same intact peptide without the phosphor group ("precursor-98", Fig 3.4C). This peptide mapped to the region displayed in Fig 3.4C with one phosphorylation site (T87) on protein VII (Fig 3.5C), which is near previously reported phosphorylation sites in the primary sequence (T72, S79)[83,84]. Furthermore, we see a large peak in the WT sample of the chromatography retention time plot (Fig 3.4D, left) that corresponds to the phosphopeptide. This peak is absent in the ΔPTM sample (Fig 3.4D, right), confirming that this phosphorylation was not detected in the ΔPTM virion. The lack of phosphorylation within the ΔPTM virions may be due to low abundance of the phosphorylation and is thus undetectable by mass spectrometry. Therefore, we conclude from our data and previously published work that protein VII within the virion is unmodified or minimally phosphorylated. It is important to note that because many of these modifications are only detected at a low abundance, we cannot determine what percentage of protein VII molecules may be modified within the virion. Because at least one phosphorylation site has been detected on protein VII within virions in several cases[83,84], it is likely that a small fraction of packaged protein VII is phosphorylated.

Protein VII's interaction with E1A is chromatin dependent and PTMs are dispensable for this interaction.

Next, we hypothesized that the PTMs may impact protein VII's interactions with other proteins that may affect infection progression. We previously determined that protein VII directly interacts with the host chromatin factor HMGB1 and that the ΔPTM mutant has a weaker interaction with HMGB1[200]. Protein VII was reported to interact with the early viral protein E1A and is hypothesized to recruit E1A to the viral genome during early infection[75]. Because the K2AK3A virus appeared to have enhanced viral genome entry and faster early gene expression during early stages of infection (Fig 3.2 and 3.3), we hypothesized that PTMs may be important for protein VII's interaction with newly expressed E1A on the viral genome, thus influencing early viral gene transcription. To test whether the two proteins directly interact, we performed a bacterial two-hybrid (B2H) analysis. Surprisingly, neither WT nor ΔPTM showed a positive interaction with E1A in our B2H, suggesting that they do not interact directly (Fig 3.6A, **B2H assay performed by K. Leung*). Because the B2H setting does not contain chromatin or other cellular factors, we sought to recapitulate the reported interaction in cells in the context of adenovirus infection. We infected A549 cells with the WT and ΔPTM viruses and assessed the interaction between protein VII and E1A by IP at 24 h p.i. In contrast to our B2H results, we observed that E1A co-immunoprecipitated with WT protein VII, indicating the two proteins interact in cells during infection (Fig 3.6B). Furthermore, because protein VII ΔPTM also co-immunoprecipitated with E1A, this suggests that the mutated sites are not critical for this interaction. These results suggest that while there is likely no direct interaction between protein VII and E1A, both proteins are found on chromatin throughout infection. Taken together, these findings suggest that it may be through interacting with chromatin, viral or host, that protein VII and E1A come into contact.

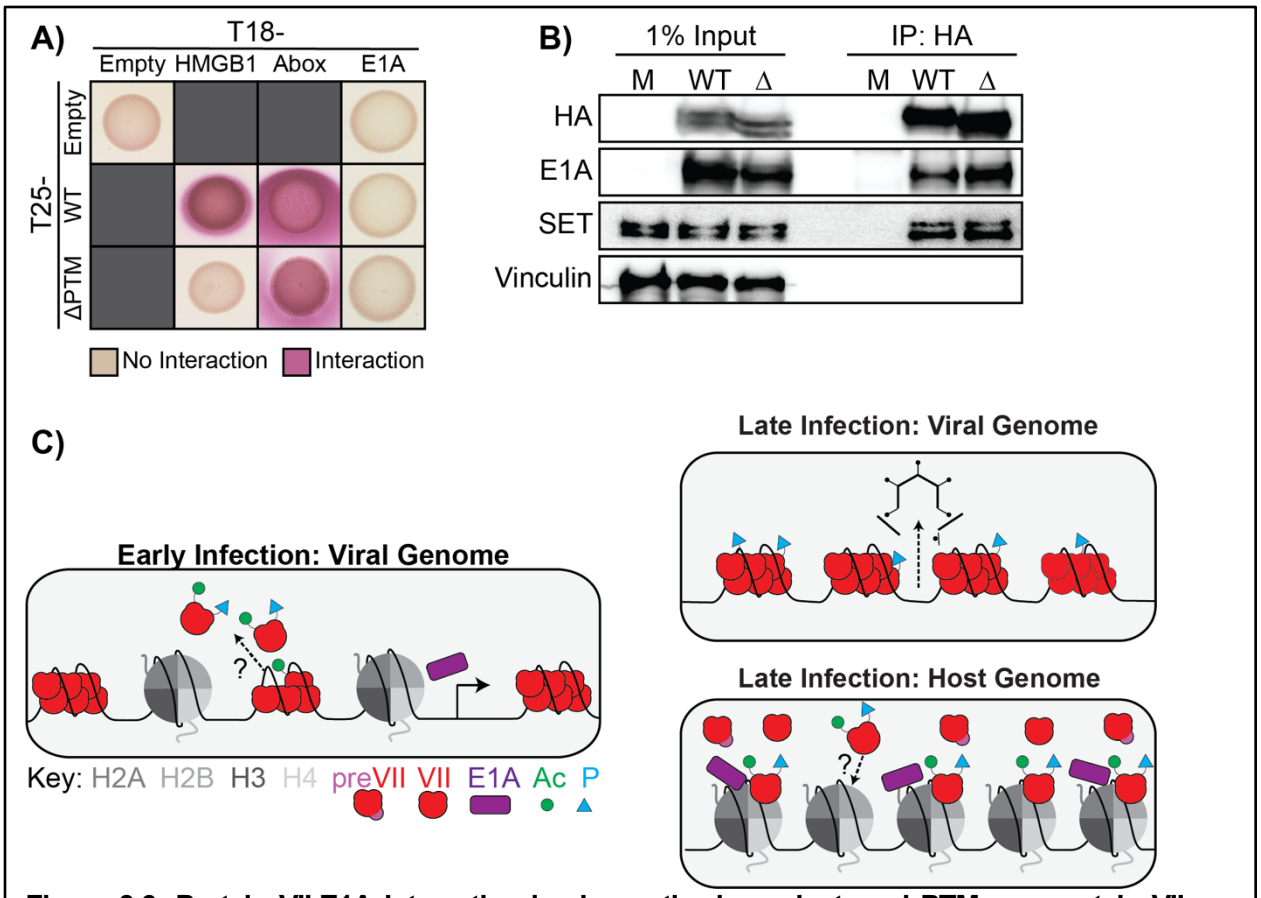

Figure 3.6: Protein VII-E1A interaction is chromatin dependent, and PTMs on protein VII are dispensable for this interaction. A) Bacterial two hybrid results of the interaction between E1A and WT and ΔPTM protein VII. Controls include empty vector (negative control), HMGB1 (positive control), or the A-box of HMGB1 (positive control). A positive interaction results in a pink color while a negative interaction remains beige. Representative image of 4 biological replicates. **B2H assay performed by K. Leung.* **B)** Representative western blot results from immunoprecipitation of HA from A549 cells infected with WT or ΔPTM viruses at 24 h p.i. Blots were stained for HA (protein VII), E1A, SET (positive control), and vinculin (negative control). n = 3 biological replicates. Of note, HA i.p. is same as in Fig 3B. **C)** Model of the role of post-translational modifications on protein VII during early and late adenovirus infection.

Discussion

In this study, we sought to determine how PTMs on the histone-like protein VII affect its function and in turn adenovirus infection. To our knowledge, this is the first attempt to characterize the function of these PTMs on protein VII during infection. We found that when acetylation of K2 and K3 of protein VII was prevented, adenovirus nuclear entry and early gene expression were both enhanced (Fig 3.2-3). Changes in early gene expression did not impact late infection, as genome replication, late gene expression, and progeny production were comparable to wild type virus (Fig 3.4). Furthermore, mutating protein VII to mimic or prevent modification during infection had no effect on protein VII localization to chromatin or nucleoli late in infection (Fig 3.4D). Interestingly, we also found that protein VIIΔPTM is likely acetylated at alternative residues to compensate for the introduced mutations (Fig 3.5). What is the significance of acetylation on protein VII? In the literature, there are conflicting reports on whether protein VII is an activator or repressor of the initial burst of viral transcription[67,70,75,196–199]. Reported results may be difficult to interpret due to different methods used with the complicating layer of regulation dictated by protein VII PTMs. Our results indicate that acetylation at the K2/K3 locus on protein VII is important for viral genome entry as loss of this site led to enhanced nuclear entry and earlier viral gene expression. Because this acetylation was identified upon ectopic expression, that is with no other viral proteins present, it is likely that a host protein is depositing the acetyl mark. Taken together, these observations suggest that a host acetyltransferase may be acting in a defense mechanism to delay viral entry. Nevertheless, the virus is able to overcome this barrier as the loss of these sites results in viral infection dynamics that are indistinguishable from wild type. Our finding that protein VIIΔPTM is still acetylated despite the mutations suggests that either acetylation is critical for protein VII function, or the host defenses are ineffective. Future work to identify the enzyme or enzymes responsible will shed light on whether innate immune signals are responsible.

We found that protein VII's interaction with the early viral protein, E1A, is mediated by chromatin and that PTM sites on protein VII are dispensable for this interaction (Fig 3.6). It is well-established that the first gene expressed upon entry of the viral genome into the nucleus is E1A. Newly translated E1A then binds to active viral genomes to initiate transcription of further viral genes while also binding to the host genome to influence multiple pathways for viral benefit[195,207,208]. Evidence for the interaction of protein VII with E1A[75] led to a model in which the newly translated E1A localizes to the viral genome by binding directly to protein VII, which is still present on the incoming viral genomes. Our results in this study suggest that E1A binds to protein VII only in a chromatin-mediated manner, which would suggest that the order of events is for (1) histones to be deposited on the viral genome together with protein VII, and then (2) E1A binds to activate the expression of other viral genes. While we cannot rule out other models, we propose that protein VII promotes the remodeling of the incoming viral genome to encourage deposition of host histones, together with TAF-1β/SET, which in turn allow for the expression of E1A, that then binds to these genomes and promotes further viral gene expression (Fig 3.6C). On the host genome, E1A has also been well-established to alter histone acetylation and promote an S-like phase. Protein VII also localizes to the host genome, although whether protein VII and E1A localize to the same host genomic loci is unknown. Future work with genomic profiling methods will elucidate the overlap of these two viral proteins on host chromatin and the direct outcome on host transcription.

The K2/K3 site of modification in the wild-type virus is an AKKRS motif, which is reminiscent of the canonical histone ARSK motif. Histone mimics have been observed on Influenza A Virus H3N2 NS1 protein and SARS-CoV-2 ORF8, where viral proteins mimic the histone H3-tail to subvert immune responses[209–211]. In the case of protein VII, it is possible that this AKKRS motif is a viral mimic of the histone motif[212,213]. Protein VII is highly conserved amongst human adenoviruses, and the histone mimic motif is also conserved across HAdV

species as well as within other vertebrate adenoviruses, including an ARKRS motif in MAdV-1. Despite the conservation of this motif, protein VII in general varies widely across different adenovirus species in sequence and length. Surprisingly, protein VII from reptilian and avian adenoviruses are only 128 and 78 amino acids in length, respectively[214,215]. While the origins of protein VII are not known, given its generally poor conservation across non mammalian species, it is clear that protein VII is rapidly evolving and mimicking histones may be a recent adaptation by adenovirus to hijack host processes. Future work into the evolution of protein VII will shed more light on the importance of the conservation and function of potential PTMs at these sites.

We found that increased early gene expression had no significant impact on later stages of infection or the production of infectious progeny (Fig 3.4). We also found that the ΔPTM protein VII was still acetylated during infection, suggesting that other sites on protein VII may be modified to compensate for the mutations we introduced (Fig 3.5). We observed the distinctive double band of protein VII in the WT and ΔPTM samples, suggested that the both the preVII and mature VII proteins are acetylated in ΔPTM. Thus, either K73 or K75 in mature VII is likely acetylated since there are no other lysine residues within mature protein VIIΔPTM. In contrast, there are twelve threonine and six serine residues throughout protein VII (e.g. S5, T28, T48, S130, S161, T169). Thus, it is possible that mutation of the three phosphorylated sites in ΔPTM may not produce an observable defect in the virus due to compensation by phosphorylation of another site. Another possibility is that phosphorylation of various serine and threonine residues within protein VII may be non-specific and dynamic. Future studies employing kinase screens may be more effective at identifying potential enzymes or pathways responsible for protein VII phosphorylation and how phosphorylation of protein VII impacts infection.

During infection, protein VII is first expressed as a precursor protein, preVII, which is cleaved by a viral protease to produce the mature protein[40,56], the latter of which has been the focus of this study. Because the prior ectopic expression analyses were done with the mature

protein only, it is possible that the presence of the precursor peptide may mask the effects of the PTMs. Indeed, the precursor fragment contains both a nucleolar localization and reported PTMs[68,216], which may impact its function. While the function of the precursor is not well understood beyond virion packaging, the ratio of precursor to mature protein heavily favors the precursor based on western blotting during late infection. Furthermore, the exact amount of mature protein VII in the nucleus that is not packaged within progeny virions is unknown. Taken together, these observations indicate that further study is needed to elucidate the functional differences between the mature and precursor proteins. In summary, our study underscores the importance of PTMs on viral proteins during infection while highlighting that these modifications may be pro or antiviral.

Methods and Materials

Cell lines, viruses, and infections

A549 cells were purchased from ATCC and cultured in Kaighn's modification of Ham's F-12 medium (F-12K) containing 100 U/ml of penicillin and 100 mg/ml of streptomycin and supplemented with 10% fetal bovine serum (FBS). HEK293T cells were purchased from ATCC and HEK293Q cells were purchased from Qiagen. Both were cultured in Dulbecco's Modified Eagle Medium (DMEM) containing 100 U/mL of penicillin and 100 mg/ml of streptomycin and supplemented with 10% fetal bovine serum (FBS). HeLa cells were purchased from ATCC and cultured in Eagle's Minimum Essential Medium (EMEM) containing 100 U/mL of penicillin and 100 mg/ml of streptomycin and supplemented with 10% fetal bovine serum (FBS).

Ad5 VIIΔPTM-HA, VIIK2AK3A-HA, and VIIK3Q-HA were all generated by recombineering using a bacterial artificial chromosome containing the genome of a replication-competent, E3-deleted HAdV-5-based vector containing an HA-tagged protein VII[179,200]. Successful recombineering was verified through restriction digest and Sanger sequencing. To produce virus, viral genomes were linearized by *Pac* I endonuclease digestion and transfected into 293β5 cells[217]. The resulting virus was amplified by repeated passaging in 293β5 cells[217], purified with two rounds of ultracentrifugation in a CsCl gradient, snap frozen in liquid nitrogen, and then stored in a 20% glycerol buffer at -80˚C[218]. Viral titers were determined by flow cytometry and plaque assay. Infections for figures 1-2 were performed at a multiplicity of infection of 10 or 25 plaque forming units per cell. Infections were synchronized by adding inoculum to cells on ice and incubating for 1 h while rocking every 20 min. Cells were moved to 37˚C for an additional 2 h with rocking every 20 min before the inoculum was removed and replaced with fresh media. Infections for Figures 3-5 were carried out likewise but without synchronization on ice.

Plaque assays

Cell pellets from time course infections of A549 cells were collected at 24, 36, and 48 h p.i. Cell pellets were resuspended in 100 µL PBS, freeze-thawed 4x, and pelleted in a table-top centrifuge at max speed, and virus containing supernatant was collected for plaque assays. Plaque assays were performed on HEK293Q cells. Cells were seeded in 6-well plates, infected the next day with serial dilutions of virus samples, and overlayed with a 4% SeaPlaque agarose. Plates were incubated at 37 ˚C until plaques developed, approximately 6-7 days. The agarose overlay was dissolved by incubating with 10% trichloroacetic acid in phosphate buffered saline at RT for 30 min and then stained with crystal violet. Plaques were counted by eye, and the count was used to determine the concentration of infectious units.

Antibodies

Commercially available antibodies were purchased through Abcam (HMGB1 [18526], H3 [ab1791], HA-tag [ab9110], SET [ab181990], Adenovirus Late Proteins [ab6982]), Sigma-Aldrich (Vinculin [V9131]), and BD Biosciences (E1A [554155]). Protein VII antibodies were a generous gift from the Gerace and Wodrich labs. DBP antibodies were a generous gift from the Levine lab. Secondary antibodies used for immunoblotting were obtained from Jackson ImmunoResearch (115-035-003 and 111-035-045). Secondary antibodies for immunofluorescence microscopy were obtained from Thermo Fisher Scientific (A-11011, A-11001). DAPI stain was obtained from Fisher Scientific (50-874-10001).

Immunofluorescence microscopy

Immunofluorescence microscopy was performed as previously described[82,94]. Briefly, cells were seeded on poly-L-lysine coated coverslips in a 24-well plate. Cells were infected with viruses, and coverslips were fixed at 0, 2, 4, 6 and 8 hh p.i. with 4% paraformaldehyde. After fixation, cells were permeabilized with 0.5% Triton-X, washed three times with phosphate buffered saline (PBS), and blocked with 3% BSA. Cells were incubated with primary antibodies for 1 h at RT,

washed three times in PBS, incubated with secondary antibody and DAPI for 1 h in the dark, and then washed three times in PBS. Coverslips were then mounted on slides with ProLong Gold Antifade Mountant (Thermo Fisher Scientific) and allowed to dry overnight. High resolution confocal microscopy was performed with a Leica Stellaris Confocal Microscope using a 63x oil objective.

RT-qPCR and qPCR

For qPCR, gDNA was extracted from cells with Qiagen QIAamp DNA kit. Extracted gDNA was normalized to 50 ng/µL and then used for qPCR with primers targeting viral DBP and cellular tubulin for normalization. qPCR results in Fig 2C were determined by performing a standard curve with viral DBP primers against a BAC containing the HAdV-5 VII-HA viral genome. The standard curve was used to determine ng of input DNA for each virus, which was converted to the number of total genomes, and then divided by the number of cells present to quantify the number of genomes per cell. qPCR results in Fig 4 are depicted as fold-change over an input control at 4 h p.i.

For RT-qPCR, RNA was extracted from cells with Trizol. Extracted RNA was converted to cDNA with Iscript Reverse Transcription Supermix (BioRad). cDNA at a concentration of 50 ng/µl was used for qPCR with iTaq Universal SYBR Green Supermix (BioRad) with primers spanning an exon-intron boundary of E1A and RPLP0 for normalization (see primers table below). RT-qPCR results are depicted as fold-change over internal control gene RPLP0. For transcriptional and replication analysis, qPCR was performed with the BioRad CFX384 Real-Time System.

Western blotting

Samples were resuspended in 1X Laemmli sample buffer with 5% β-mercaptoethanol (200µL per 10^6 cells), separated on 12% or 15% polyacrylamide gels, and then transferred to nitrocellulose. Membranes were blocked in 5% milk in TBST buffer or 5% BSA in TBST buffer for 30 min, and then probed with primary antibodies at 4°C overnight. Blots were then washed

with TBST buffer for 30 min, probed with HRP-conjugated secondary antibodies for 1 h at RT, washed with TBST buffer for 30 min, and developed with Clarity Western ECL Substrate, and imaged with a Biorad ChemiDoc MP Imaging System.

Protein prediction

Amino acid sequence of wild-type protein VII (NCBI accession ID AAW65510) was run on the protein prediction software I-TASSER[58,59]. The top predicted model was selected, and the 3D model was formatted in PyMOL.

Bacterial 2-hybrid

Plasmids (pUT18, pUT18C, pKT25, and pKNT25) containing fusion constructs of HMGB1, A-box, protein VII, and E1A were co-transformed into the B2H assay strain BTH101. Four replicates from each transformation were picked, grown in M63 minimal media for 48 h, and spotted on MacConkey agar plates supplemented with carbenicillin, kanamycin, 1% maltose, and 1mM IPTG. Plates were incubated at 30°C and imaged after 72 hrs. Interaction between protein VII and E1A (e.g., T25-VII with T18-E1A, T25-VII with E1A-T18, VII-T25 with T18-E1A, and VII-T25 with E1A-T18).

Immunoprecipitation

A549 cells were infected with Ad5 VII-HA or Ad5 VIIΔPTM-HA at an MOI of 10. Cell pellets were collected at 24h p.i. and stored at -80˚C until ready to proceed to IP. Cells were thawed on ice, resuspended in 1mL of lysis buffer (20mM Hepes pH 7.4, 110mM KOAc, 2mM $MgCl_2$, 0.1% Tween-20. 0.5% Triton-X 100, 200mM NaCl, protease/phosphatase inhibitors (Thermo Fisher A32961, added fresh before use), and incubated on ice for 10 min mixing intermittently. The lysate was then treated with 5µL of benzonase (Fisher Scientific 71-205-3) for one h at 4˚C with rocking. Lysates were pelleted at 4˚C at max speed for 15 min. The supernatant was transferred to new tubes and then protein concentration from each sample was measured by Bradford assay. Samples were normalized to 1 ml of 2mg/mL protein, and 100µL was removed as 10%

input sample. 60µL of HA-conjugated beads was washed twice with lysis buffer and then ~20µL of beads was added to remaining 900µL of protein samples. Samples were incubated with rocking at 37˚C. Beads were washed two times with 1 mL of lysis buffer, and then eluted with 100µL of 1X sample buffer (10% DTT) at 95˚C for 20 min. Eluted samples were then separated from beads with a magnetic stand. 30µL of IP sample and 10µL of input sample (1%) were run on an SDS-PAGE gel for western blotting.

Statistical analyses

All statistical analyses were performed using GraphPad Prism v10. Statistical tests and n values are described in the figure legends. Statistical significance was defined as $p<0.05$ in all experiments. Specifically, we used a one-way ANOVA with Dunnett's multiple comparisons test or a two-way ANOVA with a Tukey's multiple comparisons test where described. Only p-values less than cutoff are reported in figures.

Primers

Description	Sequence 5' to 3'	Usage
Protein-T25 (pNKT25) and Protein-T18 (pUT18)	TATGCTTCCGGCTCGTATG	sequencing
T18-Protein (pUT18C)	ATGTACTGGAAACGGTGC	sequencing
T25-Protein (pKT25) forward	GGTGACCAGCGGCGATTC	sequencing
T25-Protein (pKT25) reverse	GTGCTGCAAGGCGATTAAG	sequencing
T18-Protein (pUT18C) reverse	GGGCTGGCTTAACTATGC	sequencing/ onetaq
Protein-T18 (pUT18) reverse	AACAAGTCGATGCGTTCG	sequencing/ onetaq
Protein-T25 (pNKT25) reverse	GCGTTTGCGTAACCAGC	sequencing/ onetaq
E1A forward (5')	GTCGACTCTAGAGATGAGACATAT TATCTGCCA	cloning
E1A reverse (3')	GAGCTCGGTACCCGCTTACTGTAG ACAAACATGCC	cloning
DBP forward	GCCATTGCGCCCAAGAAGAA	qPCR
DBP reverse	CTGTCCACGATTACCTCTGGTGAT	qPCR
Tubulin forward	AGTTCTCCATTTACCCAGCA	qPCR
Tubulin reverse	TTCAGGGCTCCATCAAATCTC	qPCR
E1A forward	AGTGACGACGAGGATGAAGAG	RT-qPCR
E1A reverse	GTTCAGACACAGGACTGTAGAC	RT-qPCR
RPLPO forward	GCAGCATCTACAACCCTGAAG	RT-qPCR
RPLPO reverse	CACTGGCAACATTGCGGAC	RT-qPCR
VII-HA K3Q fwd	CAAGCAGCGCTCCGACCAACA	PCR Mutagenesis/ Recombineering
VII-HA K3Q rev	TTGGTCGGAGCGCTGCTT	PCR Mutagenesis/ Recombineering
VII-HA_K2A K3A_fwd	TGCTGCGGCCCCGCCAAACATC	PCR Mutagenesis/ Recombineering
VII-HA_K2A K3A_rev	GTGGGCTTGTACTCGGTCAT	PCR Mutagenesis/ Recombineering

Chapter 4: Divergence in function of protein VII in murine adenoviruses.

Abstract

Protein VII is highly conserved amongst human adenoviruses but is particularly divergent in different adenoviruses that infect different animals, such as murine adenovirus. In this chapter, I leveraged this divergence to interrogate the difference in function of protein VII from human and murine adenoviruses. I utilized a chimeric human adenovirus-5 that contains a murine adenovirus-1 protein VII (hereto referred to as mVII) to determine that mVII does not interact with the host protein HMGB1, but HMGB1 is still retained on chromatin during infection. Furthermore, I observed differing localization patterns of mVII in comparison to protein VII from HAdV-C5 (hereto referred to as hVII). Lastly, I demonstrate that the chimeric adenovirus has similar infection dynamics to the wild-type virus but produces less protein VII, which also results in a drop in infectious progeny production. These findings collectively illustrate the variance in protein VII function across distinct adenovirus species, which have adapted to different ecological niches.

Introduction

Murine adenovirus (MAdV) was first isolated in 1960, and there are currently three known serotypes of MAdV[219]. While MAdVs, like all adenoviruses, are genetically and physiologically similar to HAdVs, the two families of viruses differ in many aspects. The MAdV-1 genome is shorter at approximately 31 kb in length, while the HAdV genome is approximately 36 kb; however, it is structured the same as HAdVs[220,221]. MAdV contains the E1-E4 genes, a MLP, and late genes encoding the major and minor virion proteins, which have sequence and functional similarity to HAdVs. While HAdVs primarily infect epithelial cells, MAdV-1 largely infect endothelial cells and monocytes/macrophages[222–225]. MAdV-1 causes CNS infections and

A

```
                        Pre-peptide
                  P      Ac                    Ac
HAdV-5    1 MSILISPSNNTGWGLRFPSKMFGGAKKRSDQHPVRVRGHYRAPWGAHKRG
            ||||||||:||||||   .||:|||:||| :|||:||.::|| ||:::|
MAdV-1    1 MSILISPSDNTGWGLGT-GKMYGGARKRSAEHPVHVRSYWRAAWGSRNRR

                 P                 P
HAdV-5   51 RTGRTTVDDAIDAVVEEARNYTPTPPPVSTVDAAIQ--TVVRGARRYAKM
            |.. .:.:||    :|:. :   | | |      :   : .|| |: |::
MAdV-1   50 RVATVAAEDAEAPQLEDVAQAPATVPIVRRHRRRVGGSARTRGLRKSARV

HAdV-5   99 KRRRRRVARRHRRRPGTAAQRA--AAALLNRARRTGRRAAMR---AARRL
            :   | :.|      |:||  |  . |  | |  .|  |  |     ||
MAdV-1  100 RAAARAIVRA---VNGAAAAAAPTVPASANFAAMVGAIANARAAYRHRRS

                                                   P
HAdV-5  144 AAGIVTVPPRSRRRAAAAAAAAISAMTQGRRGNVYWVRDSVSGLRVPVRT
             |||  ||       .    :.    : |   . :|  .: .  :. ||
MAdV-1  147 RAGINPVPASRSTTRVRLPRTVRFHPSMGAFHRRWWRIHTRGRRKASVRR

HAdV-5  194 RPPRN
            |
MAdV-1  197 RRT--
```

B

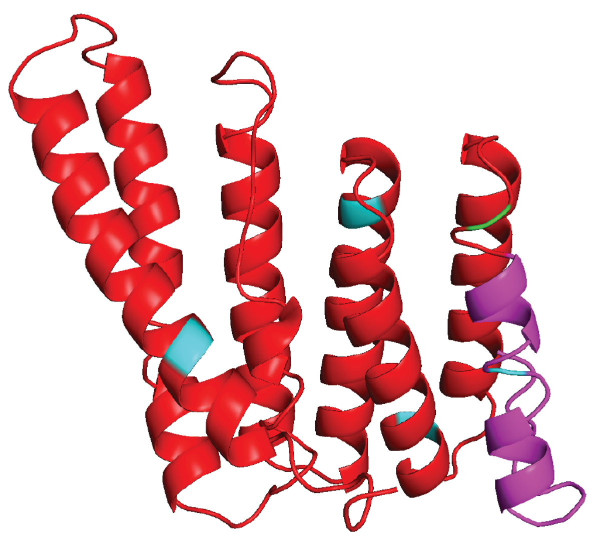

Figure 4.1: MAdV-1 protein VII is divergent from HAdV-5 protein VII. A) Amino acid sequence alignment of protein VII from HAdV-5 (top) and MAdV-1 (bottom). Location of known PTMs within HAdV-5 protein VII indicated above modified residues. Acetylation (Ac) in green, phosphorylation (P) in cyan, and pre-peptide is in magenta. A straight line (|) is conserved amino acid, a colon (:) is similar amino acid, a period (.) is semi-similar amino acid, and empty space is non-similar amino acid. **B)** I-TASSER prediction of MAdV-1 protein VII. Protein VII is in red, and color scheme is same as **A.**

encephalitis and can also cause respiratory infections and myocarditis[226–232]. MAdV-2 is primarily found within the GI tract, but causes no apparent disease in mice, and MAdV-3 has a primary tropism for cardiac tissue, but can also be pan-tropic, similar to MAdV-1[233–236]. While MAdV disease does not mimic that of HAdV, it can be used by virologists as a small animal model to understand adenovirus pathogenesis *in vivo*[222]. MAdVs are also used to study how host-pathogen interactions drive evolution of the virus and its host and understand the mechanisms behind these interactions.

MAdVs also encode protein VII, however, it is quite divergent from that of HAdVs. MAdV-1 protein VII (mVII) is approximately 39% similar to protein VII from HAdV-5 (Fig 4.1A). The majority of the similarity is within the N-termini of the proteins, especially the pre-portion of the proteins, which are close to identical. Despite this divergence in amino acid sequence, mVII is similar in length at 199 amino acids long while hVII is 198 amino acids, is highly basic, and positively charged (+39.4 for hVII and +36.5 for mVII) and packages with the MAdV genome within the core of the virion. The I-TASSER prediction software suggests that structurally mVII is similar to hVII, in that mVII consists of a bundle of seven to eight α-helices (Fig 4.1B)[58–60]. It is unknown if PTMs from hVII are also present on mVII, but many of the residues that are modified on hVII are conserved on mVII or contain residues nearby that are potentially modified (Fig 4.1). There is little known about the functions of mVII during infection, besides that it is packaged with the viral genome. Furthermore, the localization of mVII and whether it can distort host chromatin during infection has not been reported. Thus, studies with mVII will inform on how the different ecological niche and evolution of MAdVs have contributed to a divergence of function in protein VII within different adenoviruses.

In this chapter, we sought to better understand the functions of mVII during adenovirus infection and how it interacts with the host chromatin factor, HMGB1. We utilized a chimeric adenovirus containing the MAdV-1 protein VII gene in place of the native gene within the HAdV-

5 genome to characterize the function of mVII and compare the functions of mVII to hVII during infection. We observed that while mature mVII does not interact with HMGB1 by B2H and fractionation of transfected cells, during infection mVII does appear to have a modest interaction with HMGB1 by fractionation. This interaction mislocalizes HMGB1 and retains it on chromatin, similar to hVII. We also showed that mVII has different localization patterns during infection in comparison to hVII, frequently localizing to the nucleolus, but not to VRCs. We also determined that infection with the mVII chimera had similar infection dynamics to the WT HAdV-5 but produced less protein VII and less infectious progeny. Removing HMGB1 did not rescue titers, suggesting that HMGB1 is not the cause for reduced progeny. We used mass spectrometry to measure the amount of mVII that was packaged within purified virions and saw a reduction in the quantity of packaged mVII. Lastly, we observed that the reduction in packaged mVII had no impact on virion stability. In total, this study is the first to characterize functions of the murine adenovirus core protein and what role it has in adenovirus infection.

Results

MAdV-1 protein does not directly interact with HMGB1.

Since mVII is dissimilar to HAdV-5 protein VII (Fig 4.1A), we hypothesized that this would impact mVII's interaction with HMGB1. HMGB1 is a highly conserved protein amongst animals, and is 99% identical in humans and mice, with the only difference being two amino acids in the C-terminal tail. Since hVII binds the A-box of HMGB1, any difference in the interaction would be due to differences in hVII and mVII. First, we wanted to see if HMGB1 is released and elevated in mouse sera during MAdV-1 infection. We obtained serum samples from C57BL/6 mice that were either mock infected or infected with MAdV-1 and performed an ELISA to measure HMGB1 levels. Mice that were infected with MAdV-1 had elevated levels of HMGB1 in their sera in comparison to their uninfected counterparts (Fig 4.2A). These results suggest that HMGB1 is released during MAdV-1 infection.

Because HMGB1 levels are elevated in MAdV-1 infected mice, we hypothesized that HMGB1 is released during infection. Since we know hVII retains HMGB1 on chromatin during HAdV-5 infection, we predicted that mVII does not interact with HMGB1. We used a bacterial two-hybrid analysis to test if there was a direct interaction between mVII and HMGB1 and observed that mVII did not interact with HMGB1, while hVII does (Figure 4.2A, *of note, B2H was performed by K. Leung of Monica Guo's lab*). To confirm the result in eukaryotic cells, we transfected HeLa cells with mature hVII or mature mVII and fractionated the cells at 72 hours post transfection (same fractionation as Chapter 2). We observed that while hVII retains HMGB1 within the insoluble fraction, mVII was unable to do so, confirming what we observed in our B2H (Fig 4.2B). To verify this result in the context of infection and to observe the impact that HMGB1 may have on infection, we created chimeric adenoviruses via BAC-mediated recombineering that replaced hVII with mVII in the HAdV-5 genome, creating HAdV-5 mVII-HA. We infected A549 cells with HAdV-5 VII-HA and HAdV-5 mVII-HA and fractionated cell pellets at

24 hpi. As expected, HAdV-5 VII-HA retained HMGB1 in the insoluble fraction (Fig 4.2C). Surprisingly, a faint band of HMGB1 was noticeable within the insoluble fraction during HAdV-5 mVII-HA infection (Fig 4.2D). This could be due to several different factors. One, there is a weak

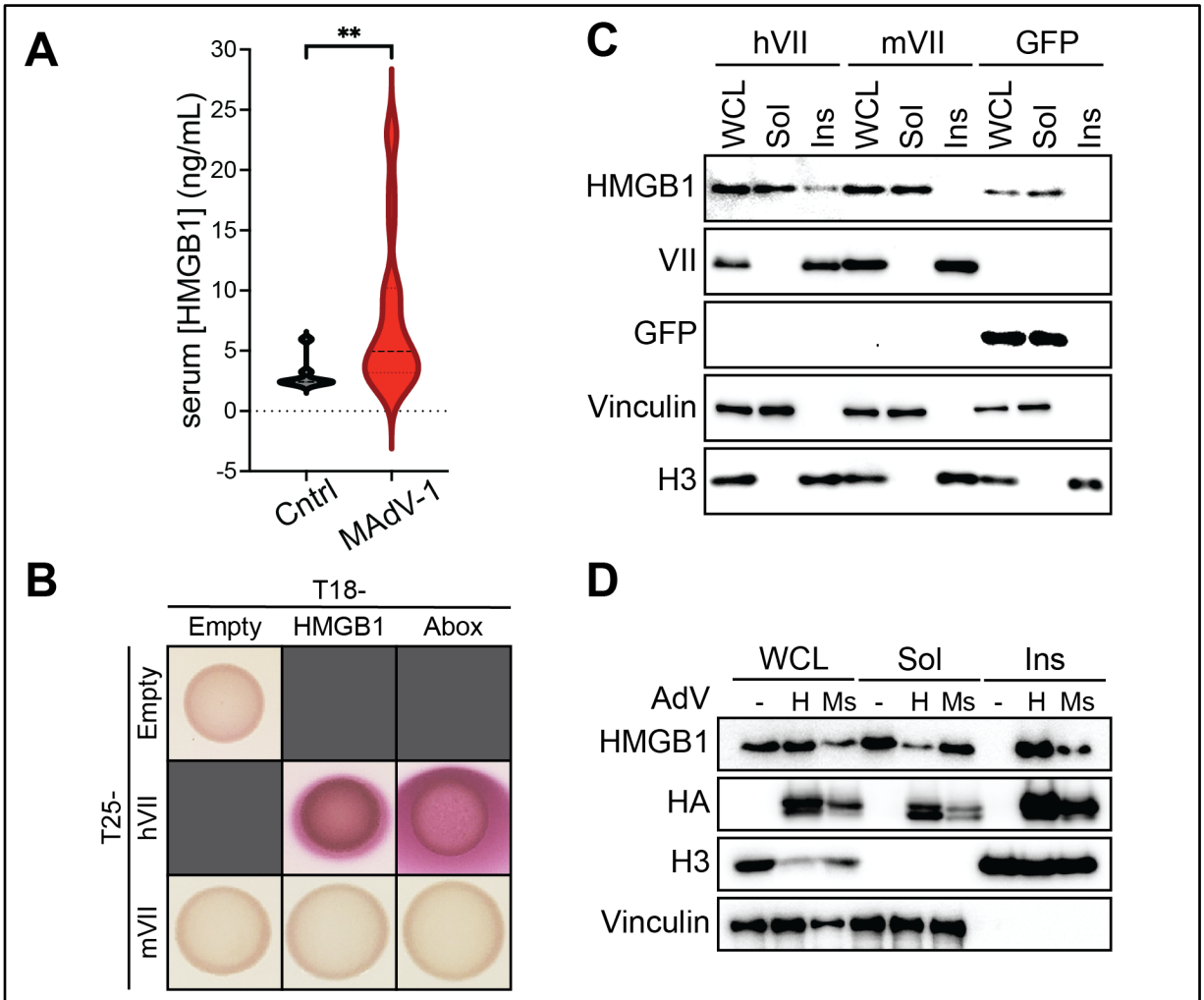

Figure 4.2: HMGB1 is elevated in mouse sera during MAdV-1 infection and mVII does not directly interact with HMGB1. A) ELISA of mock or MAdV-1 infected C57BL/6 mice showing increased concentration of HMGB1 in serum of MAdV-1 infected mice. ** is p<.01 by Mann-Whitney Test. N is 8 for mock, 23 for MAdV-1. **B)** Bacterial 2-hybrid analysis of interaction of protein VII from HAdV-5 (hVII) and MAdV-1 (mVII) with full length HMGB1 or Abox alone. *Performed by K. Leung.* **C)** Fractionation of HeLa cells transfected with hVII (lanes 1-3), mVII (lanes 4-6), or GFP (lanes 7-9), showing hVII retains HMGB1 in the insoluble fraction but mVII does not. Fractionated at 72 h post-transfection. N is three biological replicates. WCL is whole cell lysate, Sol is soluble fraction, Ins is insoluble fraction. **D)** Fractionation of A549 cells infected with HAdV-5 VII-HA (H), HAdV-5 mVII-HA (Ms), or mock infection (-) showing HMGB1 is retained in the insoluble fraction during infection with both viruses. N is three biological replicates.

interaction between mVII and HMGB1 during infection. Two, if there is no direct interaction between mVII and HMGB1, a separate aspect of HAdV-5 infection could retain HMGB1 within the insoluble fraction, such as a different viral protein. Lastly, a complex could be formed between mVII, host chromatin, and HMGB1 during infection, that retains HMGB1 within the insoluble fraction.

HMGB1 is mislocalized and retained on chromatin during HAdV-5 mVII-HA infection.

Because our fractionation during HAdV-5 mVII-HA infection supported a potential interaction between mVII and HMGB1, we hypothesized that mVII is likely mislocalizing HMGB1 within the nucleus as well. We used confocal microscopy to observe the distribution and localization of HMGB1 and mVII during HAdV-5 mVII-HA infection. In steady-state conditions, HMGB1 maintains a dispersed localization within the nucleus (see Chapter 2). During times of stress or infection, it is released from the nucleus and the cell. During infection with HAdV-5 VII-HA, HMGB1 colocalizes with hVII, and is retained on chromatin, preventing its release (Fig 4.3A). When we infected A549 cells with HAdV-5 mVII-HA, we observed that HMGB1 colocalized with mVII during infection (Fig 4.3A). Additionally, we frequently observed that mVII localized to large centers in the nucleus that we hypothesized was the nucleolus. Furthermore, HMGB1 was excluded from these centers (Fig 4.3A, white arrow). We quantified the number of cells that contained these “nucleolar” centers in both viruses. While the centers were uncommon during HAdV-5 VII-HA infection, over 60% of HAdV-5 mVII-HA infected cells contained them (Fig 4.3B). This suggests that the colocalization of mVII and HMGB1 is not as strong as HMGB1 with hVII or that HMGB1 is excluded from these large centers of mVII.

Since mVII was capable of mislocalizing HMGB1 within HAdV-5 infection, we next hypothesized that this interaction, like the hVII-HMGB1 interaction, would require chromatin. We repeated the IF microscopy experiment with a pre-extraction step (see Chapter 2). During mock infection, the soluble HMGB1 was no longer visible within the nucleus (Fig 4.3B). As expected, HMGB1 was still visible during infection with HAdV-5 VII-HA. HMGB1 was also observable

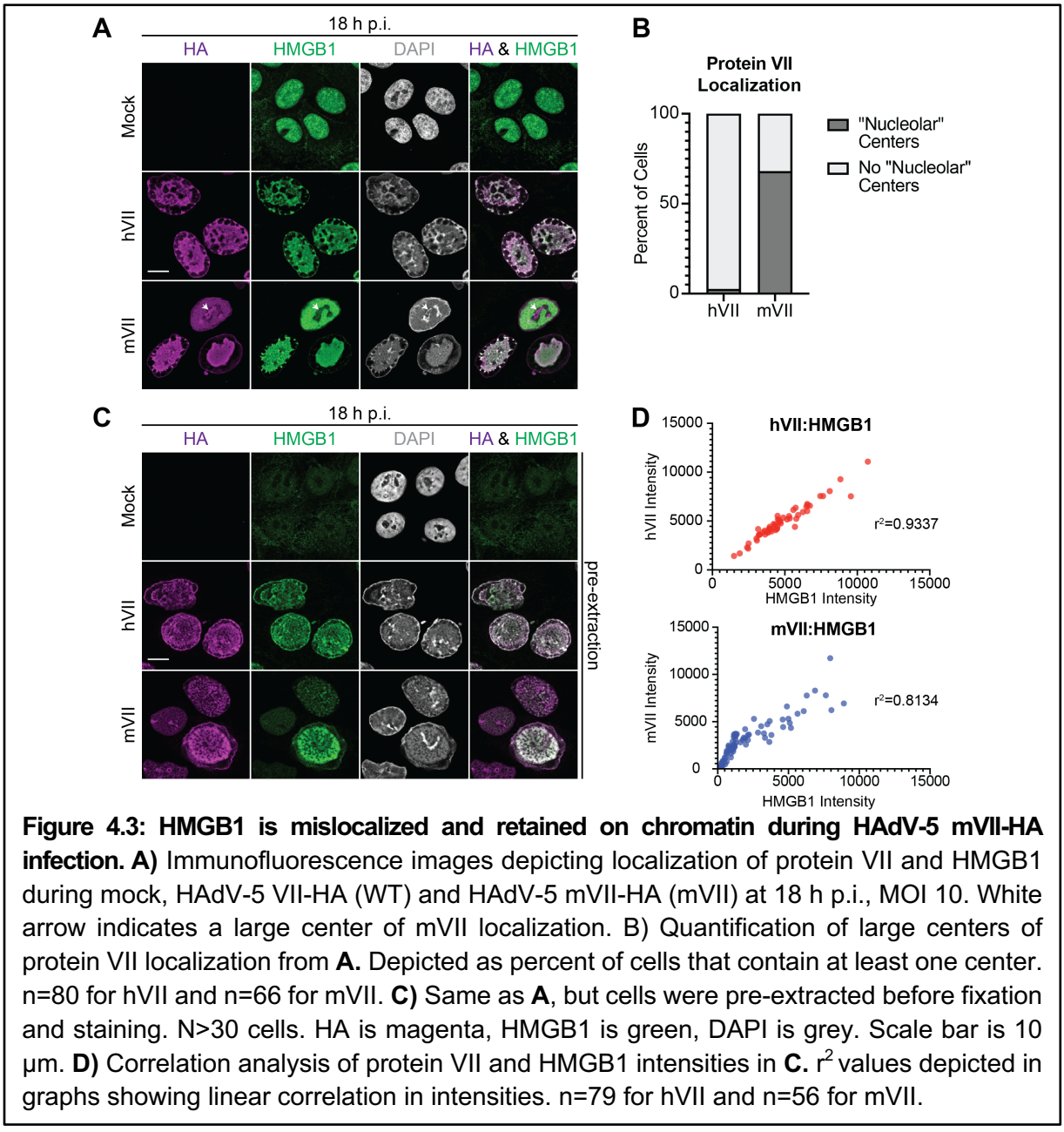

Figure 4.3: HMGB1 is mislocalized and retained on chromatin during HAdV-5 mVII-HA infection. A) Immunofluorescence images depicting localization of protein VII and HMGB1 during mock, HAdV-5 VII-HA (WT) and HAdV-5 mVII-HA (mVII) at 18 h p.i., MOI 10. White arrow indicates a large center of mVII localization. B) Quantification of large centers of protein VII localization from **A.** Depicted as percent of cells that contain at least one center. n=80 for hVII and n=66 for mVII. **C)** Same as **A**, but cells were pre-extracted before fixation and staining. N>30 cells. HA is magenta, HMGB1 is green, DAPI is grey. Scale bar is 10 µm. **D)** Correlation analysis of protein VII and HMGB1 intensities in **C.** r^2 values depicted in graphs showing linear correlation in intensities. n=79 for hVII and n=56 for mVII.

within nuclei during HAdV-5 mVII-HA infection, albeit the HMGB1 signal intensity was weaker in many cells when compared to the WT virus (Fig 4.3 B). The reduced HMGB1 signal intensity generally correlated with cells that had a reduced mVII signal intensity as well, likely due to lower expression levels of mVII within these infected cells. To confirm this observation, we measured and compared the intensity of protein VII to HMGB1 after pre-extraction and saw a strong linear correlation during HAdV-5 VII-HA (r^2=0.9337) and HAdV-5 mVII-HA infection (r^2=0.8134) (Fig 4.3D). Overall, the pre-extraction data suggests that this interaction does require the insoluble chromatin, and that HMGB1 is being retained on the insoluble chromatin during HAdV-5 infection, by hVII or mVII.

A separate observation that we made during HAdV-5 mVII-HA infection is the localization pattern of mVII. While hVII forms a dispersed and punctate appearance during infection, mVII would frequently accumulate in large centers throughout the nucleus that appeared nucleolar (Fig 4.3A white arrows and Fig 4.3B). To confirm if these large centers of mVII were in the nucleolus, we performed IF microscopy on cells infected with HAdV-5 VII-HA, HAdV-5 mVII-HA, or mock infected and co-stained with nucleolar resident protein nucleophosmin/B23. We observed that during mock infection, B23 would localize to the nucleolus (Fig 4.4A, top left). During HAdV-5 mVII-HA infection at 12 h p.i., mVII would localize to large, more intensely stained centers within the nucleus, that colocalized with B23 (Fig 4.4A, top right). During HAdV-5 VII-HA infection, both B23 and hVII were dispersed throughout the nucleus, with modest colocalization between the two proteins. At 18 h p.i., mVII continued to form these large centers and would also form more intense staining within the center of the nucleus with less at the nuclear periphery and still colocalizing with B23 (Fig 4.4A, bottom left). In hVII infected cells at 18 h p.i., hVII appeared more at the nuclear periphery while B23 localized more to the nuclear center in areas of low hVII staining. Finally, at 24 h p.i., both mVII and hVII were dispersed throughout the nucleus, with some areas of more punctate and intense

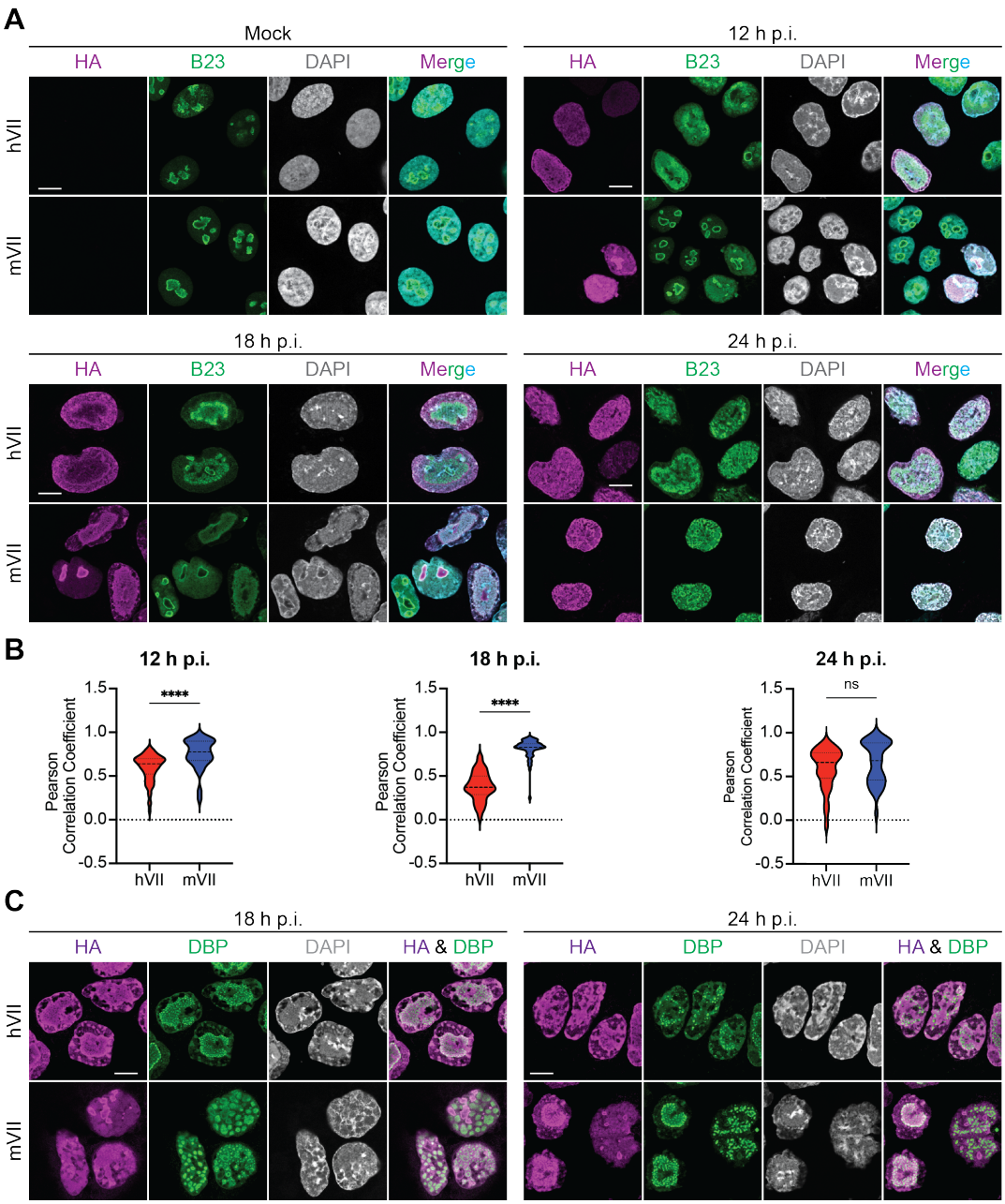

Figure 4.4: mVII colocalizes with nucleolar proteins during HAdV-5 infection. A) Immunofluorescence images of HAdV-5 VII-HA and HAdV-5 mVII-HA infection depicting localization of protein VII and B23 during infection at mock, 12, 18, and 24 h p.i. **B)** Quantification of colocalization of protein VII and B23 from **A** using Pearson Correlation Coefficient. n is 71, 45, and 59 for hVII at 12, 18, and 24 h p.i., respectively. n is 49, 59, and 33 for mVII at 12, 18, and 24 h p.i., respectively. **** is $p<0.0001$ and ns is not significant by Welch's t-test. **C)** Confocal microscopy of protein VII and DBP during infection at 18 and 24 h p.i. Protein VII (HA) in magenta, B23 and DBP in green, DAPI in grey. MOI is 10. Scale bar is 10 μm.

staining (Fig 4.4A, bottom right). At this time, B23 was also dispersed throughout the nucleus and appeared to somewhat colocalize with both hVII and mVII.

To confirm our observations from our microscopy data, we quantified the colocalization of hVII and mVII with B23 using the Pearson's Correlation Coefficient (PCC). At 12 and 18 h p.i. mVII had a significantly higher average PCC than hVII (Fig 4.4B). Interestingly, the average PCC of hVII with B23 started at 0.59 at 12 h p.i. before falling to 0.38 at 18 h p.i. and then rising back to 0.59 at 24 h p.i. (Fig 4.4 B). In contrast, the average PCC for mVII was 0.75 and .81 at 12 and 18 h p.i., until falling at 24 h p.i. to 0.66. By 24 h p.i., both viruses had similar average PCC values, likely because protein VII and B23 have dispersed throughout the entire nucleus leading to some colocalization (Fig 4.4B). B23 has been previously identified to interact with protein V and protein VII and is hypothesized to act as a chaperone of viral core proteins to help assemble viral chromatin during late infection and aid in maturation of viral progeny[237,238]. Perhaps mVII is less efficient at assembling on the viral genome, leading to the increased colocalization with B23 to assist in viral chromatin formation. While mVII does appear to be localizing to the nucleolus, during later stages of adenovirus infection, the nucleolus becomes distorted, and many nucleolar proteins are co-opted into viral replication centers (VRCs)[85]. Perhaps this distortion of the nucleolus is delayed in HAdV-5 mVII-HA infection, which is why we see the persistence of these large centers of mVII at 12 and 18 h p.i and colocalization with B23.

During late stages of infection, protein VII localizes near VRCs where DNA is actively replicated (marked by DBP in IF microscopy) but has not been observed to colocalize with DBP at sites of active DNA replication. Since mVII colocalized with the nucleolar protein B23, we hypothesized that mVII also localized to VRCs during infection. In HAdV-5 VII-HA infection, protein VII continued to localize near VRCs, but did not colocalize with DBP (Fig 4.4C). We observed a similar pattern during HAdV-5 mVII-HA infection, with mVII frequently localizing near

VRCs but not colocalizing with DBP. Higher resolution confocal microscopy would provide better quality images to fully determine the spatial relationship of hVII and mVII with VRCs, but this suggests that mVII, like hVII, is not localizing to sites of active genome replication. In total, this data shows that mVII has a different localization pattern than hVII during infection, and frequently localizes to the nucleolus, but not to VRCs.

HAdV-5 mVII-HA has similar infection dynamics to HAdV-5 VII-HA but produces less protein VII and fewer infectious progeny.

Thus far, we determined that mVII does not directly interact with HMGB1 but may have a potential indirect interaction during infection and that mVII has different localization patterns than hVII in infected cells. We hypothesized that these differences during HAdV-5 mVII-HA infection would have an impact on the infection cycle of HAdV-5 mVII-HA. We performed time course infections and collected samples to measure genome replication, protein production, and infectious progeny production. Western blot and qPCR data showed that protein production and genome replication, while slightly delayed in the chimeric virus, are similar to that of WT, and the mutant virus HAdV-5 VIIΔPTM-HA (Fig 4.5A-B). However, protein VII levels appeared much lower in HAdV-5 mVII-HA infection. Furthermore, the levels of preVII to mature VII seemed even in HAdV-5 mVII-HA infection, while in HAdV-5 VII-HA and HAdV-5 VIIΔPTM-HA infection there is more preVII present than mature VII. Strikingly, we did observe a 7-, 8.5-, and 3.8-fold reduction in viral titers of the chimeric virus by plaque assay at 24, 36, and 48 h p.i., respectively (Fig 4.5C). Since HMGB1 has potential roles in immune signaling, we hypothesized that the differences in binding HMGB1 by hVII and mVII contributed to the reduction in titers. To test this, we performed similar experiments in A549 cells that did not express HMGB1 via CRISPR-

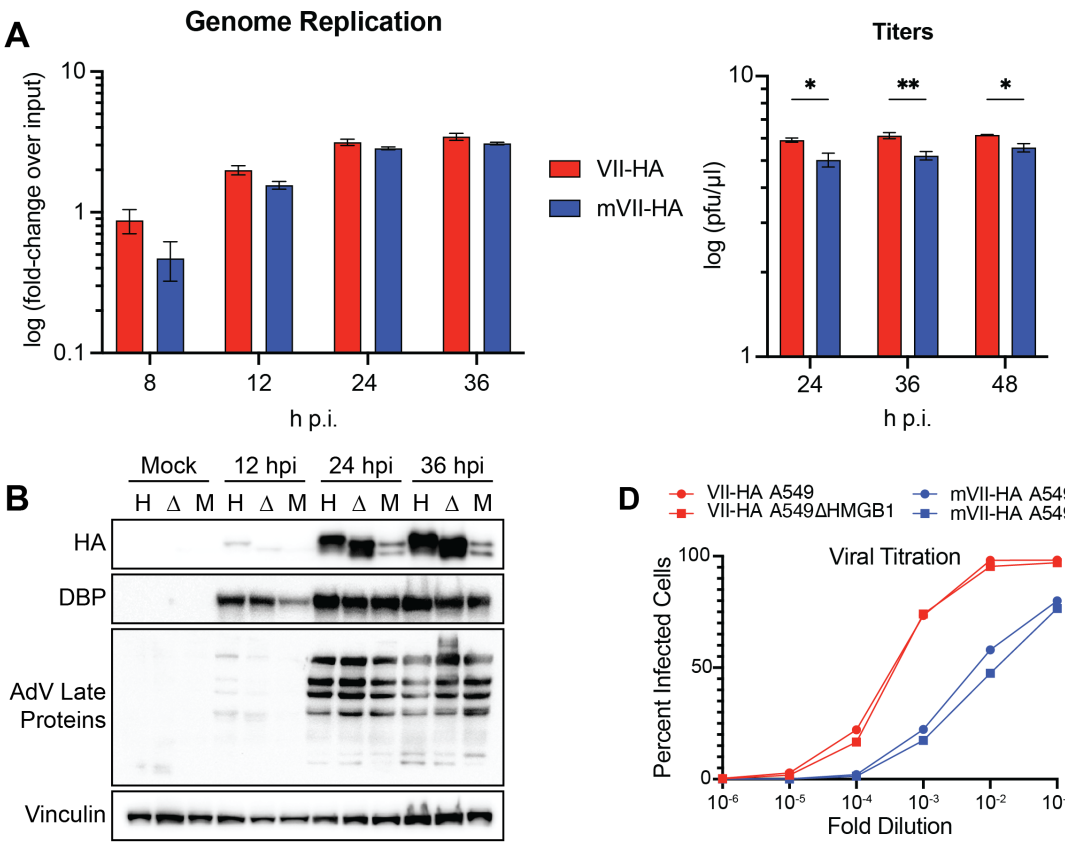

Figure 4.5: HAdV-5 mVII-HA produces less infectious progeny than HAdV-5 VII-HA. Time course infection of A549 cells with HAdV-5 VII-HA and HAdV-5 mVII-HA measuring genome replication by qPCR **(A)**, protein production by western blot **(B)**, and viral progeny production by plaque assay **(C)**. For **B**, HA is protein VII, DBP is early viral protein, AdV late proteins is virion capsid and core proteins, H is hVII, Δ is HAdV-5 VIIΔPTM-HA, and M isHAdV-5 mVII-HA. For **C**, ns is not significant, * is p<.05, ** is p<.01 by 2-way ANOVA with Tukey's multiple comparisons test. **D)** Viral titration of HAdV-5 VII-HA (red) and HAdV-5 mVII-HA (blue) collected from A549 cells (circles) or A549ΔHMGB1 cells (squares) at 36hpi. Virus titrated on A549 cells, and percent infected cells at 24hpi determined by flow cytometry. N of three biological replicates for each experiment.

Cas9 knockout[91,200]. Virus obtained from A549ΔHMGB1 cells was serially diluted and used to infect A549 cells. Infected cells were fixed at 24 h p.i., stained for a viral late protein, and the percentage of infected cells was quantified by flow cytometry. Surprisingly, we did not observe a change in titers from A549ΔHMGB1 cells in comparison to WT A549 cells (Fig 4.5D). This demonstrates that the reduction in titers for the chimeric HAdV-5 mVII-HA is not caused by the presence or absence of HMGB1.

HAdV-5 mVII-HA packages significantly less protein VII than HAdV-5 VII-HA.

While performing the western blots from our time course infections, we noticed that the early and late gene protein levels during HAdV-5 mVII-HA infection were comparable to that of the WT virus, but the protein levels of mVII were noticeably much lower. Since protein VII is essential for infection (see Chapter 1)[79], we hypothesized that due to reduced mVII protein production, less mVII is packaged, which would result in fewer infectious progeny being formed. To test this, we performed mass spectrometry on purified virions to quantify the amount of mVII present in virions. From the mass spectrometry data, we normalized the intensity Based Absolute Quantification (iBAQ) value for protein VII to the iBAQ value for hexon for each virus. From there, we set the HAdV-5 VII-HA value as 100% and normalized the HAdV-5 mVII-HA sample to the VII-HA sample. HAdV-5 mVII-HA virions had approximately 9% of the protein VII within the virion that HAdV-5 VII-HA virions contained, suggesting that the HAdV-5 mVII-HA virus contains significantly less protein VII (Fig 4.6A). While mass spectrometry was only performed on one viral prep, lower protein VII levels and lower viral titers have been observed by western blotting and plaque assay in multiple virus preps, suggesting that this is not unique

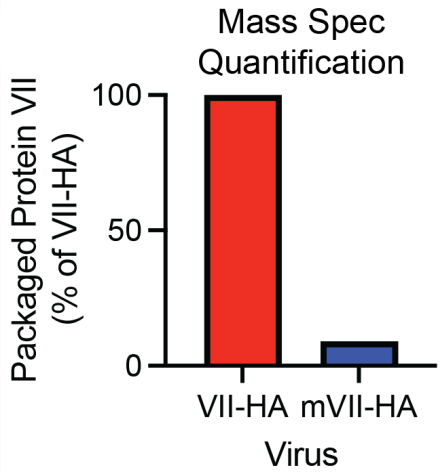

Figure 4.6: HAdV-5 mVII-HA virions have less packaged protein VII and a higher particle to PFU ratio. Quantity of packaged protein VII within HAdV-5 VII-HA and HAdV-5 mVII-HA virions, normalized as a percentage of HAdV-5 VII-HA. n=1 biological replicate

to an individual virus prep but an inherent phenotype of the virus. Protein VII is necessary to establish infection[79,80] and since less mVII is packaged, this would possibly explain why there is less infectious progeny being produced. It is possible that a threshold amount of protein VII is necessary to be packaged in order for the progeny to be infectious and that many of the progeny do not meet this threshold. This would suggest that some progeny package the standard ~800 copies of protein VII per virion, while some produce very little to none, making them non-infectious and explaining why the particle to pfu ratio is higher for HAdV-5 mVII-HA. However, it is possible that all viral progeny package ~10% of the standard 800 copies/virion, which would also cause less infectious progeny to form.

The diminished protein VII content within HAdV-5 mVII-HA virions does not result in reduced stability of HAdV-5 mVII-HA virions.

Previous studies determined that protein VII null virions are less mechanically and thermally stable than WT virions[80]. While the HAdV-5 mVII-HA virions still contain protein VII, our mass spectrometry experiments determined that there is considerably less mVII within the virions, which may further destabilize the capsid. Thus, we hypothesized that differences between the quantity of mVII and hVII within the virions may cause defects in capsid stability. To test if the HAdV-5 mVII-HA are less stable, we performed a thermostability assay, where purified virions are incubated with the fluorescent DNA dye SYBR, and the temperature is raised incrementally over a short period. As the capsid falls apart, the dsDNA genome is exposed to the solvent and DNA dye which will intercalate and fluoresce, giving off a measurable signal. The experiment provides a half-transition temperature (T_M), where approximately 50% of the capsids have fallen apart. The results from this experiment showed that the thermostability between the chimeric and WT virus were similar with only negligible differences in their T_M (46.22 $\pm$ 0.61˚C for WT and 45.77$\pm$0.45˚C for mVII) and is similar to values previously reported

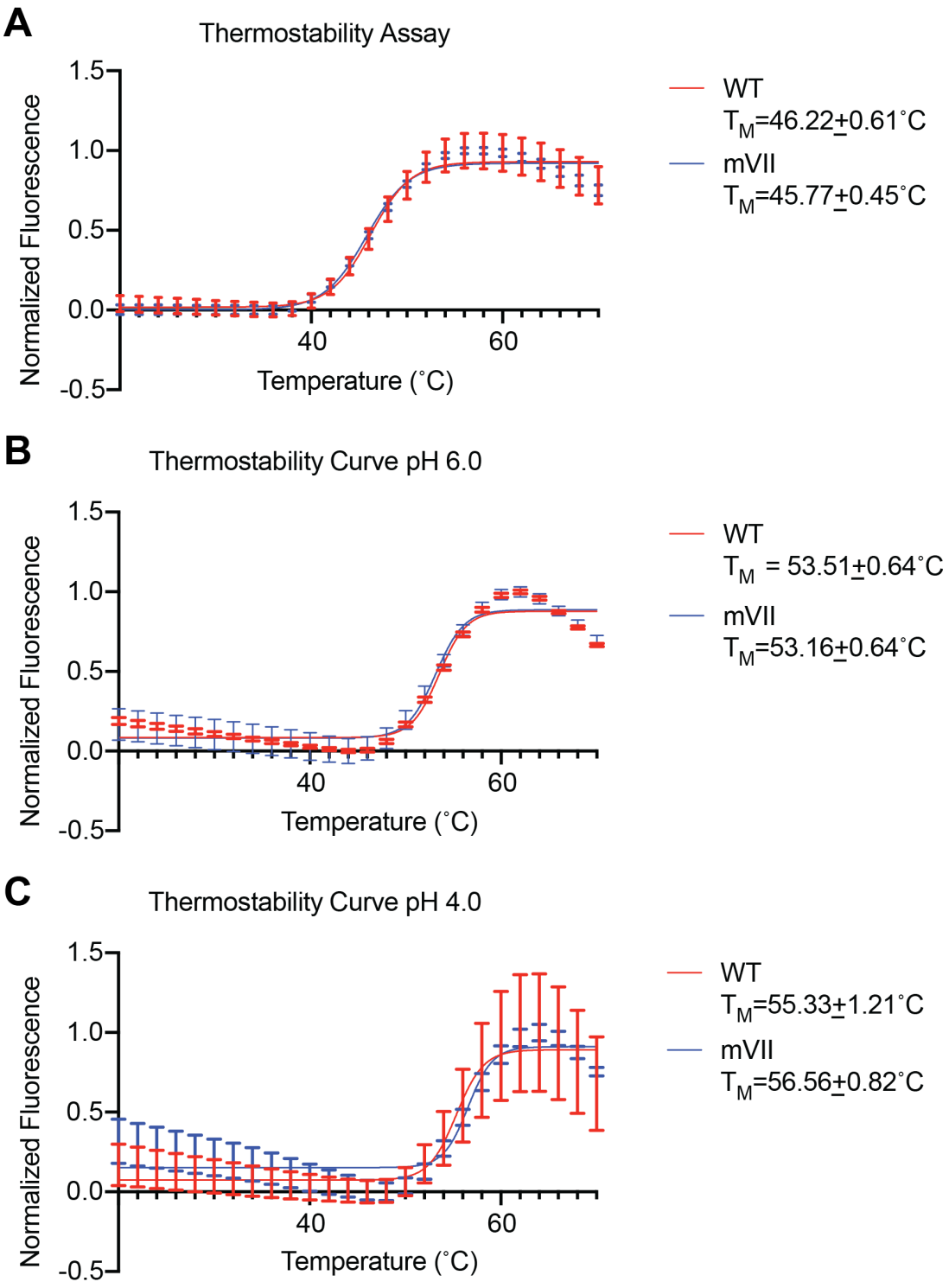

Figure 4.7: HAdV-5 mVII-HA thermal stability is similar to HAdV-5 VII-HA. Normalized thermostability curves of designated viruses at pH **A)** 7.4, **B)** 6.0, and **C)** 4.0. T_M value for each virus given in key of each graph. Line for each graph is line of best fit. Error bars represent SEM. N of 3 biological replicates for each virus in each graph.

(Fig 4.7A)[33]. Thus, even with less mVII-HA present, the chimera's capsids are not inherently less thermally stable than that of the WT virus.

The adenovirus virion begins to disassemble upon internalization and within the endosome. Acidification of the endosome is hypothesized to play a role in adenovirus disassembly and uncoating, and other studies have shown that acidification may impact the stability of the virion[81,239,240]. To test if the HAdV-5 mVII-HA capsid was more or less stable at acidic pHs compared to the HAdV-5 VII-HA capsid, we repeated the thermostability assay at the endosomal acidic pH of 6.0 and then a more extreme acidic pH of 4.0. We observed that acidification increased the thermostability of the virions and the T_M values were similar to that of previous reports (Fig 4.7 B-C)[239]. There was still no significant difference in the stability of the WT and mVII virions, suggesting that the mVII virion is not inherently more or less stable than the WT virion, even at extreme pHs and is likely not the cause for lower titers. Previous results found that at a physiological pH VII-null virions had a T_M approximately 3˚C lower than a WT virion. Here we show that even with much less mVII in the virion compared to hVII, there is not a significant difference in T_M values, suggesting that only a small fraction of protein VII is needed to stabilize the HAdV-5 capsid.

Discussion

In this study we sought to leverage the diversity of adenoviruses to better understand how the protein VII-HMGB1 interaction impacts infection. We showed that HMGB1 sera levels are significantly higher in MAdV-1 infected mice, in comparison to mock infected mice, suggesting that HMGB1 is released from cells and elevated in mice experiencing MAdV-1 disease (Fig 4.2A). We used a B2H and cellular fractionation to determine that protein VII from MAdV-1 does not directly interact with HMGB1 (Fig 4.2B) nor did mVII retain HMGB1 within the insoluble fraction of cells when transfected (Fig 4.2C). However, we found that during infection, mVII did retain a faint band of HMGB1 within the insoluble fraction (Fig 4.2D). We showed that HMGB1 frequently colocalizes with mVII during infection and is retained on the insoluble chromatin (Fig 4.3). We also observed by IF that mVII has a localization pattern distinct from that of hVII, and will colocalize with the nucleolar protein B23, but not VRCs (Fig 4.4). HAdV-5 mVII-HA had similar infection kinetics to HAdV-5 VII-HA but produced less infectious progeny (Fig 4.5 A-C), which was not rescued by knocking out HMGB1 (Fig 4.5D). We also observed that protein levels of mVII were significantly lower during infection by western blot (Fig 4.5B), and that there was significantly less mVII within purified virions, as quantified by mass spectrometry (Fig 4.6). Lastly, the reduction in mVII levels had no adverse impact on virion thermostability, which suggests that the drop in titers is not due to unstable virions (Fig 4.7).

Since mVII is so dissimilar to hVII (Fig 4.1) and because we measured elevated HMGB1 serum levels during MAdV-1 infection, we were surprised that fractionation of infected cells contradicted the results from our B2H and fractionation of transfected cells (Fig 4.2). One possible reason may be that our transfection of mVII and B2H did not contain the full length mVII protein, but only the truncated mature protein. These results suggest that there is possibly a weak interaction taking place between mVII and HMGB1, possibly facilitated by the presence

of the pre-peptide. Future experiments will test of pre-mVII is capable of directly binding HMGB1 or retaining it on chromatin outside of infection.

Because hVII is capable of mislocalizing HMGB1 within the nucleus, we also tested if HMGB1 was mislocalized during HAdV-5 mVII-HA infection by IF microscopy. We were again surprised to see that it was mislocalized (Fig 4.3) contradictory to our B2H and transfection fractionation (Fig 4.2A-B), but in agreement with our infection fractionation (Fig 4.2C). Furthermore, when we pre-extracted cells, we still observed a retention of HMGB1 within the nucleus and mislocalization throughout the nucleus, albeit the staining of HMGB1 appeared weaker than in HAdV-5 VII-HA infection (Fig 4.3C-D). These results suggest that HMGB1 is being retained on the insoluble chromatin during infection. It is possible that an adenovirus protein besides mVII is facilitating this retention. Further characterizing the potential interaction between mVII and HMGB1 would inform if mVII is retaining HMGB1 on chromatin.

Since mVII is potentially interacting with HMGB1, we hypothesized that this would have an impact on HAdV-5 infection. We tested infection dynamics and found that there was no significant difference in viral genome replication and protein production with the mVII and WT viruses (Fig 4.5 A-B). However, we did observe that HAdV-5 mVII-HA produced ~10 fold less infectious progeny and had a reduced protein level of mVII during infection by plaque assay (Fig 4.5B-C). Knocking out HMGB1 did not rescue viral titers, suggesting that HMGB1 is not the cause for HAdV-5 mVII-HA being less infectious (Fig 4.5D). It is possible that another host factor is the cause for reduced titers during HAdV-5 mVII-HA infection. Furthermore, HMGB2 and HMGB3 are still present during infection, and the HMGB proteins have some overlapping functions which may be contributing to the reduced titers[113,117]. Another possibility is that the lower protein levels of mVII are the cause for less infectious progeny production. Our mass spectrometry quantification data showed that the HAdV-5 mVII-HA virions had approximately 10-fold less protein VII than HAdV-5 VII-HA virions (Fig 4.6). Prior quantitative mass spec on

adenovirus virions has shown that there are approximately 800 copies of protein VII per virion[84]. Whether each HAdV-5 mVII-HA progeny virion contains ~10% of the standard quantity, or if some virions contain ~800 mVII molecules while the rest contain a negligible amount is unknown and future studies will attempt to answer this question.

To further explore what is causing the drop in viral titers, we hypothesized that the reduction in mVII within virions impacted virion stability. Protein VII has been previously shown to contribute to the stability of the particle, and VII null virions are less mechanically and thermally stable than the wild-type particle[80]. Our thermal stability assays showed that the presence of mVII within the virions did not adversely affect virion thermostability at neutral or acidic pHs (Fig 4.7). This suggests that protein VII packaging is a conserved function, and while the core of the HAdV and MAdV virions is likely different, the role of protein VII within them is potentially similar.

The cause for the lower mVII protein levels during infection is unknown, but one hypothesis is that mVII is not being transcribed efficiently. However, since adenovirus transcribes its late genes as one long transcript and then alternatively splices out individual genes and the protein levels of other later proteins are comparable to the WT virus, this hypothesis seems unlikely (Fig 4.5B)[54,55]. A more plausible hypothesis is that mVII is unstable in human cells during infection. The nucleolus has been reported to be a phase-separated compartment, where misfolded nuclear proteins aggregate to be refolded or eventually degraded if they do not refold properly[241]. Since we observed that mVII frequently colocalizes with the nucleolar resident protein B23 (Fig 4.4A-B), it may be that it is localizing to the nucleolus to be refolded or degraded. It is also possible that mVII naturally localizes to the nucleolus during MAdV infection, and this aspect of mVII function is different than that of hVII. An alternative hypothesis is that mVII is selectively targeted for degradation by some host cell factor. Treating cells with a proteasome inhibitor, such as MG132, may potentially confirm this

hypothesis and recover mVII protein levels during infection. Future studies will aim to ‘rescue’ mVII protein levels, so that it’s functions can be studied during infection. In total, our work with HAdV-5 mVII-HA has led to many interesting insights into the conservation and divergence of the various functions and interactions of protein VII in human and murine adenoviruses.

Methods and Materials

Cell culture and viruses

A549 cells were purchased from ATCC and A549ΔHMGB1 were previously engineered by CRISPR-Cas9 knockout[91]. Both cell types were cultured using standard methods in Kaighn's modification of Ham's F-12 medium (F-12K) containing 100 U/ml of penicillin and 100 mg/ml of streptomycin and supplemented with 10% fetal bovine serum (FBS). HEK293Q and HEK293β5 cells were purchased from ATCC and cultured using standard methods in Dubelco's Modified Eagle Medium (DMEM) containing 100 U/mL of penicillin and 100 mg/ml of streptomycin and supplemented with 10% fetal bovine serum (FBS).

All infections were performed using a multiplicity of infection of 10 plaque forming units per cell. HAdV-5 mVII-HA was generated by bacterial recombineering with an E3-deleted Ad5 bacterial artificial chromosome[179]. Briefly, protein VII from MAdV-1 was PCR amplified with 50bp overhangs on the 5' and 3' ends that were homologous to the regions directly upstream and downstream of protein VII in HAdV-5. MAdV-1 protein VII was then introduced into the HAdV-5 genome via recombineering. An HA-tag was later added to the c-terminus of mVII in HAdV-5 mVII through another round of recombineering. Successful recombineering was verified through restriction digest and sanger sequencing. The Ad5 genomes were linearized by PacI digest, transfected into HEK293β5 cells, amplified by repeated passaging, and then virus was extracted by freeze-thawing cell pellets. Extracted virus was purified with two rounds of ultracentrifugation in a cesium-chloride gradient, and then stored in a 20% glycerol buffer at -80˚C. Viral titers were determined by flow cytometry and plaque assay.

ELISA

HMGB1 ELISAs were performed with the Chondrex HMGB1 detection kit using manufacturers protocol. Serum samples were provided by Jason Smith Lab at UW Microbiology. Serum

samples were obtained from mock infected or MAV-1 infected C57BL/6 mice. Serum was gathered from mice that met euthanasia criteria at 11-12 days post infection.

Bacterial growth conditions and chemical treatments.

Escherichia coli strains were grown in LB (5 g / L NaCl, 10 g / L tryptone, 5 g / L yeast extract) at 37 °C with shaking at 200 rpm. Antibiotics were supplemented as needed (carbenicillin: 50 µg / mL liquid / 100 µg / mL plate, and kanamycin: 30 µg / mL / 50 µg / mL). Optical density was measured at 600 nm using an Eppendorf BioPhotometer. For bacterial two-hybrid assays, *E. coli* BTH101 was grown in M63 minimal media (0.4 g / L ammonium sulfate, 2.72 g / L monopotassium phosphate, 0.1 mg / L ferrous sulfate heptahydrate [pH 7.0], 1 mM magnesium sulfate, 0.2 % maltose, 0.4 % glucose, and 0.0001% vitamin B1) supplemented with carbenicillin, kanamycin, and 1 mM IPTG for 48 hours at 30°C with shaking before spotting on MacConkey agar (BD Difco) plates.

Bacterial two-hybrid

Plasmids (pUT18, pUT18C, pKT25, and pKNT25) containing fusion constructs of HMGB1, protein VII, and variants were co-transformed into the B2H assay strain BTH101. Four replicates from each transformation were picked, grown in M63 minimal media for 48 hours, and spotted on MacConkey agar plates supplemented with carbenicillin, kanamycin, 1% maltose, and 1mM IPTG. Plates were incubated at 30 °C and imaged after 72 hrs. Interaction between protein VII and HMGB1 and A-box was probed in four orientations (e.g., T25-VII with T18-HMGB1, T25-VII with HMGB1-T18, VII-T25 with T18 HMGB1, and VII-T25 with HMGB1-T18).

Cellular fractionation

The cellular fractionation protocol was adapted from Suzuki *et al.* [181]. Briefly, cell pellets were thawed on ice for 5 minutes and then resuspended in 900µL of ice-cold 0.5% NP-40. 300 µL was added to 100µL of 4X sample buffer as whole cell lysate. The remaining 600µL was incubated at room temperature for 5 minutes and then centrifuged at 13,000 RPM for 30

seconds. 300μL of the supernatant was added to 100μL of 4X sample buffer as the soluble fraction. The remaining 300μL was discarded and the pellet was resuspended in 900μL of ice-cold 0.5% NP-40 and incubated at room temperature for 5 minutes. The mixture was centrifuged at 13,000 RPM for 30 seconds, the supernatant was discarded, and the remaining pellet was resuspended in 200μL of 1X sample buffer as the insoluble fraction. All three fractions were boiled at 95˚C for 20 minutes.

Western blotting

Samples were run on 12% poly-acrylimide gels or 4-20% and then transferred to nitrocellulose. The membranes were blocked in 5% milk in TBST, and then probed with primary antibodies at 4˚C overnight. Blots were then washed in TBST buffer for 30 minutes, probed with secondary antibodies for one hour, washed in in TBST buffer for 30 minutes, developed with Clarity Western ECL Substrate, and then imaged with a Biorad ChemiDoc MP Imaging System.

Immunofluorescence microscopy

Immunofluorescence microscopy was performed using standard methods as previously described [94]. Briefly, cells were seeded on poly-L-lysine coated coverslips in a 24-well plate. Cells were infected with Ad5, and coverslips were collected at 18 hours post infection and fixed with 4% paraformaldehyde. After fixation, cells were permeabilized with 0.5% Triton-X, and blocked with 3% BSA. Cells were incubated with primary antibodies for 1 hour, washed three times in PBS, incubated with secondary antibody and DAPI for 1 hour in the dark, and then washed three times in PBS. Coverslips were then mounted on slides with ProLong Gold Antifade Mountant (Thermo Fisher Scientific), and then allowed to dry overnight. High resolution confocal microscopy was performed with a Leica Stellaris Confocal Microscope using a 63x oil objective.

Nuclear pre-extraction

Cells were prepared for immunofluorescence microscopy as stated above. Before fixation, cells were treated with nuclear pre-extraction buffer (20mM Hepes, 20mM NaCl, 5mM $MgCl_2$, 1mM DTT, 0.5% NP-40, 1X phosphatase inhibitor and 1X protease inhibitor) for 20 minutes on ice. After this treatment, cells were washed with PBS and then fixation with paraformaldehyde and the staining process proceeded as stated above.

IF Quantification

For the quantification of the large protein VII centers in Fig 4.3A, images were blind scored by hand on whether an infected cell contained at least one of the large protein VII centers. For the quantification comparing intensities of protein VII to HMGB1 in Fig 4.3 C, images were analyzed by a CellProfiler pipeline that quantified the intensities via integrated density of each signal within the nucleus. These values were plotted against each other (hVII to HMGB1 and mVII to HMGB1) in GraphPad Prism and a correlation analysis was performed to obtain the r^2 value. For the quantification of colocalization of hVII and mVII to B23, images were analyzed in Fiji using the Coloc2 plugin. Briefly, a DAPI stained image was used to determine a region of interest (ROI). The ROI was used with the protein VII and B23 stained images with the Coloc2 plugin on Fiji. Pearson correlation coefficients were recorded and plotted in GraphPad prism. Only cells with visible protein VII staining were selected to be analyzed by Coloc2.

qPCR

For qPCR, gDNA was extracted from cells with Qiagen QIAamp DNA kit. Extracted gDNA was normalized to 50ng/uL and then used for qPCR with viral DNA with primers targeting DBP and cellular tubulin (primers in table below) on a BioRad CFX384 Real-Time System thermocycler with the following procedure (95˚C for 3 minutes, 40 cycles of 95˚C for 10 seconds, 60˚C for 30 seconds, and plate fluorescence read, followed by 65-95˚C with 0.5˚C/cycle and holding for 5 seconds).

Plaque assays

Cell pellets from time course infections of A549 cells were collected at 24, 36, and 48 hpi. Cell pellets were resuspended in 100µL of PBS, freeze-thawed 4x, pelleted in a table-top centrifuge at max speed, and virus containing supernatant was collected for plaque assays. Plaque assays were performed on HEK293Q cells. Cells were seeded in 6-well plates, and then infected the next day with serial dilutions of virus samples, and overlayed with a 4% SeaPlaque agarose overlay. Plates were incubated at 37˚C until plaques developed. The agarose overlay was dissolved and cells were fixed by incubating with a 10% trichloroacetic acid solution at room temp for 30 minutes, and then stained with crystal violet. Plaques were counted by eye.

Viral titration

A549 and A549ΔHMGB1 cells were infected for with HAdV-5 VII-HA or HAdV-5 mVII-HA at an MOI 10. At 36 hpi, cell pellets from infections were collected, suspended in 100 µL of PBS, and freeze-thawed four times to release the virus, centrifuged at max speed, and then the supernatant containing virus was transferred to new tubes. Virus from infections was then titrated out on A549 cells at 10-fold dilutions, and infectious were halted at 24hpi by fixation with ice-cold 90% methanol for 30 minutes. Cells were stained with the monoclonal 8C4 antibody recognizing adenovirus hexon protein, and then stained with alexa-flour 488, both for 1 hour at room temp in the dark. Cells were suspended in 300 µL of FACS buffer, and then counted by flow cytometry with the BD Canto II. FlowJo software was used for gating and calculating the percentage of infected cells at each dilution, by positive 8C4 staining. The percent positive cells were plotted against fold-dilution in GraphPad Prism.

Mass Spectrometry

Purified HAdV-5 VII-HA and HAdV-5 mVII-HA virions were digested by chymotrypsin, analyzed on the Thermo Eclipse.Label free quantification (LFQ) was performed to calculate the abundances for each peptide and protein. Protein abundance was determined from the sum of

the peptide abundances for that protein, which are determined from the peak areas from the mass spectra data.

Thermostability Assays

Approximately $5x10^9$ particles of HAdV-5 VII-HA or HAdV-5 mVII-HA were suspended in PBS buffer and incubated overnight at 4˚C. For acidic pHs, PBS was buffered with 1M HCl to reach indicated pH. 1000X SYBR green was added to the virus mixture at a 1:1000 dilution and then the mixture was incubated in a BioRad CFX384 Real-Time System thermocycler. The sample was equilibrated at 20˚C for five minutes before the temperature was increased from 20˚C to 70˚C, with fluorescence readings every 2˚C after holding for 0.5 min for equilibration. Fluorescence values were 0,1 normalized and plotted in GraphPad Prism, with a line of best fit and T_M calculated for each line.

Antibodies

Commercially available antibodies were purchased through Abcam (GFP [ab290], HMGB1 [18256], H3 [ab1791], B23 [ab10530], HA tag [ab9110], Adenovirus Late Proteins/Anti-Adenovirus Type 5 [ab6982]), Sigma-Aldrich (Vinculin [V9131]). DBP antibodies were a generous gift from the Levine lab [183]. Secondary antibodies used for immunoblotting were obtained from Jackson ImmunoResearch (115-035-003 and 111-035-045). Secondary antibodies for immunofluorescence microscopy were obtained from Thermo Fisher Scientific (A-11011, A-11001).

Statistical analyses

All statistical analyses were performed using GraphPad Prism v10. Statistical tests and n values are described in the figure legends. Statistical significance was defined as $p<0.05\%$ in all experiments. Specifically, we used a two-way ANOVA with Tukey's multiple comparisons test, Welch's t-test, and correlation analysis where described. Only p-values less than cutoff are reported in figures.

Plasmids

Description	Use
DA0045 HAdV-5 VII-HA	Transfection Fractionation
DA0116 MAdV-1 VII-HA	Transfection Fractionation
pUT18	Bacterial Two-Hybrid
pUT18C	Bacterial Two-Hybrid
pKT25	Bacterial Two-Hybrid
pKNT25	Bacterial Two-Hybrid

Primers

Description	Sequence 5' to 3'	Use
VII-HA_50bphomology-fwd	TGGGCATAGTCTCGC	Recombineering sequencing
VII-HA_50bphomology_rev	GCCGCTGGATACATAC	Recombineering sequencing
mVII_AddPre_Fwd	ATGAGTATTTTGATCTCGCCCAGC GACAACACCGGTTGGGGCTTGG GGACGGGTAAAATGTACGGCGGT GCTAGAAAGAGATCTGCCGA	recombineering
HATag_Rev	CTAAGCGTAATCTGGAACATCG	recombineering
mVII_Addhomology_Fwd	TGGGCATAGTCTCGCCGCGCGTC CTATCGAGCCGCACTTTTTGAGC AAGCATGAGTATTTTGATCTCGCC	recombineering
mVII_Addhomology_Rev	GCCGCTGGATACATACAACAGTA CGAGTCTAAGTAGTTTTTTCTTGC AATCTAAGCGTAATCTGGAACAT	recombineering
Ad5 DBP qPCR FP	GCCATTGCGCCCAAGAAGAA	qPCR
Ad5 DBP qPCR RP	CTGTCCACGATTACCTCTGGTGA T	qPCR
Tubulin gDNA qPCR 2 FP	AGTTCTCCATTTACCCAGCA	qPCR
Tubulin gDNA qPCR 2 RP	TTCAGGGCTCCATCAAATCTC	qPCR
Protein-T25 (pNKT25) and Protein-T18 (pUT18)	TATGCTTCCGGCTCGTATG	sequencing
T18-Protein (pUT18C)	ATGTACTGGAAACGGTGC	sequencing
T25-Protein (pKT25) forward	GGTGACCAGCGGCGATTC	sequencing
T25-Protein (pKT25) reverse	GTGCTGCAAGGCGATTAAG	sequencing
T18-Protein (pUT18C) reverse	GGGCTGGCTTAACTATGC	sequencing/onetaq
Protein-T18 (pUT18) reverse	AACAAGTCGATGCGTTCG	sequencing/onetaq
Protein-T25 (pNKT25) reverse	GCGTTTGCGTAACCAGC	sequencing/onetaq
mouse protein VII forward (5')	GTCGACTCTAGAGGGTATGGCTA GAAAGAGATCTGC	cloning
mouse protein VII reverse (3')	GAGCTCGGTACCCGAGTTCTACG ACGACGCACAGAG	cloning

Chapter 5: Discussion and Future Directions

Viruses must interact with the host environment in order to establish infection and produce infectious progeny. Many nuclear-replicating viruses have have evolved to interact with chromatin and chromatin associated proteins. These virus-host interactions are vital for either the success of the virus or for the host to inhibit and prevent further infection. Therefore, it is important that we understand how viruses interact with their environment, so that we may improve strategies for combatting viruses and the diseases they cause. Moreover, viruses such as adenovirus are frequently used as vectors for vaccines, gene-therapy, and within research. Understanding how specific viral proteins function and interact with the cellular environment can help improve their use as tools within medicine and scientific research. In this thesis, I have addressed how adenovirus utilizes the histone-like core protein, protein VII, to hijack host chromatin for viral benefit and how protein VII function has diverged in different vertebrate adenoviruses. In **chapter 2**, I characterized how protein VII interacts with the chromatin-associated and alarmin protein, HMGB1, and how this promotes inhibition of the Type-I interferon response. In **chapter 3**, I described how PTMs on protein VII may impact its function during early and late stages of infection and what impact this has on adenovirus infection. Lastly, in **chapter 4**, I utilized a chimeric human adenovirus with a murine adenovirus protein VII to study how divergent evolution of human and murine adenovirus has altered protein VII function. Furthermore, I examined how divergence between hVII and mVII impacts protein VII's interaction with HMGB1, and what effect this has on adenovirus infection. These projects have furthered our knowledge on protein VII function and how protein VII contributes to adenovirus infection.

How does protein VII inhibit expression of interferon-β, what host factors contribute to this phenotype, and is this specific to interferon-β?

In chapter two, we discovered that expression of protein VII alone was sufficient to suppress expression of interferon-β (IFNβ), and we measured an approximate three-log reduction in expression by RT-ddPCR. In this study, we did not explore the mechanism of how protein VII is repressing IFNβ expression, which remains an important open question to be answered. We stimulated the Type-I Interferon response by treating cells with poly(dA:dT), a dsDNA agonist, that is likely stimulating the cGAS-STING response or some other cytoplasmic dsDNA sensor in our experiments[242–244]. Activation of the Type-I Interferon response can occur through multiple different pathways through recognition of different PAMPs, such as RIG-I, MDA5, or TLR3 with foreign RNA or TLR4 with LPS[245–248]. Since we only tested inhibition of IFNβ with dsDNA, it would be prudent to test if protein VII can prevent IFNβ expression with a different type of agonist, such as poly(I:C) or LPS. It is possible that expression of protein VII prevents activation of cGAS-STING alone, implying that it is preventing the recognition of dsDNA in the cytoplasm. This is plausible, since protein VII coats the genome within the virion, and may prevent the recognition of the dsDNA genome by cGAS during trafficking to the nucleus when the capsid is partially disassembled, and the genome is exposed to the cytoplasm. Alternatively, if protein VII blocks IFNβ expression when cells are stimulated with poly(I:C) or LPS, this would suggest that it is not targeting a specific activation pathway of the Type-I Interferon response, but possibly a downstream step within the Type-I Interferon signaling pathway. Furthermore, since protein VII exclusively localizes to the nucleus, except during entry and for brief periods after it is initially translated, it is unlikely that it is inhibiting a cytoplasmic portion of the initiation of the Type-I Interferon response. Therefore, we would expect protein VII to inhibit IFNβ expression when cells are treated with different immunostimulants than poly(dA:dT).

Since protein VII localizes exclusively to the nucleus, it is most likely that protein VII is inhibiting expression of IFNβ within the nucleus. One hypothesis is that protein VII sequesters transcription factors of *IFNβ1*, the gene that encodes IFNβ, such as IRF3, away from the IFNβ locus, preventing transcription[249–252]. Immunofluorescence microscopy would inform where IRF3 localizes within the nucleus and whether it colocalizes with protein VII or the IFNβ locus, which can be visualized with fluorescence in-situ hybridization (FISH). An alternative hypothesis is that protein VII blocks transcription of *IFNβ1*by reducing its accessibility through distortion of host chromatin. The current model for how protein VII distorts chromatin is that protein VII competes with the linker histone H1 for access to the nucleosome[94]. HMGB1 is an H1 antagonist and competes with H1 for access to the linker DNA, which HMGB1 can bind to and bend to displace H1[102,253–255]. Thus, protein VII utilizes HMGB1 to gain access to chromatin by displacing H1[94]. If protein VII is inhibiting IFNβ expression through chromatin distortion, then an interesting hypothesis would be that protein VII utilizes the DNA bending property of HMGB1 to help inhibit IFNβ expression. We can test this hypothesis by repeating the RT-ddPCR experiment with our HMGB1 DNA binding mutant cell line. This cell line has HMGB1 present that protein VII interacts with but has a reduced capacity to bind and bend DNA. If we observe similar results to that of the A549ΔHMGB1 cells, then this would suggest that the DNA bending function of HMGB1 is playing a role in inhibiting IFNβ.

When we removed HMGB1 we still observed an inhibition of IFNβ, suggesting that HMGB1 is not necessary for this phenotype. There are a few possibilities for why this is. First, is the presence of the other HMGB proteins, most notably HMGB2 and HMGB3, both of which have some redundant functions with HMGB1 within the nucleus[117,145,254]. While they are less abundant than HMGB1, they may contribute to inhibiting IFNβ. Removing them or inhibiting them by knockout or knockdown may further decrease protein VII's ability to inhibit IFNβ expression. Second, the host protein SET functions as a chaperone of the linker histone,

H1[256,257]. Protein VII interacts with SET, which contributes to inhibiting the DNA damage response to adenovirus infection, blocking cell cycle progression, and facilitating the deposition of histone proteins on the viral genome during early infection[70,82,87,88,91,94]. Since SET is hypothesized to contribute to protein VII's distortion of chromatin, it is possible that it is also aiding in repression of IFNβ expression. SET is involved in chromosome segregation during mitosis and knocking it out leads to eventual cell death[258]. However, it can be knocked down via RNAi, and is worth testing to determine mechanistically how protein VII inhibits IFNβ expression and what host factors contribute to this.

Protein VIIΔPTM localizes to the nucleolus during ectopic expression and does not distort host chromatin[82]. Furthermore, the PTM mutant is incapable of blocking cell cycle progression[94]. If localization to and disruption of chromatin is required to inhibit expression of IFNβ, then we would predict that cells expressing protein VIIΔPTM would be incapable of inhibiting the expression of IFNβ. This would be another interesting avenue to explore and would help determine if the localization of protein VII or if the PTMs are essential for inhibiting IFNβ. Furthermore, if protein VII inhibits IFNβ expression through disruption of chromatin, then we would expect it to also inhibit expression of other genes. We did not see any significant inhibition of the panel of ISGs we tested; however, we performed this with our cell lines that contain dox inducible protein VII. While useful, these cell lines produce much less protein VII than the recombinant adenovirus expressing protein VII-GFP or WT HAdV-5. Thus, protein VII's inhibition of IFNβ and potentially other genes could be dose dependent. Lastly, all our experiments to date have tested inhibition of IFNβ through expression of protein VII alone. Future studies will also aim to examine this phenotype during the context of adenovirus infection. Adenovirus has many strategies for inhibiting the innate immune response, which is mostly regulated by the early E1, E3, and E4 genes[154]. Understanding how adenovirus and more specifically how protein VII antagonizes the innate immune response, is essential for

determining how adenovirus causes disease. Moreover, this also provides a novel way for studying how viruses specifically target chromatin to alter gene expression during infection.

What enzyme deposits PTMs on protein VII? How well are PTMs conserved in different adenoviruses? Do PTMs facilitate removal of protein VII from the viral genome?

In chapter 3, we explored how PTMs on protein VII may impact its function during early and late infection. One question that remains to be addressed is what enzymes are modifying protein VII? We know that protein VII is modified by a host enzyme, since modifications can be detected on protein VII expressed in eukaryotic cells[82]. Furthermore, adenovirus is not known to encode its own kinase or acetyl transferase. We previously used IP-mass spec on cells expressing protein VII or protein VII∆PTM to screen for interacting partners with protein VII[82]. This result did not identify any acetyl transferases that were significantly enriched in the WT sample or the ∆PTM sample. Moreover, this screen was not performed during adenovirus infection, as the HAdV-5 VII∆PTM virus was not created until a later date. The proper comparison during infection is now possible since the appropriate viruses are available to be used. However, as we identified in chapter 3, it appears that protein VII∆PTM could still be acetylated during adenovirus infection. Mass spectrometry on protein VII isolated during HAdV-5 VII∆PTM-HA infection could identify which specific lysine is still acetylated. There are only three remaining lysine residues that are not modified within the VII∆PTM, which we can mutate and introduce into the viral genome to create a fully unacetylatable protein VII virus. With this virus, repeating the IP-mass spec screen may obtain a better comparison of what acetyl transferases are responsible for modifying protein VII.

It is also possible that there were no significant hits in the initial screen because the interaction between protein VII and the acetyltransferase enzyme is weak or transient. An alternative method would be a BioID labeling approach, where a biotin ligase is attached to

protein VII, which will biotinylate proteins within close proximity to protein VII[259,260]. Biotinylated proteins can then be pulled down and run through mass-spec to identify interacting proteins. This approach would require engineering a new virus with the BioID fusion protein on protein VII or expressing both the WT and ΔPTM protein VII ectopically with the BioID fusion proteins. This approach may be more fruitful in generating potential interacting partners with protein VII. BioID represents a robust approach for identifying interacting partners, albeit constrained by the production of background. Conducting knockdown/knockout screens of acetyltransferase and kinase candidates identified through BioID would serve as a valuable method to validate enzymes involved in the modification of protein VII.

As to which enzymes are modifying protein VII, P300 is an acetyl transferase that we predict is interacting with protein VII. P300 is well-known for its interaction with the early viral protein E1A, where this interaction is necessary for E1A to transform rodent cells[261–266]. P300 functions by acetylating core histone proteins, which can promote gene expression. E1A utilizes P300 to acetylate histones within the promoter of host genes to alter gene expression that is conducive for adenovirus infection[207,267]. It is hypothesized that protein VII recruits E1A to the viral genome, and our data in chapter 3 showed that while protein VII and E1A don't directly interact, they may interact in a chromatin-mediated interaction since both proteins are found on chromatin during infection[75]. It is possible that E1A recruited to protein VII during early infection shuttles P300 with it, and then protein VII is acetylated by P300. If our hypothesis that PTMs, specifically acetylation, facilitate the removal of protein VII from the viral genome, then this model of E1A/P300 mediated acetylation is worth testing. This mechanism would not explain how protein VII is acetylated during ectopic expression, when there is no E1A present to deliver P300, or during late stages of infection when the dynamics of E1A and protein VII expression are much different than early infection. However, protein VII's localization to chromatin during expression or late infection likely places it near P300 or other acetyl transferases that are

interacting with chromatin. Thus, it is important that we identify the enzymes responsible for modifying protein VII and other adenovirus proteins, as these are potentially pro-viral factors that can be targeted for inhibiting adenovirus infection.

Further expanding on removal of protein VII, it has been hypothesized that protein VII is slowly removed from the viral genome during early infection as it is replaced with histone proteins[66,67,72,73,75,194]. We attempted to visualize the removal of protein VII in our early IF microscopy experiments in chapter 3, as protein VII foci during early infection are representative of viral genomes.[65,66,70,74,193] However, while we saw differences in the quantity of foci, we saw no clear difference in reduction of foci throughout early infection with our mutant viruses. What happens to protein VII after it is removed is unknown, so it is possible that it remains as foci within the nucleus, which are mistakenly identified as viral genomes. To this extent, it was demonstrated with click chemistry that during infection with labeled viral genomes, some protein VII foci are visualized not overlapping with viral genomes during early infection[202]. This suggests that protein VII foci can still be visualized within the nucleus, even after it's been removed from the viral genome. We can utilize the labeled genome approach with our mutant viruses to test our hypothesis that PTMs on protein VII facilitate its removal from the viral genome. Ultimately, it is vital that we determine how protein VII is modified and how it is removed from the viral genome. This is not exclusively important for understanding more about adenovirus infection but since protein VII influences expression of the viral genome, it may help with improve trans-gene expression via adenovirus vectors.

Protein VII undergoes modifications during late-stage infection. Previously, we proposed a model in which acetylated protein VII specifically localizes to host chromatin, while non-modified protein VII associates with the viral genome[82]. This was based on studies of ectopically expressed protein VII. However, our observations in Chapter 3 indicate no significant difference in the localization of wild-type protein VII compared to mutant protein VIIs during infection.

During infection, the precursor form is highly expressed, and the exact ratio of mature protein VII to precursor is unknown, but there is likely more of the precusor based on western blots during late infection. Thus, it is possible that our PTM mutations have the expected change in localization of the mature protein, but it is difficult to observe and distinguish from the large quantity of precursor within the nucleus. It is also plausible that PTMs exert distinct effects on the localization of precursor protein VII. Moreover, acetylation at K20 and phosphorylation at S19 have been detected on the precursor, but these residues were not mutated in our PTM mutants[82–84]. Therefore, elucidating how PTMs at these sites in the precursor influence the localization and function of protein VII during infection could provide insights into its roles in late-stage infection.

What impact does HMGB1 have on murine adenovirus infection?

In chapter 4, we explored the role mVII has on human adenovirus infection, and how it interacts with HMGB1 during infection. We reported conflicting results on whether mVII interacts with HMGB1. Our transfection data and bacterial two-hybrid (B2H) analysis suggested that mVII doesn't interact with HMGB1, while our work with HAdV-5 mVII-HA suggests that there is a possible interaction. Therefore, further work will aim to characterize the nature of the interaction between mVII and HMGB1. Since we did not test pre-mVII in our B2H and transfection fractionation, it is possible that the pre portion of mVII is required to bind HMGB1. In chapter 2, we concluded that hVII bound the A-box, and that the C-terminal tail inhibited this interaction. In our B2H, mVII did not bind to the A-box either, however we did not test any of the other domains of HMGB1. Thus, a B2H analysis of mVII and pre-mVII with the remaining HMGB1 domain constructs by B2H or by cellular fractionation may inform on how mVII interacts with HMGB1.

We used HAdV-5 mVII-HA virus to understand the impact of the mVII-HMGB1 interaction on infection. However, the more appropriate context for studying this interaction

would be within MAdV. To address this, we used BAC-mediated recombineering to create the reverse of HAdV-5 mVII-HA, a MAdV-1 chimera that contains protein VII from HAdV-5 (MAdV-1 hVII). MAdV-1 has a primary tropism for endothelial cells, which can often present as encephalomyelitis due to disruption of the blood brain barrier and inflammation[268,269]. HMGB1, is a major driver of inflammation and can promote disruption of the blood brain barrier through positive feedback loop where inflammation stimulates more HMGB1 release and inflammation[270–272]. As such, release of HMGB1 may exacerbate disease in mice leading to worse outcomes during MAdV-1 infection. We showed in chapter 4, that MAdV-1 infected mice had significantly higher serum levels of HMGB1 compared to mock infected mice, suggesting that HMGB1 is released during MAdV-1 infection and potentially driving worse disease. Thus, it is important to understand how mVII regulates HMGB1, if at all, during infection and we hypothesize that infection of mice with MAdV-1 hVII would retain HMGB1 within chromatin of infected cells. We can test this by repeating many of the experiments performed in chapter 2 and 4, but in the context of MAdV-1 and MAdV-1 hVII infection. Furthermore, *in vivo* infections of mice with MAdV-1 and MAdV-1 hVII will help determine the effects that hVII has on HMGB1 retention during infection, how it impacts inflammation, and if it affects disease outcomes in mice.

How conserved are protein VII functions within mVII and hVII?

To our knowledge, protein VII has not been studied in the context of MAdV. Outside of packaging with the viral genome inside progeny virions, the exact functions of mVII are unknown. We suspect that there is some conservation in function between hVII and mVII, but due to their divergent evolution over time the two proteins have likely gained separate functions as well. For example, it is not known if mVII is dispensable for virion production, like hVII is[79]. The core of the MAdV virion is likely different to that of HAdV[1]. Thus, studying deletion of the

mVII from the virion may determine what role it has in packaging and stability of the virion, and in viral entry. Furthermore, the studies that characterized how protein VII interacts with and distorts chromatin specifically focused on protein VII from HAdV-C5 only[82,91,94]. We observed through DAPI staining of mVII expressing cells that host chromatin is distorted and that mVII expression is sufficient to block cell cycle progression. This suggests that many of hVII's chromatin distortion functions are conserved within mVII, however, they may differ in how they are accomplished mechanistically. For example, hVII traps HMGB1 on chromatin, preventing its release and likely using it to help disrupt chromatin. If mVII is incapable of interacting with HMGB1, then perhaps it disrupts chromatin through a different mechanism. By studying how mVII interacts with and distorts host chromatin, we may learn more about how these two proteins have evolved to perform similar and possible divergent functions.

In chapter 4, we observed that mVII differed from hVII in a few different functional aspects. First, the localization pattern of mVII was frequently different than that of hVII. mVII would often localize to large centers nucleolus during infection, that colocalized with the nucleolar resident protein B23. Protein VII, and a separate core protein, protein V, have been reported to interact with B23 during human adenovirus infection[237,238]. B23 acts as a chaperone of the core proteins during late infection, aiding in their assembly on the viral genome. In our IF data, while we observed that mVII frequently colocalized with B23 in large centers, we did not observe hVII repeating this pattern. It is possible be that mVII is less efficient at assembling on viral DNA that needs to be packaged, and that is why we see such a large colocalization within the nucleolus. We know that ectopically expressed protein VIIΔPTM localizes to the nucleolus as well. PTMs may also play a role for localization of mVII, and that we see a large quantity of nucleolar mVII because it is unmodified within human cells. Furthermore, whether mVII is modified in mouse cells and whether it can be modified in human cells is unknown. An alignment of the hVII and mVII amino acid sequences determined that many of the identified

PTM sites within hVII are conserved within mVII. Moreover, mVII contains a histone mimic sequence at the N-terminus of the mature protein (ARKRS) similar to that of hVII (AKKRS). Thus, it would be worthwhile to test if mVII contains PTMs, and to perform mutational studies to see if PTMs also impact localization of mVII.

We observed that less mVII protein is present during adenovirus infection. It is unlikely that it isn't efficiently transcribed, seeing as the remaining late genes are all robustly expressed, and this can be easily answered through a RT-qPCR assay. Other possibilities are that mVII is degraded or is not translated efficiently. If the former is true, it would be intriguing to identify how mVII is targeted for degradation, and if some host protein is identifying it and marking it for degradation. To that end, verifying what proteins hVII and mVII interact with during HAdV and MAdV infection through an IP-mass spec screen may identify host proteins that are potentially targeting protein VII during infection. For the latter possibility, ribosome profiling would be a useful assay to determine if mVII is not as efficiently translated as compared to other late genes. Furthermore, the mVII gene could be codon optimized to try and improve translation efficiency during infection.

Since mVII distorts host chromatin, which likely impacts gene expression, it would be interesting to determine mVII impacts gene expression during infection. We used a targeted approach in chapter 2, to show that hVII inhibits IFNβ expression. Is mVII capable of inhibiting IFNβ expression, and, if so, does HMGB1 also aid in this inhibition like it does for hVII? It is likely that hVII and mVII's distortion of host chromatin also impacts the expression of multiple host genes. We can test this with RNAseq, which would help determine what host genes hVII and mVII regulate during HAdV infection. The same experiment would also be useful with MAdV-1 and MAdV-1 hVII in the context of infecting mice. Mice also contain a Type-I Interferon response[173], and it would be important to know if mVII and hVII can stunt the interferon response in mice. While MAdV does not infect humans, it serves as an excellent small animal

model for studying adenovirus pathogenesis and disease in an *in vivo* setting[222]. Therefore, it is critical that we know more about the functions of protein VII within the context of MAdV infection. Lastly, these results may inform on mechanistic differences in how mVII and hVII distort host chromatin and regulate gene expression and how the two proteins have evolved to have similar and potentially distinct functions.

Concluding Remarks

Protein VII is an essential viral protein, that serves many roles throughout the adenovirus infection cycle. The work within this thesis has attempted to elucidate how protein VII interacts with host proteins, how PTMs impact protein VII's function, how protein VII can influence gene expression and the innate immune response, and how conserved protein VII function is within different adenoviruses. By advancing our knowledge of protein VII, we can understand more about how adenovirus successfully infects cells, and potentially identify new targets for combatting infection and disease.

References

1. Davison AJ, Benkő M, Harrach B. Genetic content and evolution of adenoviruses. *J Gen Virol*. 2003;84(11):2895-2908. doi:10.1099/vir.0.19497-0

2. Rowe WP, Huebner RJ, Gilmore LK, Parrott RH, Ward TG. Isolation of a Cytopathogenic Agent from Human Adenoids Undergoing Spontaneous Degeneration in Tissue Culture. *Proc Soc Exp Biol Med*. 1953;84(3):570-573. doi:10.3181/00379727-84-20714

3. Robinson CM, Singh G, Lee JY, et al. Molecular evolution of human adenoviruses. *Sci Rep*. 2013;3(1):1812. doi:10.1038/srep01812

4. Garcia-Zalisnak D, Rapuano C, Sheppard JD, Davis AR. Adenovirus Ocular Infections. *Eye Contact Lens: Sci Clin Pr*. 2018;44(NA;):S1-S7. doi:10.1097/icl.0000000000000226

5. Sandkovsky U, Vargas L, Florescu DF. Adenovirus: Current Epidemiology and Emerging Approaches to Prevention and Treatment. *Curr Infect Dis Rep*. 2014;16(8):416. doi:10.1007/s11908-014-0416-y

6. Greber UF, Flatt JW. Adenovirus Entry: From Infection to Immunity. *Annu Rev Virol*. 2019;6(1):1-21. doi:10.1146/annurev-virology-092818-015550

7. Ghebremedhin B. Human adenovirus: Viral pathogen with increasing importance. *Eur J Microbiol Immunol*. 2014;4(1):26-33. doi:10.1556/eujmi.4.2014.1.2

8. Al-Heeti OM, Cathro HP, Ison MG. Adenovirus Infection and Transplantation. *Transplantation*. 2022;106(5):920-927. doi:10.1097/tp.0000000000003988

9. Lion T. Adenovirus persistence, reactivation, and clinical management. *FEBS Lett*. 2019;593(24):3571-3582. doi:10.1002/1873-3468.13576

10. Hierholzer JC. Adenoviruses in the immunocompromised host. *Clin Microbiol Rev*. 1992;5(3):262-274. doi:10.1128/cmr.5.3.262

11. Majorant D, Qiu F, Kalil AC, Wilson N, Florescu DF. Adenovirus—A Deadly Disease in the Solid Organ Transplant Population: Risk Factors and Outcomes. *Transplant Proc*. 2018;50(10):3769-3774. doi:10.1016/j.transproceed.2018.07.004

12. Lieberman PM. Epigenetics and Genetics of Viral Latency. *Cell Host Microbe*. 2016;19(5):619-628. doi:10.1016/j.chom.2016.04.008

13. Kosulin K, Geiger E, Vécsei A, et al. Persistence and reactivation of human adenoviruses in the gastrointestinal tract. *Clin Microbiol Infect*. 2016;22(4):381.e1-381.e8. doi:10.1016/j.cmi.2015.12.013

14. Lynch JP, Kajon AE. Adenovirus: Epidemiology, Global Spread of Novel Serotypes, and Advances in Treatment and Prevention. *Semin Respir Crit Care Med*. 2016;37(04):586-602. doi:10.1055/s-0036-1584923

15. Lenaerts L, Naesens L. Antiviral therapy for adenovirus infections. *Antivir Res*. 2006;71(2-3):172-180. doi:10.1016/j.antiviral.2006.04.007

16. Chamberlain JM, Sortino K, Sethna P, et al. Cidofovir Diphosphate Inhibits Adenovirus 5 DNA Polymerase via both Nonobligate Chain Termination and Direct Inhibition, and Polymerase Mutations Confer Cidofovir Resistance on Intact Virus. *Antimicrob Agents Chemother*. 2019;63(1). doi:10.1128/aac.01925-18

17. Kager J, Schneider J, Rasch S, et al. Fulminant Adenoviral-Induced Hepatitis in Immunosuppressed Patients. *Viruses*. 2022;14(7):1459. doi:10.3390/v14071459

18. Ganapathi L, Arnold A, Jones S, et al. Use of cidofovir in pediatric patients with adenovirus infection. *F1000Research*. 2016;5:758. doi:10.12688/f1000research.8374.2

19. Collins ND, Adhikari A, Yang Y, et al. Live Oral Adenovirus Type 4 and Type 7 Vaccine Induces Durable Antibody Response. *Vaccines*. 2020;8(3):411. doi:10.3390/vaccines8030411

20. Sanchez JL, Cooper MJ, Myers CA, et al. Respiratory Infections in the U.S. Military: Recent Experience and Control. *Clin Microbiol Rev*. 2015;28(3):743-800. doi:10.1128/cmr.00039-14

21. Chen S, Tian X. Vaccine development for human mastadenovirus. *J Thorac Dis*. 2018;10(19):S2280-S2294. doi:10.21037/jtd.2018.03.168

22. Sakurai F, Tachibana M, Mizuguchi H. Adenovirus vector-based vaccine for infectious diseases. *Drug Metab Pharmacokinet*. 2022;42:100432. doi:10.1016/j.dmpk.2021.100432

23. Wold W, Toth K. Adenovirus Vectors for Gene Therapy, Vaccination and Cancer Gene Therapy. *Curr Gene Ther*. 2014;13(6):421-433. doi:10.2174/1566523213666131125095046

24. Ang L, Li J, Dong H, et al. Chimeric Oncolytic Adenovirus Armed Chemokine Rantes for Treatment of Breast Cancer. *Bioengineering*. 2022;9(8):342. doi:10.3390/bioengineering9080342

25. Heiniö C, Clubb J, Kudling T, et al. Effective Combination Immunotherapy with Oncolytic Adenovirus and Anti-PD-1 for Treatment of Human and Murine Ovarian Cancers. *Diseases*. 2022;10(3):52. doi:10.3390/diseases10030052

26. Sallard E, Zhang W, Aydin M, Schröer K, Ehrhardt A. The Adenovirus Vector Platform: Novel Insights into Rational Vector Design and Lessons Learned from the COVID-19 Vaccine. *Viruses*. 2023;15(1):204. doi:10.3390/v15010204

27. Bulcha JT, Wang Y, Ma H, Tai PWL, Gao G. Viral vector platforms within the gene therapy landscape. *Signal Transduct Target Ther*. 2021;6(1):53. doi:10.1038/s41392-021-00487-6

28. Atasheva S, Shayakhmetov DM. Adenovirus sensing by the immune system. *Curr Opin Virol*. 2016;21:109-113. doi:10.1016/j.coviro.2016.08.017

29. Fejer G, Freudenberg M, Greber UF, Gyory I. Adenovirus-triggered innate signalling pathways. *Eur J Microbiol Immunol*. 2011;1(4):279-288. doi:10.1556/eujmi.1.2011.4.3

30. Wang Y, Shao W. Innate Immune Response to Viral Vectors in Gene Therapy. *Viruses*. 2023;15(9):1801. doi:10.3390/v15091801

31. Gallardo J, Pérez-Illana M, Martín-González N, Martín CS. Adenovirus Structure: What Is New? *Int J Mol Sci*. 2021;22(10):5240. doi:10.3390/ijms22105240

32. Reddy VS, Nemerow GR. Structures and organization of adenovirus cement proteins provide insights into the role of capsid maturation in virus entry and infection. *Proc Natl Acad Sci*. 2014;111(32):11715-11720. doi:10.1073/pnas.1408462111

33. Martín-González N, Hernando-Pérez M, Condezo GN, et al. Adenovirus major core protein condenses DNA in clusters and bundles, modulating genome release and capsid internal pressure. *Nucleic Acids Res*. 2019;47(17):9231-9242. doi:10.1093/nar/gkz687

34. Anderson CW, Young ME, Flint SJ. Characterization of the adenovirus 2 virion protein, Mu. *Virology*. 1989;172(2):506-512. doi:10.1016/0042-6822(89)90193-1

35. Mirza MA, Weber J. Structure of adenovirus chromatin. *Biochim Biophys Acta (BBA) - Gene Struct Expr*. 1982;696(1):76-86. doi:10.1016/0167-4781(82)90012-4

36. Vayda ME, Rogers AE, Flint SJ. The structure of nucleoprotein cores released from adenovirions. *Nucleic Acids Res*. 1983;11(2):441-460. doi:10.1093/nar/11.2.441

37. Pérez-Vargas J, Vaughan RC, Houser C, Hastie KM, Kao CC, Nemerow GR. Isolation and Characterization of the DNA and Protein Binding Activities of Adenovirus Core Protein V. *J Virol*. 2014;88(16):9287-9296. doi:10.1128/jvi.00935-14

38. Chatterjee PK, Vayda ME, Flint SJ. Interactions among the three adenovirus core proteins. *J Virol*. 1985;55(2):379-386. doi:10.1128/jvi.55.2.379-386.1985

39. Rekosh DMK, Russell WC, Bellet AJD, Robinson AJ. Identification of a protein linked to the ends of adenovirus DNA. *Cell*. 1977;11(2):283-295. doi:10.1016/0092-8674(77)90045-9

40. Webster A, Russell S, Talbot P, Russell WC, Kemp GD. Characterization of the Adenovirus Proteinase: Substrate Specificity. *J Gen Virol*. 1989;70(12):3225-3234. doi:10.1099/0022-1317-70-12-3225

41. Greber UF, Webster P, Weber J, Helenius A. The role of the adenovirus protease on virus entry into cells. *EMBO J*. 1996;15(8):1766-1777.

42. Tyler RE, Ewing SG, Imperiale MJ. Formation of a Multiple Protein Complex on the Adenovirus Packaging Sequence by the IVa2 Protein. *J Virol*. 2007;81(7):3447-3454. doi:10.1128/jvi.02097-06

43. Wickham TJ, Mathias P, Cheresh DA, Nemerow GR. Integrins αvβ3 and αvβ5 promote adenovirus internalization but not virus attachment. *Cell*. 1993;73(2):309-319. doi:10.1016/0092-8674(93)90231-e

44. Suomalainen M, Nakano MY, Keller S, Boucke K, Stidwill RP, Greber UF. Microtubule-dependent Plus- and Minus End–directed Motilities Are Competing Processes for Nuclear Targeting of Adenovirus. *J Cell Biol*. 1999;144(4):657-672. doi:10.1083/jcb.144.4.657

45. Nacht A. The use of blood products in shock. *Crit care Clin*. 1992;8(2):255-291.

46. Trotman LC, Mosberger N, Fornerod M, Stidwill RP, Greber UF. Import of adenovirus DNA involves the nuclear pore complex receptor CAN/Nup214 and histone H1. *Nat Cell Biol*. 2001;3(12):1092-1100. doi:10.1038/ncb1201-1092

47. Cassany A, Ragues J, Guan T, et al. Nuclear Import of Adenovirus DNA Involves Direct Interaction of Hexon with an N-Terminal Domain of the Nucleoporin Nup214. *J Virol*. 2015;89(3):1719-1730. doi:10.1128/jvi.02639-14

48. Hoeben RC, Uil TG. Adenovirus DNA Replication. *Cold Spring Harb Perspect Biol*. 2013;5(3):a013003. doi:10.1101/cshperspect.a013003

49. Voelkerding K, Klessig DF. Identification of two nuclear subclasses of the adenovirus type 5-encoded DNA-binding protein. *J Virol*. 1986;60(2):353-362. doi:10.1128/jvi.60.2.353-362.1986

50. Pied N, Wodrich H. Imaging the adenovirus infection cycle. *FEBS Lett*. 2019;593(24):3419-3448. doi:10.1002/1873-3468.13690

51. Komatsu T, Robinson DR, Hisaoka M, et al. Tracking adenovirus genomes identifies morphologically distinct late DNA replication compartments. *Traffic*. 2016;17(11):1168-1180. doi:10.1111/tra.12429

52. Sugawara K, Gilead Z, Wold WSM, Green M. Immunofluorescence Study of the Adenovirus Type 2 Single-Stranded DNA Binding Protein in Infected and Transformed Cells. *J Virol*. 1977;22(2):527-539. doi:10.1128/jvi.22.2.527-539.1977

53. Genoveso MJ, Hisaoka M, Komatsu T, Wodrich H, Nagata K, Okuwaki M. Formation of adenovirus DNA replication compartments and viral DNA accumulation sites by host chromatin regulatory proteins including NPM1. *FEBS J*. 2020;287(1):205-217. doi:10.1111/febs.15027

54. Akusjärvi G, Persson H. Controls of RNA splicing and termination in the major late adenovirus transcription unit. *Nature*. 1981;292(5822):420-426. doi:10.1038/292420a0

55. Shaw AR, Ziff EB. Transcripts from the adenovirus-2 major late promoter yield a single early family of 3′ coterminal mRNAs and five late families. *Cell*. 1980;22(3):905-916. doi:10.1016/0092-8674(80)90568-1

56. Weber J. Genetic analysis of adenovirus type 2 III. Temperature sensitivity of processing viral proteins. *J Virol*. 1976;17(2):462-471. doi:10.1128/jvi.17.2.462-471.1976

57. Hernando-Pérez M, Martín-González N, Pérez-Illana M, et al. Dynamic competition for hexon binding between core protein VII and lytic protein VI promotes adenovirus maturation and entry. *Proc National Acad Sci*. 2020;117(24):13699-13707. doi:10.1073/pnas.1920896117

58. Zhang Y. I-TASSER server for protein 3D structure prediction. *BMC Bioinform*. 2008;9(1):40. doi:10.1186/1471-2105-9-40

59. Roy A, Kucukural A, Zhang Y. I-TASSER: a unified platform for automated protein structure and function prediction. *Nat Protoc*. 2010;5(4):725-738. doi:10.1038/nprot.2010.5

60. Yang J, Yan R, Roy A, Xu D, Poisson J, Zhang Y. The I-TASSER Suite: protein structure and function prediction. *Nat Methods*. 2015;12(1):7-8. doi:10.1038/nmeth.3213

61. Appelquist G, Baglin C, Beringer J, et al. Strangelet Search in Pb-Pb Interactions at 158 GeV /c per Nucleon. *Phys Rev Lett*. 1996;76(21):3907-3910. doi:10.1103/physrevlett.76.3907

62. Ercius P, Alaidi O, Rames MJ, Ren G. Electron Tomography: A Three-Dimensional Analytic Tool for Hard and Soft Materials Research. *Adv Mater*. 2015;27(38):5638-5663. doi:10.1002/adma.201501015

63. Vayda ME, Flint SJ. Isolation and characterization of adenovirus core nucleoprotein subunits. *J Virol*. 1987;61(10):3335-3339. doi:10.1128/jvi.61.10.3335-3339.1987

64. Chatterjee PK, Vayda ME, Flint SJ. Adenoviral protein VII packages intracellular viral DNA throughout the early phase of infection. *EMBO J*. 1986;5(7):1633-1644. doi:10.1002/j.1460-2075.1986.tb04406.x

65. Karen KA, Hearing P. Adenovirus Core Protein VII Protects the Viral Genome from a DNA Damage Response at Early Times after Infection. *J Virol*. 2011;85(9):4135-4142. doi:10.1128/jvi.02540-10

66. Xue Y, Johnson JS, Ornelles DA, Lieberman J, Engel DA. Adenovirus Protein VII Functions throughout Early Phase and Interacts with Cellular Proteins SET and pp32. *J Virol*. 2005;79(4):2474-2483. doi:10.1128/jvi.79.4.2474-2483.2005

67. Komatsu T, Haruki H, Nagata K. Cellular and viral chromatin proteins are positive factors in the regulation of adenovirus gene expression. *Nucleic Acids Res*. 2011;39(3):889-901. doi:10.1093/nar/gkq783

68. Wodrich H, Cassany A, D'Angelo MA, Guan T, Nemerow G, Gerace L. Adenovirus Core Protein pVII Is Translocated into the Nucleus by Multiple Import Receptor Pathways. *J Virol*. 2006;80(19):9608-9618. doi:10.1128/jvi.00850-06

69. Komatsu T, Dacheux D, Kreppel F, Nagata K, Wodrich H. A Method for Visualization of Incoming Adenovirus Chromatin Complexes in Fixed and Living Cells. *PLoS ONE*. 2015;10(9):e0137102. doi:10.1371/journal.pone.0137102

70. Haruki H, Okuwaki M, Miyagishi M, Taira K, Nagata K. Involvement of Template-Activating Factor I/SET in Transcription of Adenovirus Early Genes as a Positive-Acting Factor. *J Virol*. 2006;80(2):794-801. doi:10.1128/jvi.80.2.794-801.2006

71. Kyriakis SC, Olsson NG, Martinsson K, Bjork AKK. Observations on the action of amperozide: are there social influences on sow-litter productivity? *Res Vet Sci*. 1991;51(2):169-173. doi:10.1016/0034-5288(91)90008-c

72. Ross PJ, Kennedy MA, Christou C, Quiroz MR, Poulin KL, Parks RJ. Assembly of Helper-Dependent Adenovirus DNA into Chromatin Promotes Efficient Gene Expression. *J Virol*. 2011;85(8):3950-3958. doi:10.1128/jvi.01787-10

73. Giberson AN, Saha B, Campbell K, Christou C, Poulin KL, Parks RJ. Human adenoviral DNA association with nucleosomes containing histone variant H3.3 during the early phase of infection is not dependent on viral transcription or replication. *Biochem Cell Biol*. 2018;96(6):797-807. doi:10.1139/bcb-2018-0117

74. Chen J, Morral N, Engel DA. Transcription releases protein VII from adenovirus chromatin. *Virology*. 2007;369(2):411-422. doi:10.1016/j.virol.2007.08.012

75. Johnson JS, Osheim YN, Xue Y, et al. Adenovirus Protein VII Condenses DNA, Represses Transcription, and Associates with Transcriptional Activator E1A. *J Virol*. 2004;78(12):6459-6468. doi:10.1128/jvi.78.12.6459-6468.2004

76. Sharma G, Moria N, Williams M, Krishnarjuna B, Pouton CW. Corrigendum: Purification and characterization of adenovirus core protein VII: a histone-like protein that is critical for adenovirus core formation. *J Gen Virol*. 2018;99(6):860-860. doi:10.1099/jgv.0.001078

77. Komatsu T, Quentin-Froignant C, Carlon-Andres I, et al. In Vivo Labelling of Adenovirus DNA Identifies Chromatin Anchoring and Biphasic Genome Replication. *J Virol*. 2018;92(18):e00795-18. doi:10.1128/jvi.00795-18

78. Pablo PJ de, Martín CS. Seeing and touching adenovirus: complementary approaches for understanding assembly and disassembly of a complex virion. *Curr Opin Virol*. 2022;52:112-122. doi:10.1016/j.coviro.2021.11.006

79. Ostapchuk P, Suomalainen M, Zheng Y, Boucke K, Greber UF, Hearing P. The adenovirus major core protein VII is dispensable for virion assembly but is essential for lytic infection. Imperiale MJ, ed. *PLoS Pathog*. 2017;13(6):e1006455. doi:10.1371/journal.ppat.1006455

80. Hernando-Pérez M, Martín-González N, Pérez-Illana M, et al. Dynamic competition for hexon binding between core protein VII and lytic protein VI promotes adenovirus maturation and entry. *Proc Natl Acad Sci*. 2020;117(24):13699-13707. doi:10.1073/pnas.1920896117

81. Wiethoff CM, Wodrich H, Gerace L, Nemerow GR. Adenovirus Protein VI Mediates Membrane Disruption following Capsid Disassembly. *J Virol*. 2005;79(4):1992-2000. doi:10.1128/jvi.79.4.1992-2000.2005

82. Avgousti DC, Herrmann C, Kulej K, et al. A core viral protein binds host nucleosomes to sequester immune danger signals. *Nature*. 2016;535(7610):173-177. doi:10.1038/nature18317

83. Zarei M, Jonveaux J, Wang P, et al. Proteomic Analysis of Adenovirus 5 by UHPLC-MS/MS: Development of a Robust and Reproducible Sample Preparation Workflow. *ACS Omega*. 2022;7(41):36825-36835. doi:10.1021/acsomega.2c05325

84. Lind SB, Artemenko KA, Elfineh L, Zhao Y, Bergquist J, Pettersson U. The phosphoproteome of the adenovirus type 2 virion. *Virology*. 2012;433(1):253-261. doi:10.1016/j.virol.2012.08.012

85. Lam YW, Evans VC, Heesom KJ, Lamond AI, Matthews DA. Proteomics Analysis of the Nucleolus in Adenovirus-infected Cells. *Mol Cell Proteom*. 2010;9(1):117-130. doi:10.1074/mcp.m900338-mcp200

86. Scaffidi P, Misteli T, Bianchi ME. Release of chromatin protein HMGB1 by necrotic cells triggers inflammation. *Nature*. 2002;418(6894):191-195. doi:10.1038/nature00858

87. Gyurcsik B, Haruki H, Takahashi T, Mihara H, Nagata K. Binding Modes of the Precursor of Adenovirus Major Core Protein VII to DNA and Template Activating Factor I: Implication for the Mechanism of Remodeling of the Adenovirus Chromatin †. *Biochemistry*. 2006;45(1):303-313. doi:10.1021/bi051248+

88. Haruki H, Gyurcsik B, Okuwaki M, Nagata K. Ternary complex formation between DNA-adenovirus core protein VII and TAF-Iβ/SET, an acidic molecular chaperone. *FEBS Lett*. 2003;555(3):521-527. doi:10.1016/s0014-5793(03)01336-x

89. McCarthy-Leo C, Darwiche F, Tainsky MA. DNA Repair Mechanisms, Protein Interactions and Therapeutic Targeting of the MRN Complex. *Cancers*. 2022;14(21):5278. doi:10.3390/cancers14215278

90. Stracker TH, Carson CT, Weitzman MD. Adenovirus oncoproteins inactivate the Mre11–Rad50–NBS1 DNA repair complex. *Nature*. 2002;418(6895):348-352. doi:10.1038/nature00863

91. Avgousti DC, Fera AND, Otter CJ, Herrmann C, Pancholi NJ, Weitzman MD. Adenovirus Core Protein VII Downregulates the DNA Damage Response on the Host Genome. *J Virol*. 2017;91(20):e01089-17. doi:10.1128/jvi.01089-17

92. Rogakou EP, Pilch DR, Orr AH, Ivanova VS, Bonner WM. DNA Double-stranded Breaks Induce Histone H2AX Phosphorylation on Serine 139*. *J Biol Chem*. 1998;273(10):5858-5868. doi:10.1074/jbc.273.10.5858

93. Stucki M, Jackson SP. γH2AX and MDC1: Anchoring the DNA-damage-response machinery to broken chromosomes. *DNA Repair*. 2006;5(5):534-543. doi:10.1016/j.dnarep.2006.01.012

94. Lynch KL, Dillon MR, Bat-Erdene M, et al. A viral histone-like protein exploits antagonism between linker histones and HMGB proteins to obstruct the cell cycle. *Curr Biol*. 2021;31(23):5227-5237.e7. doi:10.1016/j.cub.2021.09.050

95. Stros M. DNA bending by the chromosomal protein HMG1 and its high mobility group box domains. Effect of flanking sequences. *J Biol Chem*. 1998;273(17):10355-10361.

96. Jung Y, Lippard SJ. Nature of Full-Length HMGB1 Binding to Cisplatin-Modified DNA †. *Biochemistry*. 2003;42(9):2664-2671. doi:10.1021/bi026972w

97. Bianchi ME, Falciola L, Ferrari S, Lilley DM. The DNA binding site of HMG1 protein is composed of two similar segments (HMG boxes), both of which have counterparts in other eukaryotic regulatory proteins. *EMBO J*. 1992;11(3):1055-1063. doi:10.1002/j.1460-2075.1992.tb05144.x

98. Thomas JO, Travers AA. HMG1 and 2, and related 'architectural' DNA-binding proteins. *Trends Biochem Sci*. 2001;26(3):167-174. doi:10.1016/s0968-0004(01)01801-1

99. Štros M. HMGB proteins: Interactions with DNA and chromatin. *Biochim Biophys Acta (BBA) - Gene Regul Mech*. 2010;1799(1-2):101-113. doi:10.1016/j.bbagrm.2009.09.008

100. Bruni CB, Auricchio F, Covelli I. Acid alpha-D-glucosidase glucohydrolase from cattle liver. *J Biol Chem*. 1969;244(17):4735-4742.

101. Blair RH, Horn AE, Pazhani Y, Grado L, Goodrich JA, Kugel JF. The HMGB1 C-Terminal Tail Regulates DNA Bending. *J Mol Biol*. 2016;428(20):4060-4072. doi:10.1016/j.jmb.2016.08.018

102. Cato L, Stott K, Watson M, Thomas JO. The Interaction of HMGB1 and Linker Histones Occurs Through their Acidic and Basic Tails. *J Mol Biol*. 2008;384(5):1262-1272. doi:10.1016/j.jmb.2008.10.001

103. Oh YJ, Youn JH, Ji Y, et al. HMGB1 Is Phosphorylated by Classical Protein Kinase C and Is Secreted by a Calcium-Dependent Mechanism. *J Immunol*. 2009;182(9):5800-5809. doi:10.4049/jimmunol.0801873

104. Bonaldi T, Talamo F, Scaffidi P, et al. Monocytic cells hyperacetylate chromatin protein HMGB1 to redirect it towards secretion. *EMBO J*. 2003;22(20):5551-5560. doi:10.1093/emboj/cdg516

105. Youn JH, Shin JS. Nucleocytoplasmic Shuttling of HMGB1 Is Regulated by Phosphorylation That Redirects It toward Secretion. *J Immunol*. 2006;177(11):7889-7897. doi:10.4049/jimmunol.177.11.7889

106. Ito I, Fukazawa J, Yoshida M. Post-translational Methylation of High Mobility Group Box 1 (HMGB1) Causes Its Cytoplasmic Localization in Neutrophils*. *J Biol Chem*. 2007;282(22):16336-16344. doi:10.1074/jbc.m608467200

107. Tang D, Shi Y, Kang R, et al. Hydrogen peroxide stimulates macrophages and monocytes to actively release HMGB1. *J Leucoc Biol*. 2006;81(3):741-747. doi:10.1189/jlb.0806540

108. Hoppe G, Talcott KE, Bhattacharya SK, Crabb JW, Sears JE. Molecular basis for the redox control of nuclear transport of the structural chromatin protein Hmgb1. *Exp Cell Res*. 2006;312(18):3526-3538. doi:10.1016/j.yexcr.2006.07.020

109. Kang R, Tang D, Schapiro NE, et al. The receptor for advanced glycation end products (RAGE) sustains autophagy and limits apoptosis, promoting pancreatic tumor cell survival. *Cell Death Differ*. 2010;17(4):666-676. doi:10.1038/cdd.2009.149

110. Wang J, Tochio N, Takeuchi A, Uewaki J ichi, Kobayashi N, Tate S ichi. Redox-sensitive structural change in the A-domain of HMGB1 and its implication for the binding to cisplatin modified DNA. *Biochem Biophys Res Commun*. 2013;441(4):701-706.

111. Venereau E, Casalgrandi M, Schiraldi M, et al. Mutually exclusive redox forms of HMGB1 promote cell recruitment or proinflammatory cytokine release. *J Exp Med*. 2012;209(9):1519-1528. doi:10.1084/jem.20120189

112. Yang H, Hreggvidsdottir HS, Palmblad K, et al. A critical cysteine is required for HMGB1 binding to Toll-like receptor 4 and activation of macrophage cytokine release. *Proc Natl Acad Sci*. 2010;107(26):11942-11947. doi:10.1073/pnas.1003893107

113. Sharman AC, Hay-Schmidt A, Holland PWH. Cloning and analysis of an HMG gene from the lamprey Lampetra fluviatilis: gene duplication in vertebrate evolution. *Gene*. 1997;184(1):99-105. doi:10.1016/s0378-1119(96)00580-x

114. Panday A, Grove A. Yeast HMO1: Linker Histone Reinvented. *Microbiol Mol Biol Rev*. 2017;81(1):e00037-16. doi:10.1128/mmbr.00037-16

115. Calogero S, Grassi F, Aguzzi A, et al. The lack of chromosomal protein Hmg1 does not disrupt cell growth but causes lethal hypoglycaemia in newborn mice. *Nat Genet*. 1999;22(3):276-280. doi:10.1038/10338

116. Catena R, Escoffier E, Caron C, Khochbin S, Martianov I, Davidson I. HMGB4, a Novel Member of the HMGB Family, Is Preferentially Expressed in the Mouse Testis and Localizes to the Basal Pole of Elongating Spermatids1. *Biol Reprod*. 2009;80(2):358-366. doi:10.1095/biolreprod.108.070243

117. Niu L, Yang W, Duan L, et al. Biological functions and theranostic potential of HMGB family members in human cancers. *Ther Adv Méd Oncol*. 2020;12:1758835920970850. doi:10.1177/1758835920970850

118. Bustin M. Regulation of DNA-Dependent Activities by the Functional Motifs of the High-Mobility-Group Chromosomal Proteins. *Mol Cell Biol*. 1999;19(8):5237-5246. doi:10.1128/mcb.19.8.5237

119. Taniguchi N, Kawakami Y, Maruyama I, Lotz M. HMGB proteins and arthritis. *Hum Cell*. 2018;31(1):1-9. doi:10.1007/s13577-017-0182-x

120. Catena R, Escoffier E, Caron C, Khochbin S, Martianov I, Davidson I. HMGB4, a Novel Member of the HMGB Family, Is Preferentially Expressed in the Mouse Testis and Localizes to the Basal Pole of Elongating Spermatids1. *Biol Reprod*. 2009;80(2):358-366. doi:10.1095/biolreprod.108.070243

121. Bianchi ME, Agresti A. HMG proteins: dynamic players in gene regulation and differentiation. *Curr Opin Genet Dev*. 2005;15(5):496-506. doi:10.1016/j.gde.2005.08.007

122. Müller S, Ronfani L, Bianchi ME. Regulated expression and subcellular localization of HMGB1, a chromatin protein with a cytokine function. *J Intern Med*. 2004;255(3):332-343. doi:10.1111/j.1365-2796.2003.01296.x

123. Ronfani L, Ferraguti M, Croci L, et al. Reduced fertility and spermatogenesis defects in mice lacking chromosomal protein Hmgb2. *Development*. 2001;128(8):1265-1273. doi:10.1242/dev.128.8.1265

124. Nemeth MJ, Curtis DJ, Kirby MR, et al. Hmgb3: an HMG-box family member expressed in primitive hematopoietic cells that inhibits myeloid and B-cell differentiation. *Blood*. 2003;102(4):1298-1306. doi:10.1182/blood-2002-11-3541

125. Rouhiainen A, Zhao X, Vanttola P, et al. HMGB4 is expressed by neuronal cells and affects the expression of genes involved in neural differentiation. *Sci Rep*. 2016;6(1):32960. doi:10.1038/srep32960

126. Gaillard C, Strauss F. High affinity binding of proteins HMG1 and HMG2 to semicatenated DNA loops. *BMC Mol Biol*. 2000;1(1):1. doi:10.1186/1471-2199-1-1

127. Bianchi ME, Beltrame M, Paonessa G. Specific Recognition of Cruciform DNA by Nuclear Protein HMG1. *Science*. 1989;243(4894):1056-1059. doi:10.1126/science.2922595

128. Sofiadis K, Josipovic N, Nikolic M, et al. HMGB1 coordinates SASP-related chromatin folding and RNA homeostasis on the path to senescence. *Mol Syst Biol*. 2021;17(6):e9760. doi:10.15252/msb.20209760

129. Wang H, Bloom O, Zhang M, et al. HMG-1 as a Late Mediator of Endotoxin Lethality in Mice. *Science*. 1999;285(5425):248-251. doi:10.1126/science.285.5425.248

130. Yang H, Zeng Q, Silverman HA, et al. HMGB1 released from nociceptors mediates inflammation. *Proc Natl Acad Sci*. 2021;118(33):e2102034118. doi:10.1073/pnas.2102034118

131. Deng M, Tang Y, Li W, et al. The Endotoxin Delivery Protein HMGB1 Mediates Caspase-11-Dependent Lethality in Sepsis. *Immunity*. 2018;49(4):740-753.e7. doi:10.1016/j.immuni.2018.08.016

132. Gardella S, Andrei C, Ferrera D, et al. The nuclear protein HMGB1 is secreted by monocytes via a non-classical, vesicle-mediated secretory pathway. *EMBO Rep*. 2002;3(10):995-1001. doi:10.1093/embo-reports/kvf198

133. Urbonaviciute V, Fürnrohr BG, Meister S, et al. Induction of inflammatory and immune responses by HMGB1–nucleosome complexes: implications for the pathogenesis of SLE. *J Exp Med*. 2008;205(13):3007-3018. doi:10.1084/jem.20081165

134. Tang D, Kang R, Livesey KM, et al. Endogenous HMGB1 regulates autophagy. *J Cell Biol*. 2010;190(5):881-892. doi:10.1083/jcb.200911078

135. Andreeva L, Hiller B, Kostrewa D, et al. cGAS senses long and HMGB/TFAM-bound U-turn DNA by forming protein–DNA ladders. *Nature*. 2017;549(7672):394-398. doi:10.1038/nature23890

136. Yanai H, Ban T, Wang Z, et al. HMGB proteins function as universal sentinels for nucleic-acid-mediated innate immune responses. *Nature*. 2009;462(7269):99-103. doi:10.1038/nature08512

137. Moisy D, Avilov SV, Jacob Y, et al. HMGB1 Protein Binds to Influenza Virus Nucleoprotein and Promotes Viral Replication. *J Virol*. 2012;86(17):9122-9133. doi:10.1128/jvi.00789-12

138. Zhang G, Kobayashi T, Kamitani W, et al. Borna Disease Virus Phosphoprotein Represses p53-Mediated Transcriptional Activity by Interference with HMGB1. *J Virol*. 2003;77(22):12243-12251. doi:10.1128/jvi.77.22.12243-12251.2003

139. Wei J, Alfajaro MM, DeWeirdt PC, et al. Genome-wide CRISPR Screens Reveal Host Factors Critical for SARS-CoV-2 Infection. *Cell*. 2021;184(1):76-91.e13. doi:10.1016/j.cell.2020.10.028

140. Kulanayake S, Tikoo SK. Adenovirus Core Proteins: Structure and Function. *Viruses*. 2021;13(3):388. doi:10.3390/v13030388

141. Corden J, Engelking HM, Pearson GD. Chromatin-like organization of the adenovirus chromosome. *Proceedings of the National Academy of Sciences of the United States of America*. 1976;73(2):401-404.

142. Aleström P, Akusjärvi G, Lager M, Yeh-kai L, Pettersson U. Genes encoding the core proteins of adenovirus type 2. *J Biological Chem*. 1984;259(22):13980-13985.

143. Ostapchuk P, Suomalainen M, Zheng Y, Boucke K, Greber UF, Hearing P. The adenovirus major core protein VII is dispensable for virion assembly but is essential for lytic infection. Imperiale MJ, ed. *PLoS Pathog*. 2017;13(6):e1006455. doi:10.1371/journal.ppat.1006455

144. Kang R, Chen R, Zhang Q, et al. HMGB1 in health and disease. *Mol Aspects Med*. 2014;40:1-116. doi:10.1016/j.mam.2014.05.001

145. Agresti A, Bianchi ME. HMGB proteins and gene expression. *Curr Opin Genet Dev*. 2003;13(2):170-178. doi:10.1016/s0959-437x(03)00023-6

146. Belgrano FS, Silva IC de A da, Oliveira FMB de, Fantappié MR, Mohana-Borges R. Role of the Acidic Tail of High Mobility Group Protein B1 (HMGB1) in Protein Stability and DNA Bending. *Plos One*. 2013;8(11):e79572. doi:10.1371/journal.pone.0079572

147. Knapp S, Müller S, Digilio G, Bonaldi T, Bianchi ME, Musco G. The Long Acidic Tail of High Mobility Group Box 1 (HMGB1) Protein Forms an Extended and Flexible Structure That Interacts with Specific Residues within and between the HMG Boxes †. *Biochemistry-us*. 2004;43(38):11992-11997. doi:10.1021/bi049364k

148. Chen R, Kang R, Tang D. The mechanism of HMGB1 secretion and release. *Exp Mol Medicine*. 2022;54(2):91-102. doi:10.1038/s12276-022-00736-w

149. Xu J, Jiang Y, Wang J, et al. Macrophage endocytosis of high-mobility group box 1 triggers pyroptosis. *Cell Death Differ*. 2014;21(8):1229-1239. doi:10.1038/cdd.2014.40

150. Yang H, Wang H, Andersson U. Targeting Inflammation Driven by HMGB1. *Front Immunol*. 2020;11:484. doi:10.3389/fimmu.2020.00484

151. Ren J, Antony F, Rouse BT, Suryawanshi A. Role of Innate Interferon Responses at the Ocular Surface in Herpes Simplex Virus-1-Induced Herpetic Stromal Keratitis. *Pathogens*. 2023;12(3):437. doi:10.3390/pathogens12030437

152. Suzuki Y. Interferon-induced restriction of Chikungunya virus infection. *Antivir Res*. 2023;210:105487. doi:10.1016/j.antiviral.2022.105487

153. Min J, Liu W, Li J. Emerging Role of Interferon-Induced Noncoding RNA in Innate Antiviral Immunity. *Viruses*. 2022;14(12):2607. doi:10.3390/v14122607

154. Sohn S, Hearing P. Adenoviral strategies to overcome innate cellular responses to infection. *Febs Lett*. 2019;593(24):3484-3495. doi:10.1002/1873-3468.13680

155. Karimova G, Pidoux J, Ullmann A, Ladant D. A bacterial two-hybrid system based on a reconstituted signal transduction pathway. *Proc National Acad Sci*. 1998;95(10):5752-5756. doi:10.1073/pnas.95.10.5752

156. Mikolaskova B, Jurcik M, Cipakova I, et al. Identification of Nrl1 Domains Responsible for Interactions with RNA-Processing Factors and Regulation of Nrl1 Function by Phosphorylation. *Int J Mol Sci*. 2021;22(13):7011. doi:10.3390/ijms22137011

157. Fouillen A, Neves JDS, Mary C, et al. Interactions of AMTN, ODAM and SCPPPQ1 proteins of a specialized basal lamina that attaches epithelial cells to tooth mineral. *Sci Rep-uk*. 2017;7(1):46683. doi:10.1038/srep46683

158. Guzzo M, Sanderlin AG, Castro LK, Laub MT. Activation of a signaling pathway by the physical translocation of a chromosome. *Dev Cell*. 2021;56(15):2145-2159.e7. doi:10.1016/j.devcel.2021.06.014

159. Kwak MS, Rhee WJ, Lee YJ, et al. Reactive oxygen species induce Cys106-mediated anti-parallel HMGB1 dimerization that protects against DNA damage. *Redox Biol*. 2021;40:101858. doi:10.1016/j.redox.2021.101858

160. Anggayasti WL, Mancera RL, Bottomley S, Helmerhorst E. The self-association of HMGB1 and its possible role in the binding to DNA and cell membrane receptors. *Febs Lett*. 2017;591(2):282-294. doi:10.1002/1873-3468.12545

161. Ritt C, Grimm R, Fernández S, Alonso JC, Grasser KD. Basic and Acidic Regions Flanking the HMG Domain of Maize HMGa Modulate the Interactions with DNA and the Self-Association of the Protein †. *Biochemistry-us*. 1998;37(8):2673-2681. doi:10.1021/bi972620r

162. Gangelhoff TA, Mungalachetty PS, Nix JC, Churchill MEA. Structural analysis and DNA binding of the HMG domains of the human mitochondrial transcription factor A. *Nucleic Acids Res*. 2009;37(10):3153-3164. doi:10.1093/nar/gkp157

163. Herrmann C, Avgousti D, Weitzman M. Differential Salt Fractionation of Nuclei to Analyze Chromatin-associated Proteins from Cultured Mammalian Cells. *Bio-protocol*. 2017;7(6):e2175. doi:10.21769/bioprotoc.2175

164. Park JS, Arcaroli J, Yum HK, et al. Activation of gene expression in human neutrophils by high mobility group box 1 protein. *Am J Physiol-cell Ph*. 2003;284(4):C870-C879. doi:10.1152/ajpcell.00322.2002

165. Jayaraman L, Moorthy NC, Murthy KGK, Manley JL, Bustin M, Prives C. High mobility group protein-1 (HMG-1) is a unique activator of p53. *Gene Dev*. 1998;12(4):462-472. doi:10.1101/gad.12.4.462

166. Štros M, Ozaki T, Bačíková A, Kageyama H, Nakagawara A. HMGB1 and HMGB2 Cell-specifically Down-regulate the p53- and p73-dependent Sequence-specific Transactivation from the Human Bax Gene Promoter*. *J Biol Chem*. 2002;277(9):7157-7164. doi:10.1074/jbc.m110233200

167. Watson M, Stott K, Thomas JO. Mapping Intramolecular Interactions between Domains in HMGB1 using a Tail-truncation Approach. *J Mol Biol*. 2007;374(5):1286-1297. doi:10.1016/j.jmb.2007.09.075

168. Stott K, Watson M, Howe FS, Grossmann JG, Thomas JO. Tail-Mediated Collapse of HMGB1 Is Dynamic and Occurs via Differential Binding of the Acidic Tail to the A and B Domains. *J Mol Biol*. 2010;403(5):706-722. doi:10.1016/j.jmb.2010.07.045

169. Bonaldi T, Talamo F, Scaffidi P, et al. Monocytic cells hyperacetylate chromatin protein HMGB1 to redirect it towards secretion. *Embo J*. 2003;22(20):5551-5560. doi:10.1093/emboj/cdg516

170. Oh YJ, Youn JH, Ji Y, et al. HMGB1 Is Phosphorylated by Classical Protein Kinase C and Is Secreted by a Calcium-Dependent Mechanism. *J Immunol*. 2009;182(9):5800-5809. doi:10.4049/jimmunol.0801873

171. Kim YH, Kwak MS, Park JB, et al. N-linked glycosylation plays a crucial role in the secretion of HMGB1. *J Cell Sci*. 2015;129(1):29-38. doi:10.1242/jcs.176412

172. Sessa L, Bianchi ME. The evolution of High Mobility Group Box (HMGB) chromatin proteins in multicellular animals. *Gene*. 2007;387(1-2):133-140. doi:10.1016/j.gene.2006.08.034

173. Secombes CJ, Zou J. Evolution of Interferons and Interferon Receptors. *Front Immunol*. 2017;8:209. doi:10.3389/fimmu.2017.00209

174. Dhingra A, Hage E, Ganzenmueller T, et al. Molecular Evolution of Human Adenovirus (HAdV) Species C. *Sci Rep-uk*. 2019;9(1):1039. doi:10.1038/s41598-018-37249-4

175. Ullman AJ, Reich NC, Hearing P. Adenovirus E4 ORF3 Protein Inhibits the Interferon-Mediated Antiviral Response. *J Virol*. 2007;81(9):4744-4752. doi:10.1128/jvi.02385-06

176. Querido E, Blanchette P, Yan Q, et al. Degradation of p53 by adenovirus E4orf6 and E1B55K proteins occurs via a novel mechanism involving a Cullin-containing complex. *Gene Dev*. 2001;15(23):3104-3117. doi:10.1101/gad.926401

177. Fonseca GJ, Thillainadesan G, Yousef AF, et al. Adenovirus Evasion of Interferon-Mediated Innate Immunity by Direct Antagonism of a Cellular Histone Posttranslational Modification. *Cell Host Microbe*. 2012;11(6):597-606. doi:10.1016/j.chom.2012.05.005

178. Le LP, Le HN, Nelson AR, Matthews DA, Yamamoto M, Curiel DT. Core labeling of adenovirus with EGFP. *Virology*. 2006;351(2):291-302. doi:10.1016/j.virol.2006.03.042

179. Warming S, Costantino N, Court DL, Jenkins NA, Copeland NG. Simple and highly efficient BAC recombineering using galK selection. *Nucleic Acids Res*. 2005;33(4):e36-e36. doi:10.1093/nar/gni035

180. Diaz K, Hu CT, Sul Y, et al. Defensin-driven viral evolution. *PLoS Pathog*. 2020;16(11):e1009018. doi:10.1371/journal.ppat.1009018

181. Suzuki K, Bose P, Leong-Quong RY, Fujita DJ, Riabowol K. REAP: A two minute cell fractionation method. *Bmc Res Notes*. 2010;3(1):294. doi:10.1186/1756-0500-3-294

182. Komatsu T, Dacheux D, Kreppel F, Nagata K, Wodrich H. A Method for Visualization of Incoming Adenovirus Chromatin Complexes in Fixed and Living Cells. *Plos One*. 2015;10(9):e0137102. doi:10.1371/journal.pone.0137102

183. Reich NC, Sarnow P, Duprey E, Levine AJ. Monoclonal antibodies which recognize native and denatured forms of the adenovirus DNA-binding protein. *Virology*. 1983;128(2):480-484. doi:10.1016/0042-6822(83)90274-x

184. Luger K, Mäder AW, Richmond RK, Sargent DF, Richmond TJ. Crystal structure of the nucleosome core particle at 2.8 Å resolution. *Nature*. 1997;389(6648):251-260. doi:10.1038/38444

185. Bannister AJ, Kouzarides T. Regulation of chromatin by histone modifications. *Cell Res*. 2011;21(3):381-395. doi:10.1038/cr.2011.22

186. Wang Z, Zang C, Rosenfeld JA, et al. Combinatorial patterns of histone acetylations and methylations in the human genome. *Nat Genet*. 2008;40(7):897-903. doi:10.1038/ng.154

187. Barre A de la, Gerson V, Gout S, Creaven M, Allis CD, Dimitrov S. Core histone N-termini play an essential role in mitotic chromosome condensation. *EMBO J*. 2000;19(3):379-391. doi:10.1093/emboj/19.3.379

188. Komar D, Juszczynski P. Rebelled epigenome: histone H3S10 phosphorylation and H3S10 kinases in cancer biology and therapy. *Clin Epigenetics*. 2020;12(1):147. doi:10.1186/s13148-020-00941-2

189. Fischle W, Tseng BS, Dormann HL, et al. Regulation of HP1–chromatin binding by histone H3 methylation and phosphorylation. *Nature*. 2005;438(7071):1116-1122. doi:10.1038/nature04219

190. Moritz L, Hammoud SS. The Art of Packaging the Sperm Genome: Molecular and Structural Basis of the Histone-To-Protamine Exchange. *Front Endocrinol*. 2022;13:895502. doi:10.3389/fendo.2022.895502

191. Wykes SM, Krawetz SA. The Structural Organization of Sperm Chromatin*. *J Biol Chem*. 2003;278(32):29471-29477. doi:10.1074/jbc.m304545200

192. LISCHWE MA, SUNG MT. A histone-like protein from adenovirus chromatin. *Nature*. 1977;267(5611):552-554. doi:10.1038/267552a0

193. Walkiewicz MP, Morral N, Engel DA. Accurate single-day titration of adenovirus vectors based on equivalence of protein VII nuclear dots and infectious particles. *J Virol Methods*. 2009;159(2):251-258. doi:10.1016/j.jviromet.2009.04.010

194. Komatsu T, Nagata K. Replication-Uncoupled Histone Deposition during Adenovirus DNA Replication. *J Virol*. 2012;86(12):6701-6711. doi:10.1128/jvi.00380-12

195. Berk AJ, Lee F, Harrison T, Williams J, Sharp PA. Pre-early adenovirus 5 gene product regulates synthesis of early viral messenger RNAs. *Cell*. 1979;17(4):935-944. doi:10.1016/0092-8674(79)90333-7

196. Korn R, Horwitz MS. Adenovirus DNA synthesis in Vitro is inhibited by the virus-coded major core protein. *Virology*. 1986;150(2):342-351. doi:10.1016/0042-6822(86)90299-0

197. Nakanishi Y, Maeda K, Ohtsuki M, Hosokawa KI, Natori S. Invitro transcription of a chromatin-like complex of major core protein VII and DNA of adenovirus serotype 2. *Biochem Biophys Res Commun*. 1986;136(1):86-93. doi:10.1016/0006-291x(86)90880-6

198. Vayda ME, Leong K, Flint SJ. Transcription of adenovirus cores in vitro. *Virology*. 1984;139(1):152-163. doi:10.1016/0042-6822(84)90336-2

199. Schwartz U, Komatsu T, Huber C, et al. Changes in adenoviral chromatin organization precede early gene activation upon infection. *EMBO J*. Published online 2023. doi:10.15252/embj.2023114162

200. Arnold EA, Kaai RJ, Leung K, et al. Adenovirus protein VII binds the A-box of HMGB1 to repress interferon responses. *PLOS Pathog*. 2023;19(9):e1011633. doi:10.1371/journal.ppat.1011633

201. Greber UF, Suomalainen M, Stidwill RP, Boucke K, Ebersold MW, Helenius A. The role of the nuclear pore complex in adenovirus DNA entry. *EMBO J*. 1997;16(19):5998-6007. doi:10.1093/emboj/16.19.5998

202. Wang IH, Suomalainen M, Andriasyan V, et al. Tracking Viral Genomes in Host Cells at Single-Molecule Resolution. *Cell Host Microbe*. 2013;14(4):468-480. doi:10.1016/j.chom.2013.09.004

203. Bertzbach LD, Seddar L, Stromberg K von, Ip WH, Dobner T, Hidalgo P. The adenovirus DNA-binding protein DBP. *J Virol*. 2024;98(2):e01885-23. doi:10.1128/jvi.01885-23

204. Chow LT, Lewis JB, Broker TR. RNA Transcription and Splicing at Early and Intermediate Times after Adenovirus-2 Infection. *Cold Spring Harb Symp Quant Biol*. 1980;44(0):401-414. doi:10.1101/sqb.1980.044.01.044

205. Pombo A, Ferreira J, Bridge E, Carmo-Fonseca M. Adenovirus replication and transcription sites are spatially separated in the nucleus of infected cells. *EMBO J*. 1994;13(21):5075-5085. doi:10.1002/j.1460-2075.1994.tb06837.x

206. Gama-Carvalho M, Condado I, Carmo-Fonseca M. Regulation of adenovirus alternative RNA splicing correlates with a reorganization of splicing factors in the nucleus. *Exp Cell Res*. 2003;289(1):77-85. doi:10.1016/s0014-4827(03)00251-9

207. Ferrari R, Pellegrini M, Horwitz GA, Xie W, Berk AJ, Kurdistani SK. Epigenetic Reprogramming by Adenovirus e1a. *Science*. 2008;321(5892):1086-1088. doi:10.1126/science.1155546

208. Ferrari R, Su T, Li B, et al. Reorganization of the host epigenome by a viral oncogene. *Genome Res*. 2012;22(7):1212-1221. doi:10.1101/gr.132308.111

209. Krug RM. Functions of the influenza A virus NS1 protein in antiviral defense. *Curr Opin Virol*. 2015;12:1-6. doi:10.1016/j.coviro.2015.01.007

210. Kee J, Thudium S, Renner DM, et al. Author Correction: SARS-CoV-2 disrupts host epigenetic regulation via histone mimicry. *Nature*. 2023;614(7949):E44-E44. doi:10.1038/s41586-023-05764-8

211. Marazzi I, Ho JSY, Kim J, et al. Suppression of the antiviral response by an influenza histone mimic. *Nature*. 2012;483(7390):428-433. doi:10.1038/nature10892

212. Kouzarides T. Chromatin Modifications and Their Function. *Cell*. 2007;128(4):693-705. doi:10.1016/j.cell.2007.02.005

213. Elde NC, Malik HS. The evolutionary conundrum of pathogen mimicry. *Nat Rev Microbiol*. 2009;7(11):787-797. doi:10.1038/nrmicro2222

214. Slaine PD, Ackford JG, Kropinski AM, Kozak RA, Krell PJ, Nagy É. Molecular characterization of pathogenic and nonpathogenic fowl aviadenovirus serotype 11 isolates. *Can J Microbiol*. 2016;62(12):993-1002. doi:10.1139/cjm-2016-0297

215. Pénzes JJ, Menéndez-Conejero R, Condezo GN, et al. Molecular Characterization of a Lizard Adenovirus Reveals the First Atadenovirus with Two Fiber Genes and the First Adenovirus with Either One Short or Three Long Fibers per Penton. *J Virol*. 2014;88(19):11304-11314. doi:10.1128/jvi.00306-14

216. Lee TWR, Blair GE, Matthews DA. Adenovirus core protein VII contains distinct sequences that mediate targeting to the nucleus and nucleolus, and colocalization with human chromosomes. *J Gen Virol*. 2003;84(12):3423-3428. doi:10.1099/vir.0.19546-0

217. Smith JG, Silvestry M, Lindert S, Lu W, Nemerow GR, Stewart PL. Insight into the Mechanisms of Adenovirus Capsid Disassembly from Studies of Defensin Neutralization. *PLoS Pathog*. 2010;6(6):e1000959. doi:10.1371/journal.ppat.1000959

218. Nguyen EK, Nemerow GR, Smith JG. Direct Evidence from Single-Cell Analysis that Human α-Defensins Block Adenovirus Uncoating To Neutralize Infection. *J Virol*. 2010;84(8):4041-4049. doi:10.1128/jvi.02471-09

219. Hartley JW, Rowe WP. A new mouse virus apparently related to the adenovirus group. *Virology*. 1960;11(3):645-647. doi:10.1016/0042-6822(60)90109-4

220. Meissner JD, Hirsch GN, LaRue EA, Fulcher RA, Spindler KR. Completion of the DNA sequence of mouse adenovirus type 1: Sequence of E2B, L1, and L2 (18–51 map units). *Virus Res*. 1997;51(1):53-64. doi:10.1016/s0168-1702(97)00079-8

221. Temple M, Antoine G, Stahl S, Winnacker EL, Delius H. Replication of mouse adenovirus strain FL DNA. *Virology*. 1981;109(1):1-12. doi:10.1016/0042-6822(81)90466-9

222. Hemmi S, Spindler KR. Murine adenoviruses: tools for studying adenovirus pathogenesis in a natural host. *FEBS Lett*. 2019;593(24):3649-3659. doi:10.1002/1873-3468.13699

223. Guida JD, Fejer G, Pirofski LA, Brosnan CF, Horwitz MS. Mouse adenovirus type 1 causes a fatal hemorrhagic encephalomyelitis in adult C57BL/6 but not BALB/c mice. *J Virol*. 1995;69(12):7674-7681. doi:10.1128/jvi.69.12.7674-7681.1995

224. Ashley SL, Pretto CD, Stier MT, et al. Matrix Metalloproteinase Activity in Infections by an Encephalitic Virus, Mouse Adenovirus Type 1. *J Virol*. 2017;91(6). doi:10.1128/jvi.01412-16

225. Kajon AE, Brown CC, Spindler KR. Distribution of Mouse Adenovirus Type 1 in Intraperitoneally and Intranasally Infected Adult Outbred Mice. *J Virol*. 1998;72(2):1219-1223. doi:10.1128/jvi.72.2.1219-1223.1998

226. Weinberg JB, Stempfle GS, Wilkinson JE, Younger JG, Spindler KR. Acute respiratory infection with mouse adenovirus type 1. *Virology*. 2005;340(2):245-254. doi:10.1016/j.virol.2005.06.021

227. Blailock ZR, Rabin ER, Melnick JL. Adenovirus Endocarditis in Mice. *Science*. 1967;157(3784):69-70. doi:10.1126/science.157.3784.69

228. Blailock ZR, Rabin ER, Melnick JL. Adenovirus myocarditis in mice An electron microscopic study. *Exp Mol Pathol*. 1968;9(1):84-96. doi:10.1016/0014-4800(68)90053-1

229. McCarthy MK, Procario MC, Twisselmann N, et al. Proinflammatory Effects of Interferon Gamma in Mouse Adenovirus 1 Myocarditis. *J Virol*. 2015;89(1):468-479. doi:10.1128/jvi.02077-14

230. Spindler KR, Fang L, Moore ML, Hirsch GN, Brown CC, Kajon A. SJL/J Mice Are Highly Susceptible to Infection by Mouse Adenovirus Type 1. *J Virol*. 2001;75(24):12039-12046. doi:10.1128/jvi.75.24.12039-12046.2001

231. Kring SC, King CS, Spindler KR. Susceptibility and signs associated with mouse adenovirus type 1 infection of adult outbred Swiss mice. *J Virol*. 1995;69(12):8084-8088. doi:10.1128/jvi.69.12.8084-8088.1995

232. Procario MC, Levine RE, McCarthy MK, et al. Susceptibility to Acute Mouse Adenovirus Type 1 Respiratory Infection and Establishment of Protective Immunity in Neonatal Mice. *J Virol*. 2012;86(8):4194-4203. doi:10.1128/jvi.06967-11

233. Klempa B, Krüger DH, Auste B, et al. A Novel Cardiotropic Murine Adenovirus Representing a Distinct Species of Mastadenoviruses. *J Virol*. 2009;83(11):5749-5759. doi:10.1128/jvi.02281-08

234. Hashimoto K, Sugiyama T, Sasaki S. An Adenovirus Isolated from the Feces of Mice. *Jpn J Microbiol*. 1966;10(2):115-125. doi:10.1111/j.1348-0421.1966.tb00298.x

235. Takeuchi A, Hashimoto K. Electron microscope study of experimental enteric adenovirus infection in mice. *Infect Immun*. 1976;13(2):569-580. doi:10.1128/iai.13.2.569-580.1976

236. Hashimoto K, Sugiyama T, Yoshikawa M, Sasaki S. Intestinal Resistance in the Experimental Enteric Infection of Mice with a Mouse Adenovirus. *Jpn J Microbiol*. 1970;14(5):381-395. doi:10.1111/j.1348-0421.1970.tb00538.x

237. Samad MA, Komatsu T, Okuwaki M, Nagata K. B23/nucleophosmin is involved in regulation of adenovirus chromatin structure at late infection stages, but not in virus replication and transcription. *J Gen Virol*. 2012;93(Pt_6):1328-1338. doi:10.1099/vir.0.036665-0

238. Samad MA, Okuwaki M, Haruki H, Nagata K. Physical and functional interaction between a nucleolar protein nucleophosmin/B23 and adenovirus basic core proteins. *FEBS Lett*. 2007;581(17):3283-3288. doi:10.1016/j.febslet.2007.06.024

239. Pérez-Illana M, Martín-González N, Hernando-Pérez M, et al. Acidification induces condensation of the adenovirus core. *Acta Biomater*. 2021;135:534-542. doi:10.1016/j.actbio.2021.08.019

240. Pérez-Berná AJ, Ortega-Esteban A, Menéndez-Conejero R, et al. The Role of Capsid Maturation on Adenovirus Priming for Sequential Uncoating*. *J Biol Chem*. 2012;287(37):31582-31595. doi:10.1074/jbc.m112.389957

241. Frottin F, Schueder F, Tiwary S, et al. The nucleolus functions as a phase-separated protein quality control compartment. *Science*. 2019;365(6451):342-347. doi:10.1126/science.aaw9157

242. Ablasser A, Goldeck M, Cavlar T, et al. cGAS produces a 2′-5′-linked cyclic dinucleotide second messenger that activates STING. *Nature*. 2013;498(7454):380-384. doi:10.1038/nature12306

243. Gao P, Ascano M, Wu Y, et al. Cyclic [G(2′,5′)pA(3′,5′)p] Is the Metazoan Second Messenger Produced by DNA-Activated Cyclic GMP-AMP Synthase. *Cell*. 2013;153(5):1094-1107. doi:10.1016/j.cell.2013.04.046

244. Zhang X, Shi H, Wu J, et al. Cyclic GMP-AMP Containing Mixed Phosphodiester Linkages Is An Endogenous High-Affinity Ligand for STING. *Mol Cell*. 2013;51(2):226-235. doi:10.1016/j.molcel.2013.05.022

245. Hornung V, Ellegast J, Kim S, et al. 5’-Triphosphate RNA Is the Ligand for RIG-I. *Science*. 2006;314(5801):994-997. doi:10.1126/science.1132505

246. Kato H, Takeuchi O, Sato S, et al. Differential roles of MDA5 and RIG-I helicases in the recognition of RNA viruses. *Nature*. 2006;441(7089):101-105. doi:10.1038/nature04734

247. Reikine S, Nguyen JB, Modis Y. Pattern Recognition and Signaling Mechanisms of RIG-I and MDA5. *Front Immunol*. 2014;5:342. doi:10.3389/fimmu.2014.00342

248. Pichlmair A, Schulz O, Tan CP, et al. RIG-I-Mediated Antiviral Responses to Single-Stranded RNA Bearing 5’-Phosphates. *Science*. 2006;314(5801):997-1001. doi:10.1126/science.1132998

249. Yoneyama M, Suhara W, Fukuhara Y, Fukuda M, Nishida E, Fujita T. Direct triggering of the type I interferon system by virus infection: activation of a transcription factor complex containing IRF-3 and CBP/p300. *EMBO J*. 1998;17(4):1087-1095. doi:10.1093/emboj/17.4.1087

250. Weaver BK, Kumar KP, Reich NC. Interferon Regulatory Factor 3 and CREB-Binding Protein/p300 Are Subunits of Double-Stranded RNA-Activated Transcription Factor DRAF1. *Mol Cell Biol*. 1998;18(3):1359-1368. doi:10.1128/mcb.18.3.1359

251. Liu S, Cai X, Wu J, et al. Phosphorylation of innate immune adaptor proteins MAVS, STING, and TRIF induces IRF3 activation. *Science*. 2015;347(6227):aaa2630. doi:10.1126/science.aaa2630

252. Lin R, Heylbroeck C, Pitha PM, Hiscott J. Virus-Dependent Phosphorylation of the IRF-3 Transcription Factor Regulates Nuclear Translocation, Transactivation Potential, and Proteasome-Mediated Degradation. *Mol Cell Biol*. 1998;18(5):2986-2996. doi:10.1128/mcb.18.5.2986

253. Nightingale K, Dimitrov S, Reeves R, Wolffe AP. Evidence for a shared structural role for HMG1 and linker histones B4 and H1 in organizing chromatin. *EMBO J*. 1996;15(3):548-561.

254. Postnikov YV, Bustin M. Functional interplay between histone H1 and HMG proteins in chromatin. *Biochim Biophys Acta (BBA) - Gene Regul Mech*. 2016;1859(3):462-467. doi:10.1016/j.bbagrm.2015.10.006

255. An W, Holde K van, Zlatanova J. The Non-histone Chromatin Protein HMG1 Protects Linker DNA on the Side Opposite to That Protected by Linker Histones*. *J Biol Chem*. 1998;273(41):26289-26291. doi:10.1074/jbc.273.41.26289

256. Kajitani K, Kato K, Nagata K. Histone H1 chaperone activity of TAF-I is regulated by its subtype-dependent intramolecular interaction. *Genes Cells*. 2017;22(4):334-347. doi:10.1111/gtc.12478

257. Kato K, Okuwaki M, Nagata K. Role of Template Activating Factor-I as a chaperone in linker histone dynamics. *J Cell Sci*. 2011;124(19):3254-3265. doi:10.1242/jcs.083139

258. Asai Y, Fukuchi K, Tanno Y, et al. Aurora B kinase activity is regulated by SET/TAF1 on Sgo2 at the inner centromere. *J Cell Biol*. 2019;218(10):3223-3236. doi:10.1083/jcb.201811060

259. Roux KJ, Kim DI, Raida M, Burke B. A promiscuous biotin ligase fusion protein identifies proximal and interacting proteins in mammalian cells. *J Cell Biol*. 2012;196(6):801-810. doi:10.1083/jcb.201112098

260. Sears RM, May DG, Roux KJ. Enzyme-Mediated Ligation Methods. *Methods Mol Biol*. 2019;2012:299-313. doi:10.1007/978-1-4939-9546-2_15

261. Arany Z, Newsome D, Oldread E, Livingston DM, Eckner R. A family of transcriptional adaptor proteins targeted by the E1A oncoprotein. *Nature*. 1995;374(6517):81-84. doi:10.1038/374081a0

262. Chakravarti D, Ogryzko V, Kao HY, et al. A Viral Mechanism for Inhibition of p300 and PCAF Acetyltransferase Activity. *Cell*. 1999;96(3):393-403. doi:10.1016/s0092-8674(00)80552-8

263. Frisch SM, Mymryk JS. Adenovirus-5 E1A: paradox and paradigm. *Nat Rev Mol Cell Biol*. 2002;3(6):441-452. doi:10.1038/nrm827

264. O'Connor MJ, Zimmermann H, Nielsen S, Bernard HU, Kouzarides T. Characterization of an E1A-CBP Interaction Defines a Novel Transcriptional Adapter Motif (TRAM) in CBP/p300. *J Virol*. 1999;73(5):3574-3581. doi:10.1128/jvi.73.5.3574-3581.1999

265. Eckner R, Ewen ME, Newsome D, et al. Molecular cloning and functional analysis of the adenovirus E1A-associated 300-kD protein (p300) reveals a protein with properties of a transcriptional adaptor. *Genes Dev*. 1994;8(8):869-884. doi:10.1101/gad.8.8.869

266. Hamamori Y, Sartorelli V, Ogryzko V, et al. Regulation of Histone Acetyltransferases p300 and PCAF by the bHLH Protein Twist and Adenoviral Oncoprotein E1A. *Cell*. 1999;96(3):405-413. doi:10.1016/s0092-8674(00)80553-x

267. Lynch KL, Gooding LR, Garnett-Benson C, Ornelles DA, Avgousti DC. Epigenetics and the dynamics of chromatin during adenovirus infections. *FEBS Lett*. 2019;593(24):3551-3570. doi:10.1002/1873-3468.13697

268. Tirumuru N, Pretto CD, Jorge LAC, Spindler KR. Mouse Adenovirus Type 1 Early Region 1A Effects on the Blood-Brain Barrier. *mSphere*. 2016;1(2):e00079-16. doi:10.1128/msphere.00079-16

269. Gralinski LE, Ashley SL, Dixon SD, Spindler KR. Mouse Adenovirus Type 1-Induced Breakdown of the Blood-Brain Barrier. *J Virol*. 2009;83(18):9398-9410. doi:10.1128/jvi.00954-09

270. Liesz A, Dalpke A, Mracsko E, et al. DAMP Signaling is a Key Pathway Inducing Immune Modulation after Brain Injury. *J Neurosci*. 2015;35(2):583-598. doi:10.1523/jneurosci.2439-14.2015

271. Nishibori M, Wang D, Ousaka D, Wake H. High Mobility Group Box-1 and Blood–Brain Barrier Disruption. *Cells*. 2020;9(12):2650. doi:10.3390/cells9122650

272. Andersson U, Tracey KJ. HMGB1 Is a Therapeutic Target for Sterile Inflammation and Infection. *Annu Rev Immunol*. 2011;29(1):139-162. doi:10.1146/annurev-immunol-030409-101323